

**Faculty of Science and Engineering
Department of Chemistry
Curtin Institute of Functional Molecules and Interfaces**

Electrochemical Strategy for Detection of Biomolecules

Bren Mark Balane Felisilda

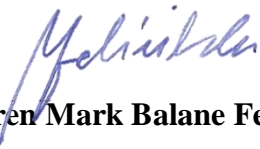
**This thesis is presented for the degree of
Doctor of Philosophy
of
Curtin University**

January 2018

Declaration

To the best of my knowledge and belief, this thesis contains no material previously published by any other person except where due acknowledgement has been made.

This thesis contains no material which has been accepted for the award of any other degree or diploma in any university or institution for higher education.



Bren Mark Balane Felisilda

PhD Candidate

[31 January 2018]

Table of Contents

Declaration	ii
Table of Contents.....	iii
List of Figures.....	vi
List of Tables.....	xii
Dedication	xiii
Acknowledgements.....	xiv
Glossary of Major Symbols.....	xvii
Glossary of Abbreviations.....	xix
Abstract	xxiii
Chapter 1. Introduction.....	1
1.1 Fundamentals of Electrochemistry.....	1
1.1.1 Solid Electrode Electrochemistry	1
1.1.2 Electron Transfer Reactions	1
1.1.3 Faradaic and Non-Faradaic Reactions	3
1.1.4 Polarisable and Non-Polarisable Electrodes	4
1.1.5 The Electrical Double Layer	5
1.1.6 Mass Transport	8
1.2 Electrochemistry at the Interface between Two Immiscible Electrolyte Solutions (ITIES)	10
1.2.1 Background on the electrochemistry at the ITIES	10
1.2.2 Structure of the ITIES.....	11
1.2.3 General Theory of the Electrochemistry at the ITIES	13
1.2.4 Polarisable and Non-polarisable ITIES	15
1.2.5 Potential Window for the ITIES.....	17
1.2.6 Forms of Charge Transfer at the ITIES	19
1.3 Micro-ITIES.....	21
1.3.1 Advantages of ITIES miniaturization	21
1.3.2 Gellification of the miniaturized ITIES	22
1.3.3 Effect of Interface Arrangement.....	23
1.4 Electroanalysis of Biological Molecules at the ITIES	28
1.5 Aims of this Work.....	33
Chapter 2. Experimental Materials and Methods.....	35
2.1 Electrochemical Set-up (ITIES).....	35
2.1.1 Electrochemical Cell.....	35
2.1.2 Electrodes and Electrolytes	37

2.2	Micro ITIES	39
2.3	Electrochemical Techniques.....	40
2.3.1	Cyclic Voltammetry	40
2.3.2	Linear Sweep Voltammetry.....	44
2.3.3	Differential Pulse Voltammetry	45
2.3.4	Stripping Voltammetry	48
Chapter 3. Electrochemical Detection of Lysozyme at a Liquid Solvent-Cast Organogel Microinterface Array		50
3.1	Introduction	50
3.2	Experimental Method.....	52
3.2.1	Reagents.....	52
3.2.2	Apparatus	52
3.2.3	Electrochemical Measurements	53
3.3	Results and Discussions	53
3.3.1	Cyclic Voltammetry	53
3.3.2	Adsorptive Stripping Voltammetry	57
3.3.3	Adsorptive Differential Pulse Stripping Voltammetry.....	61
3.4	Conclusions	64
Chapter 4. Electrochemical Behaviour of Fucoidan at Polarized Liquid-Organogel Microinterfaces.....		65
4.1	Introduction	65
4.2	Experimental Method.....	67
4.2.1	Reagents.....	67
4.2.2	Apparatus	68
4.2.3	Electrochemical Measurements	69
4.3	Results and Discussions	69
4.3.1	Cyclic Voltammetry	69
4.3.2	Adsorptive Stripping Voltammetry	76
4.3.3	Matrix Effects	79
4.4	Conclusions	82
Chapter 5. Investigation of Sulfated Carbohydrates at a Liquid-Organogel Micro-Array.....		84
5.1	Introduction	84
5.2	Experimental Method.....	87
5.2.1	Reagents.....	87
5.2.2	Apparatus	87
5.2.3	Electrochemical Measurements	88

5.3	Results and Discussions	89
5.3.1	Cyclic Voltammetry.....	89
5.3.2	Adsorptive Stripping Voltammetry	94
5.3.3	Matrix Effect	97
5.4	Conclusions.....	100
Chapter 6. Behaviour of Aptamers at Soft Polarized Microinterfaces.....		102
6.1	Introduction.....	102
6.2	Experimental Method	105
6.2.1	Reagents	105
6.2.2	Apparatus	106
6.2.3	Electrochemical Measurements.....	107
6.3	Results and Discussions	107
6.3.1	Cyclic Voltammetry.....	107
6.3.2	Effect of Surfactant Concentration	110
6.3.3	Effect of Presence of Other Species	113
6.3.4	Matrix Effects.....	115
6.4	Conclusions.....	117
Chapter 7. General Conclusions and Future Outlook.....		119
7.1	General Conclusions	119
7.2	Future Outlook.....	121
References		124
<hr/> APPENDICES		145
<hr/> Appendix A Preparation of Organic Electrolyte Salts		146
A.1	Metathesis of BTPPATPBCl	146
A.2	Metathesis of TDMATPBCl.....	147
A.3	Metathesis of CTATPBCl	148
Appendix B Research Output		149
B.4	Journal Publications	149
B.5	Research Presentations	149

List of Figures

Figure 1.1.1 Schematic representation of the electron transfer processes that occur at solid-electrolyte interfaces. (A) Circumstance without electron transfer, (B) Reduction of electrolyte species and (C) Oxidation of electrolyte species.....	2
Figure 1.1.2 Schematic illustration for a (A) polarisable and (B) non-polarisable electrode. Solid and dashed lines show theoretical as well as practical plots respectively.	5
Figure 1.1.3 (Left) Illustration of the electrical double layer according to Helmholtz while (Right) shows a schematic of a capacitor.	6
Figure 1.1.4 Schematic representation of electrical double layer showing the inner Helmholtz Plane (IHP) and outer Helmholtz Plane (OHP). ϕ_s , ϕ_2 and ϕ_m depict the Galvani potentials of the electrolyte solution, solvated cation and electrode surface, respectively.....	7
Figure 1.2.1 Illustration of the mixed solvent layer model representing the structure of the ITIES electrical double layer.....	12
Figure 1.2.2 Schematic representation of an ITIES that is polarisable and non-polarisable. For the polarisable type, A^+B^- is very hydrophilic while C^+D^- is highly hydrophobic. For the non-polarisable type, (top) A^+B^- would be common ions in the two phases or (bottom) A^+ is a common ion while B^- is very hydrophilic and C^- is just amply hydrophobic.	16
Figure 1.2.3 Cyclic voltammogram of 10 mM LiCl in the aqueous phase and 10 mM BTPPATPBCl in the gellified organic phase (10 % w/v low molecular weight poly(vinyl) chloride (PVC)/1,6-dichlorohexane) using a 30 micropore array silicon membrane. Scan rate of 5 mVs ⁻¹	19
Figure 1.2.4 Schematic illustration of the types of charge transfer phenomena. (A) Simple ion transfer (IT), (B) Facilitated/assisted ion transfer (FIT), (C) Electron transfer (ET).	20
Figure 1.3.1 Different geometries of a disc electrode with corresponding diffusion modes associated with it. The limiting current equation for each geometry is also shown. I_{lim} is the limiting current, n refers to number of electrons, F is Faraday's constant, D as the diffusion coefficient, C refers to the concentration, r is the radius of the electrode and L refers to the recessed depth when applicable.	23

Figure 1.3.2 Illustration of a single, filled microinterface showing different diffusion profiles. <i>Left</i> : Linear or Planar diffusion demonstrating movement of simple ion from organic to aqueous phase. <i>Right</i> : Radial diffusion showing transfer of simple ion from aqueous into the organic phase.	24
Figure 1.3.3 Representation of a cubic (left) and hexagonal (right) arrangement of microdisc arrays. d refers to the distance amongst pores while r is the pore radius. The greyed part depicts a diffusion zone for a single microelectrode.	25
Figure 1.3.4 Representation of diffusion profiles at the microinterface: (A) radial diffusion from aqueous to organic; (B) diffusion overlap (shielding effect); (C) linear diffusion from organic to aqueous and (D) extensive diffusion overlap inducing a linear diffusion from organic to aqueous phase.	26
Figure 2.1.1 Schematic illustration of a typical four-electrode cell set-up for an ITIES. RE is the reference electrode and CE is the counter electrode. Aq. refers to the aqueous phase while org. refers to the organic phase.	35
Figure 2.1.2 A schematic representation of a two-electrode electrochemical cell with a micropore array membrane.	36
Figure 2.2.1 Scanning Electron Microscopy (SEM) of the micropore arrays (silicon membrane). Images taken by Dr. Yang Liu and Dr. Eva Alvarez de Eulate using a Zeiss Neon 40 EsB FIBSEM microscope (Carl Zeiss Nanotechnology Systems).	39
Figure 2.3.1 Applied potential against time waveform for cyclic voltammetry.	41
Figure 2.3.2 Cyclic voltammogram of (A) cation transfer at the ITIES and (B) at the microinterface. Inset in (B) show (top) radial diffusion as cation transfer from aq. to org. phase while (bottom) linear diffusion as it back transfers from org. to aq. phase.	42
Figure 2.3.3 (A) LSV potential-time excitation signal (B) LSV cation transfer from aq. to org. phase.	45
Figure 2.3.4 (A) Plot of faradaic current, if and the charging current, ic over time after potential application; (B) Potential-time waveform for differential pulse voltammetry	46
Figure 2.3.5 (A) Sigmoidal curve of $i - \Delta\omega\phi$. Δi is higher at the rising part of the curve since $\Delta(\Delta\omega\phi)$ is inducing more changes in if (B) DPV voltammogram showing a cation transfer from aq. to org. phase.	47
Figure 2.3.6 Potential-time waveform depicting the steps in a stripping voltammetry	48
Scheme 3.2.1 Schematic representation of the electrochemical cell employed. x represents the various HEWL concentrations used in the study.	53

Figure 3.3.1 Cyclic voltammograms observed with the solvent-cast aqueous-organogel μ ITIES array (Scheme 1) in the absence and presence of TEA ⁺ and HEWL in the aqueous phase: a) 15 μ M TEA ⁺ ; b) 15 μ M HEWL and c) 15 μ M TEA ⁺ + 15 μ M HEWL. The blank experiment is shown as the dashed line. Scan rate: 5 mV s ⁻¹	55
Figure 3.3.2 Cyclic voltammograms observed with the solvent-cast aqueous-organogel μ ITIES array (Scheme 1) in the presence of increasing concentrations of HEWL, as indicated by the arrow direction (5, 10, 15, 20 and 25 μ M), in the aqueous phase. Scan rate: 5 mV s ⁻¹	56
Figure 3.3.3 Plot showing the effect on the peak current of varying the interfacial potential on the adsorption step. Aqueous phase contains: 10 mM HCl + 10 μ M HEWL. Adsorption time was 60 s, without stirring. The solvent-cast organogel was used as the organic phase (Scheme 1). Scan rate: 5 mV s ⁻¹	57
Figure 3.3.4 AdSV of 0.5 μ M HEWL + 10 mM HCl at various scan rates: 5 mV s ⁻¹ (black bold line) to 60 mV s ⁻¹ (black dotted line). Inset shows plot of peak current against scan rate. The solvent-cast organogel was used as the organic phase (Scheme 1). Pre-concentration time and potential were 60 s and 0.950 V respectively.	58
Figure 3.3.5 AdSV of 0.5 μ M HEWL + 10 mM HCl at various pre-concentration times from 5 (black bold line) to 1800 (grey bold line) s. The solvent-cast organogel was used as the organic phase (Scheme 1). Scan rate: 5 mV s ⁻¹	59
Figure 3.3.6 AdSV of various HEWL concentration for different adsorption times: (A) 60 s and (B) 300 s at an applied potential of 0.950 V. Aqueous phases contain (0 – 1.0) μ M HEWL in 10 mM HCl. The solvent-cast organogel was used as the organic phase (Scheme 1). Scan rate: 5 mV s ⁻¹	60
Figure 3.3.7 AdSV of increasing aqueous phase HEWL concentrations, as indicated by the direction of the arrow (0.02 to 0.84 μ M) at the solvent-cast aqueous-organogel μ ITIES (Scheme 1). The adsorption time and potential were 300 s and 0.950 V respectively. Scan rate: 5 mV s ⁻¹	61
Figure 3.3.8 AdDPSV of HEWL (0.02 to 0.60 μ M, increasing as directed by the arrow direction) for (A) 60 s, (B) 120 s, pre-concentration times prior to voltammetric desorption. Solutions contained increasing (0.02 - 0.60 μ M) HEWL + 10 mM HCl in the aqueous phase (Scheme 1).....	62
Scheme 4.2.1 Schematic representation of the electrochemical cells employed, where x represents the fucoidan concentrations employed in the study.	69

Figure 4.3.1	Cyclic voltammograms of 10 mM NaOH (pH 12) in the absence (grey dashed line) and presence (black line) of 1 mg mL ⁻¹ <i>Undaria p. fucoidan</i> using (A) Cell 1 and (top inset) <i>Fucus v.</i> ; (B) Cell 2 and (C) Cell 3 all in Scheme 1. (D) CVs recorded in the absence (grey dashed line) and the presence of 10 μM TPenA ⁺ (grey bold line) and with added 1 mg mL ⁻¹ <i>Undaria p. fucoidan</i> (black line) using Cell 1. Scan rate: 5 mV s ⁻¹ . Scan direction: towards negative potential; species transferred at the negative potential limit: (OH ⁻ aq → org), (BTPPA ⁺ / TDDA ⁺ / TDMA ⁺ org → aq). Bottom inset: Chemical structures of (A) BTPPA ⁺ ; (B) TDDA ⁺ ; (C) TDMA ⁺	71
Figure 4.3.2	Cyclic voltammograms of different <i>Undaria p. fucoidan</i> concentrations (10-1000 μg mL ⁻¹ for A&B; 5-25 μg mL ⁻¹ for C in 10mM NaOH (pH 12). Cell 1, 2 and 3 respectively (Scheme 1). Scan rate: 5 mV s ⁻¹ . Inset: Plot of peak current against <i>Undaria p. fucoidan</i> concentration. Scan direction: towards negative potential; species transferred at the negative potential limit: (OH ⁻ aq → org), (BTPPA ⁺ / TDDA ⁺ / TDMA ⁺ org → aq).	74
Figure 4.3.3	AdSV in the presence and absence (inset) of 500 μg mL ⁻¹ <i>Undaria p. fucoidan</i> , in aqueous phase of 10 mM NaOH (pH 12) following adsorption at different potentials. Adsorption time: 60 s, (A) Cell 1, (B) Cell 2, and (C) Cell 3 (Scheme 1). Scan rate: 5 mV s ⁻¹	77
Figure 4.3.4	Plot of peak current versus <i>Undaria p. fucoidan</i> concentrations using the optimized adsorption potential for each organic cation. Adsorption time: 180 s. Cells 1, 2 and 3 (Scheme 1).	79
Figure 4.3.5	(A) Cyclic voltammograms of pH-adjusted synthetic urine (black line) in comparison to 10 mM NaOH (pH 12) (grey dashed line) as the aqueous phase. (B) CV in the absence (grey dashed line) and presence of 1 mg mL ⁻¹ <i>Undaria p.</i> (black line) (Cell 5, Scheme1). (C) AdSV of increasing (background subtracted) <i>Undaria p.</i> fucoidan concentration (2-20 μg mL ⁻¹). Adsorption potential: -0.35 V, pre-concentration time: 180 s, Cell 5 (Scheme 1), scan rate: 5 mV s ⁻¹	81
Figure 5.1.1	Chemical structure of sucrose octasulfate (SOS).	84
Scheme 5.2.1	Schematic representation of the electrochemical cells employed, where <i>x</i> represents the sulfated carbohydrate (e.g. SOS) concentrations utilized in the study.	88
Figure 5.3.1	CV of 10 mM LiCl in the absence (grey dashed line) and presence (black line) of 10 μM sucrose octasulfate (SOS) using (A) Cell 1, (B) Cell 2 and (C) Cell 3 as shown in Scheme 5.2.1	91

Figure 5.3.2 CV of 10 mM LiCl in the absence (grey dashed line) and presence of increasing concentrations (0.25 – 6.0 μM) of SOS using Cell 2 (A) and Cell 3 (B) while (C) is with 6 μM SHpS and (D) is with 6 μM SHxS, both using Cell 3 (see Scheme 5.2.1).	92
Figure 5.3.3 AdSV of 10 mM LiCl with (A) 5 μM SOS at varying adsorption potentials applied for 60 s using Cell 3 (see Scheme 5.2.1) Inset: Corresponding blank profiles for the said experiment. And (B) 0.25-6.0 μM SOS using the optimized adsorption potential (-0.475 V, 60 s). (C) 0.03-0.15 μM SOS for 180 s. Inset: Current versus concentration plot of the said experiments; (D) Plot of peak current versus SOS concentration using optimized adsorption potentials for each chosen cation at 60 s.	95
Figure 5.3.4 (A) Cyclic voltammograms of synthetic urine (black line) in contrast to 10 mM LiCl (grey dashed line) as the aqueous phase. (B) CV in the absence (grey dashed line) and presence of 6 μM SOS. (black line) (C) AdSV of increasing SOS concentration (0.25-6.0 μM). Adsorption potential: -0.425 V, pre-concentration time: 60 s, scan rate: 5 mV s^{-1}	98
Scheme 6.2.1 Schematic illustration of the electrochemical cells utilized in the study. <i>X</i> represents the TBA concentrations used.....	107
Figure 6.3.1 Cyclic voltammograms of 10 mM LiCl (pH 8.5) (A) without (grey dashed line) and with (black line) 20 μM TBA using Cell 1; (B) with 10-100 μM of CTAB and (C) with 100 μM CTAB plus 5-25 μM TBA. Scan rate was 5 mV s^{-1}	109
Figure 6.3.2 Cyclic voltammograms of 10 mM LiCl (pH 8.5) with 10-50 μM TBA in aq. phase while (A) 5 mM CTAB + 10 mM BTTPATPBCl and (B) 10 mM CTAB + 10 mM BTTPATPBCl in org. phase; Scan rate was 5 mV s^{-1} . Top Inset: Background subtracted CVs (B), Bottom Inset: Calibration plot of top inset.	111
Figure 6.3.3 Cyclic voltammograms of 10 mM LiCl (pH 8.5) using Cell 2 (see Scheme 6.2.1) (A) with (black line) and without (grey dashed line) 10 μM TBA and (B) with varying (1-5 μM) TBA. Scan rate: 5 mV s^{-1} . Inset: Calibration plot of (B).	112

- Figure 6.3.4 Cyclic voltammograms of 10 mM LiCl (pH 8.5) using Cell 2 (see Scheme 6.2.1) (A) with (black dashed line) and without (grey dashed line) 5 μ M TBA while the dark grey line represent addition of 1 mM MgCl₂. (B) with (grey line) and without (grey dashed line) 10 μ M TBA plus different thrombin concentrations (0.13 – 0.39 mg mL⁻¹). (C) CVs in the absence (grey dashed line) and presence (black line) of 0.26 mg mL⁻¹ thrombin in 10 mM HCl. Scan rate: 5 mV s⁻¹. Inset of (B): Background subtracted CVs for (B); Inset of (C): CVs in the absence (grey dashed line) and presence (black line) of 0.26 mg mL⁻¹ thrombin in 10 mM LiCl (pH8.5)..... 114
- Figure 6.3.5 CVs of synthetic urine (black line) overlayed with that of 10 mM LiCl (pH 8.5) as the aqueous phase. (B) CVs of increasing (1-5 μ M) TBA. Scan rate: 5 mV s⁻¹. Inset: Calibration of (B)..... 117

List of Tables

Table 3.3.1 Summary of analytical performance of the solvent-casted organogel microarray for different voltammetric techniques used.	63
Table 5.3.1 Summary of analytical characteristics of SOS in the polarized liquid-organogel microarray for different voltammetric methods employed.	100
Table 6.3-1 Summary of the analytical characteristics attained for TBA using the polarized soft microinterfaces.....	116

Dedication

For my father, Melecio Sr., who taught me that life is what you make it and showed me how humility, patience, and hard-work will aid you to achieve your dreams;

For my mother, Luzvisminda, who showed me that learning is never limited to the four walls of a classroom and that even the biggest task can be accomplished if done one step at a time;

For my siblings, Melvick, April and Melecio Jr., who helped me enjoy growing up, supported me in all my endeavours and inspired me to do great things;

For my partner, Nixon, who never failed to encourage me when I needed it and for always being there throughout this journey;

And to all my teachers, advisers, and supervisors who shaped me, in one way or another, while traversing this academic journey. I dedicate this achievement to all of you.

The unexamined life is not worth living - Socrates

Acknowledgements

Reaching the finish line of this Ph.D. is one important and unforgettable event in my academic journey. Thus, I would like to grab this chance and extend my sincerest gratitude to all the people who were instrumental, in one way or another, and made this into a reality.

I would start by thanking my supervisor, Prof. Damien Arrigan, first for allowing me to join the Electrochemistry and Sensors group at Curtin. Second, for his guidance, supervision, encouragement, and patience throughout all these 3.5 years. I wouldn't have been able to start my Ph.D. without his generosity of lending me the funds needed to fulfill my OSHC requirements. His thought-provoking questions have developed the budding researcher in me and it has been really a pleasure and honour to work with such a great supervisor. I will always be grateful for all the opportunities he has given me.

Then, I would extend my deepest gratitude to Curtin University for granting me a Curtin International Postgraduate Research Scholarship (CIPRS) for the whole duration of my scholarship. Without their support, this journey would have never taken place.

I would also like to extend my thanks to the rest of my thesis committee, Dr. Franca Jones, who happens to be also the Postgraduate Research Coordinator, for her support and expert opinions, Dr. Debbie Silvester-Dean, my co-supervisor, for her suggestions and insights in my work as well as tips in becoming an early-career researcher.

A big thanks to the rest of the Electrochemistry and Sensors Group, both past and present: Eva Alvarez de Eulate (now Dr. Alvarez de Eulate) for showing me the rounds in the lab especially in the ways of the ITIES. Thanks for being an inspiration; Junqiao Lee (now Dr. Lee) for the electrochemistry discussions, Dr. Yang Liu for sharing her expertise and knowledge; Krishnan Murugappan (now Dr. Murugappan) for being a great HDR representative and connecting us new HDRs to the rest; Salmah Aziz and Masniza Sairi (now Dr. Sairi) for the nice cakes and for the beautiful group photos; Ghulam Hussain for the talks about our PhD journey and life in general; Ben

Austen, for the ideas and for introducing me to the beautiful parts of WA; Dr Terence Henares for sharing your ideas and experiences, not to mention our ‘Filipino’ sessions; and to the new members: Nasib, Jahire, and Hum as well as to the former projects and honours students, thanks for our shared experiences in and out of the labs. I will truly miss our group meetings and coffee sessions.

My gratitude also goes to the rest of the Ph.D. students who have shared the beautiful memories I had during my stay here: from birthday parties to Friday night drinks, I will definitely remember them. Then to the Department of Chemistry for providing me all the necessary things, advise and support as I ventured into my Ph.D.

Also, I extend my heartfelt thanks to the amazing people who I was able to work with on the projects during my Ph.D.: To the MARINOVA Pty Ltd group of Tasmania, Dr. Helen Fitton, and Dr. Damien Stringer for their knowledge, insightful discussions and providing the samples that aided the study in Chapter 4. Also, for their time and hospitality during my visit in their company; To Dr. Alan Payne, for discussions about the study in Chapter 5; Then to Dr Mark Hackett for his expertise in spectroscopy and informative discussions as well as to Samuel Booth (now Dr. Booth) from University of Manchester for the opportunity to work with the project on protein aggregation.

A warm thank you definitely goes to my Perth family. To Aunt Wilma and Joyvie, for welcoming me into your home especially when I needed it the most, and for helping me start my Perth life. Cheers to the shared and soon-to-be shared memories! Then to the original “Pinoy-Au Perth” gang for the friendship and support especially to Ate Maricel from our “*chikahan*” moments to your kindness and generosity, I would always be grateful. To my former Beckenham neighbours, Red and Liszt, thanks for all the things we guys have shared and the continued friendship. To the rest of the “Good Vibes” gang, exploring and living in WA has been more fun with you all. *Daghan kaayong salamat!*

My gratitude is extended to the people, who may be physically 4,586 km away from me, have been my inspiration and source of strength throughout this endeavour. To my ever-loving parents, Papa Mel and MamaVicky, I offer this success to both of you. You have done a lot for me and for my siblings and I will forever be grateful. To the rest of the family: Ate Melvick, Ate Nikki, and Sam; Ate April, Kuya

Bryne and Ben, Jay-are and Joly, thanks heaps for the prayers, love and support. Of course, to my special someone, Nixon, thanks for understanding me all these times and for always cooking the best dishes for me. We are on this journey together and I could never be happier to have spent it with you. A special mention also goes to all my “Bes” friends back home who, despite the distance, never forget the mateship and camaraderie we share.

Finally, all my praises and thanksgiving are lifted up to my dear Father in Heaven, who was always there for me despite many times I was weak. My words may not be enough to thank you, but I offer all of these to you Almighty Father.

Ad Majorem Dei Gloriam!

Glossary of Major Symbols

Roman Symbols

Symbol	Definition	Units
A	Area	cm^2
a_i	Activity of species i	-
C	capacitance	F
C_{dl}	Double-layer capacitance	F
C_i	Concentration of species i	mol cm^{-3}
d	Centre-to-centre distance in micropores	Cm
D_i	Diffusion coefficient	$\text{cm}^2 \text{s}^{-1}$
e^-	Electrons	-
E	Potential	V
E^o	Formal potential	V
E_{eq}	Equilibrium potential	V
F	Faraday's constant	C
G	Gibbs free energy	J mol^{-1}
G^o	Standard Gibbs free energy	J mol^{-1}
i	Current	A
i_{lim}	Limiting current	A
J	Flux	$\text{mol s}^{-1} \text{cm}^{-2}$
\ln	Natural logarithm	-
L	Recessed depth in microelectrodes	Cm
m	Mass	g mol^{-1}
M	Molarity	mol L^{-1}
n	Number of electrons	-
N	Number of moles	-

o	Organic phase at liquid-liquid interfaces	-
O	Oxidised species	-
Q	Charge	C
r	Radius	cm
R	Reduced species	-
	Resistance	Ω
	Resistivity	Ω
	Universal gas constant	$\text{J K}^{-1} \text{mol}^{-1}$
t	Time	s
T	Temperature	K
V	Potential difference	V
w	water/aqueous phase at liquid-liquid interface	-
z_i	charge of species i	-

Greek Symbols

Symbol	Definition	Units
α	Aqueous phase of a liquid-liquid system	-
β	Organic phase of a liquid-liquid system	-
Δ	Difference	-
Γ	Surface coverage	-
δ	Diffusion zone	-
ε	Relative permittivity of a solvent	$\text{A}^2 \text{s}^4 \text{kg}^{-1} \text{m}^{-3}$
η	Overpotential	-
μ	Micro- (prefix)	-
$\bar{\mu}_i^\alpha$	Electrochemical potential of species i in phase α	kJ mol^{-1}
μ_i^α	Chemical potential of species i in phase α	kJ mol^{-1}

$\mu_i^{\alpha,0}$	Standard chemical potential of species i in phase α	kJ mol^{-1}
v	Scan rate in voltammetry	V s^{-1}
	Hydrodynamic velocity	cm s^{-1}
ϕ	Standard Galvani potential difference	V

Glossary of Abbreviations

Abbreviation	Definition
<i>ACT</i>	Aqueous complexation followed by transfer
<i>ACV</i>	Alternating current voltammetry
<i>AdSV</i>	Adsorptive stripping voltammetry
<i>AdDPSV</i>	Adsorptive differential pulse stripping voltammetry
<i>Ag/AgCl</i>	Silver/silver chloride
<i>AOT</i>	Bis(2-ethylhexyl) sulfosuccinate
<i>ASV</i>	Anodic stripping voltammetry
<i>BESI</i>	Biphasic electrospray ionisation
<i>BTPPA</i>	Bis(triphenylphosphoranylidene) ammonium, organic cation
<i>BSA</i>	Bovine serum albumin
<i>CA</i>	Chronoamperometry
<i>CC</i>	Chronocoulometry
<i>CE</i>	Capillary electrophoresis
	Counter electrode
<i>Cl⁻</i>	Chloride ion
<i>Cs⁺</i>	Cesium ion
<i>CSV</i>	Cathodic stripping voltammetry
<i>CTAB</i>	Cetyltrimethylammonium bromide

<i>CV</i>	Cyclic voltammetry
<i>DB18C6</i>	Dibenzo-18crown-6
<i>1,2- DCE</i>	1,2-Dichloroethane
<i>1,6-DCH</i>	1,6-Dichlorohexane
<i>DEA⁺</i>	Diethylammonium ion
<i>DMFeCp₂</i>	1,1-dimethylferrocene
<i>DNA</i>	Deoxyribonucleic acid
<i>DNNS</i>	Dinonylnaphthalenesulfonate
<i>DPI</i>	Dual polarisation interferometry
<i>DPV</i>	Differential Pulse Voltammetry
<i>DRIE</i>	Deep reactive ion etching
<i>ELISA</i>	Enzyme-linked immunosorbent assay
<i>ESTASI</i>	Electrostatic spray ionisation
<i>ET</i>	Electron transfer
<i>FIA</i>	Flow-injection analysis
<i>FIB</i>	Focus-ion beam
<i>FIT</i>	Facilitated ion transfer
<i>FFTFS</i>	Front-face tryptophan fluorescence spectroscopy
<i>GC</i>	Gas chromatography
<i>HCl</i>	Hydrochloric acid
<i>HEWL</i>	Hen-egg-white lysozyme
<i>HPLC</i>	High-performance liquid chromatography
<i>HOMO</i>	Highest occupied molecular orbital
<i>IHP</i>	Inner Helmholtz Plane
<i>ISE</i>	Ion-selective electrode
<i>IT</i>	Ion transfer
<i>ITIES</i>	Interface between two immiscible electrolyte solutions
<i>LiCl</i>	Lithium chloride

<i>LSV</i>	Linear sweep voltammetry
<i>LUMO</i>	Lowest unoccupied molecular orbital
<i>MALDI</i>	Matrix-assisted laser desorption ionisation
<i>MD</i>	Molecular dynamics
<i>MS</i>	Mass spectrometry
<i>MVN</i>	Modified Verwey-Niessen model
<i>NADH</i>	Nicotinamide adenine dinucleotide
<i>NaOH</i>	Sodium hydroxide
<i>NB</i>	Nitrobenzene
<i>NMR</i>	Nuclear magnetic resonance spectrometry
<i>NPOE</i>	2-nitrophenyl octyl ether
<i>OHP</i>	Outer Helmholtz Plane
<i>PBS</i>	Phosphate buffered saline
<i>PEA</i>	Phenylethylamine
<i>pI</i>	Isoelectric point
<i>Pt</i>	Platinum
<i>PVC</i>	Poly(vinyl) chloride
<i>QELS</i>	Quasi-laser light scattering
<i>RE</i>	Reference electrode
<i>RTIL</i>	Room-temperature ionic liquid
<i>SECM</i>	Scanning electrochemical microscopy
<i>SV</i>	Stripping voltammetry
<i>SWV</i>	Square wave voltammetry
<i>SRCD</i>	Synchrotron radiation circular dichroism spectroscopy
<i>TBA</i>	Thrombin-binding aptamer
<i>TBA⁺</i>	Tetrabutyl ammonium ion
<i>TDMA⁺</i>	Tridodecylmethylammonium ion
<i>TEA⁺</i>	Tetraethylammonium ion

<i>THF</i>	Tetrahydrofuran
<i>TIC</i>	Transfer by interfacial complexation
<i>TID</i>	Transfer by interfacial dissociation
<i>TPB⁻</i>	Tetraphenylborate ion
<i>TPrA⁺</i>	Tetrapropylammonium ion
<i>TPBCl⁻</i>	Tetrakis(4-chlorophenyl)borate, organic anion
<i>UME</i>	Ultramicroelectrode
<i>UV/Vis</i>	Ultraviolet-visible
<i>WE</i>	Working electrode

Abstract

The interest in understanding the behaviour of biomolecules at aqueous-organic interfaces continue to grow as advances are made in disease diagnostics, drug delivery, and therapeutics. Along with this rise in interest is the clamour for detection techniques that are fast, affordable and sensitive. This is where the electrochemistry of the interface between two immiscible electrolyte solutions (ITIES) comes in. Mainly, this technique is based on the charge transfer across a polarized interface created when two electrolyte solutions are brought into contact. This promises a label-free detection of biologically important molecules.

Gellification of the organic phase has been reported to improve the mechanical stability of the polarized soft interface. For the start of this Ph.D., an alternative organogel preparation technique was explored. Similar to what is normally used in preparing ion-selective electrodes (ISEs), tetrahydrofuran (THF) was added to dissolve poly(vinyl) chloride (PVC), that was spiked to gellify the organic phase. Optimization of the parameters revealed that it is greatly comparable with the heat-treated organogel.

This was then utilized to investigate how a model protein, hen-egg-white lysozyme (HEWL), behaves at this aqueous-solvent-casted organogel interface. Cyclic voltammetry at the microITIES showed a broad response at the forward scan, towards positive potentials, that suggested an adsorption process and was then followed by a desorption peak at *ca.* 0.68 V, indicating the detection of HEWL in this region. Application of an adsorption step, with an optimized potential of 0.95 V, followed by a voltammetric scan afforded a linear response for concentrations 0.02-0.84 μM while a detection limit of 0.030 μM was achieved for 300 s adsorption time. The use of differential pulse stripping voltammetry (DPSV) further improved the detection limits to 0.017 μM , 0.014 μM , and 0.010 μM after pre-concentrations times of 60, 120 and 300 s respectively. These findings are an improvement against other detection methods for HEWL at the polarized soft interfaces.

Additional biologically-important molecules, fucoidans, which are sulfated polysaccharides extracted from algae, were assessed using voltammetry at an array of

microinterfaces formed between two immiscible electrolyte solutions (μ ITIES) with a gelled organic phase. Two species (*Undaria pinnatifida* and *Fucus vesiculosus*) showed different response intensity via cyclic voltammetry and it revealed an adsorption process when scanned to more negative potentials followed by a desorption peak at *ca.* -0.50 V signaling the electroactivity of both fucoidans despite *Undaria p.* showing more intense signal compared *Fucus v.* Moreover, employing tridodecylmethylammonium (TDMA⁺) or tetradodecylammonium (TDDA⁺) as the organic phase electrolyte cation enhanced the detection of both species in comparison to when bis(triphenylphosphoranylidene)ammonium (BTPPA⁺) was used as the cation. A linear response of current with fucoidan concentration of 2-20 $\mu\text{g mL}^{-1}$ for *Undaria p.* (with TDMA⁺) and 10-100 $\mu\text{g mL}^{-1}$ for *Fucus v.* (with TDDA⁺) was achieved via utilization of adsorptive stripping voltammetry. Combination of TDMA⁺ as the organic phase cation and adsorptive pre-concentration for 180 s resulted to a detection limit of 1.8 $\mu\text{g mL}^{-1}$ fucoidan (*Undaria p.*) in 10 mM NaOH and 2.3 $\mu\text{g mL}^{-1}$ in synthetic urine (pH adjusted).

Furthermore, simpler versions of these sulfated polysaccharides, in the form of sulfated carbohydrates were investigated at a μ ITIES array where the organic phase is gelled. Cyclic voltammetry of sucrose octasulfate (SOS) with the usual BTPPA⁺ in the organic phase did not show a response to a 10 μM SOS concentration. This changed when TDDA⁺ was instead used in the organic phase which revealed a distinct peak at *ca.* -0.47 V revealing a desorption process after an adsorption when scanning was at negative potentials. A similar response was shown by another negatively charged biomolecule as discussed earlier. This peak shifted to *ca.* -0.28 V when TDMA⁺ was in the organic phase. This again supports previous results suggesting increasing binding strength between of these alkylammonium cations with anionic biomolecules studied. The combination of the optimized adsorption parameters and having TDMA⁺ in the organic phase resulted to detection limits of 0.12 μM SOS in 10 mM LiCl and 0.24 μM in a synthetic urine aqueous phase. This was enhanced when the pre-concentration time was increased to 180 s and achieved 0.04 μM SOS (10 mM LiCl).

Finally, a synthetic oligonucleotide, in this case, an aptamer, was explored for its behaviour at the liquid-organogel microinterface array. Thrombin-binding aptamer (15-mer, TBA) did not display a response when BTPPA⁺ was in the organic phase. A similar observation was made with SOS as discussed previously suggesting that the

structure of BTPPA⁺ seems to hinder the interaction with such negatively charged biomolecules. Based on literature reports about surfactants affecting DNA detection, the use of CTAB was examined. CTAB showed a diffusion-controlled transfer at the polarized soft interfaces. Upon addition of increasing TBA concentrations, the peak current for CTAB decreased accordingly and indicating an interaction of CTAB with TBA thereby decreasing the amount of CTAB able to transfer across the interface. Furthermore, CTAB was incorporated into the organic phase along with 10 mM BTPPATPBCl. At a lower 5mM CTAB concentration, no response for TBA was recorded. This was not the case when CTAB concentration was increased to 10 mM. This time, a sharp peak around *ca.* -0.54 V was recorded, which is indicative of an adsorption/desorption process, as previously found for other biomolecules. Ultimately, CTATPBCl replaced BTPPATPBCl in the organic phase and this improved the response for TBA. In this case, the distinct peak response shifted to *ca.* -0.25 V, which can be credited to an early transfer of CTA⁺ across the soft polarized interface. CV at this set-up afforded a detection limit of 0.11 μ M TBA.

Also, the effect of other species on the TBA response at the μ ITIES was examined. The presence of MgCl₂ at physiological concentration caused the disappearance of the peak response corresponding to TBA. This could mean that Mg²⁺ induced the folding of TBA as suggested in the related literature. Moreover, the peak current response of TBA was decreased by the addition of different concentrations of thrombin indicating TBA interacting with it. Then, this surfactant-aptamer interaction was explored in a synthetic urine matrix. Despite the presence of other species that may interfere with TBA at this medium, the calculated detection limit was 0.29 μ M

The results discussed in this thesis offer the basis of a new bioanalytical approach for a rapid, affordable and label-free detection of various biologically-important molecules. These also provide insights of understanding the electrochemical behaviour of biomolecules at these microinterfaces formed between two electrolyte solutions.

Chapter 1. Introduction

1.1 Fundamentals of Electrochemistry

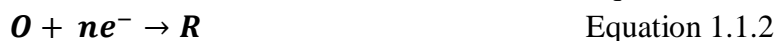
Electrochemistry is the science that deals with the relationship between chemical and electrical processes.¹ Consequently, most of these processes can be classified into two general types: (1) the examination of chemical or physical processes resulting from current flow and (2) the investigation of electrical circumstances induced by chemical reactions.²

1.1.1 Solid Electrode Electrochemistry

In general, electrochemical experiments involve the movement of charge between an electrified surface (electrode) and an ionic conducting solution (electrolyte).^{1,3}

1.1.2 Electron Transfer Reactions

When the transfer of electron happens at the (solid) electrode surface, this results in the oxidation or reduction of the electroactive species in solution. The oxidation (anodic) process entails the electroactive species in solution losing electrons towards the (solid) electrode while the reduction (cathodic) process involves the electroactive species gaining the electrons from the (solid) electrode. Equations 1.1.1 and 1.1.2 exemplifies these processes respectively, where R is the reduced species and O is the oxidized species.⁴



Such reactions happening at the electrode are affected by the application of a certain potential (voltage). By definition, a volt (V) is the energy (in Joules, J) needed for charge (in Coulombs, C) to move. Since electrons are charged species, once a potential is applied to the electrode, the energy of these electrons in the metal will change. This will produce a potential difference which will bring about a possible electron transfer. In terms of energy levels for such electron transfer processes, the

concept of Fermi level is important. Tightly packed atoms with overlapping atomic orbitals make up a metal electrode. Consequently, the metal has a continuum of energy levels, different from individual and defined energy levels of a single atom from the same material. By convention, electrons fill these levels from the bottom up while the Fermi level equates to the energy at which the top-most electrons are.¹

When a more negative potential is applied to the electrode than the potential at which the electrode has zero net current, the Fermi level in the metal is elevated. As such, the electron can be transported from a level of high-energy on the solid electrode to a lowest unoccupied molecular orbital (LUMO) for a species in solution, resulting to a current from the electrode to the solution and reduction occurs. On the other hand, when a more positive potential is employed to the electrode, this lowers the Fermi level compared to the highest occupied molecular orbital (HOMO) of the electrolyte species, producing an electron flow from the electrolyte species to the electrode and oxidation happens, giving an oxidation current. These processes are illustrated in Figure 1.1.1.

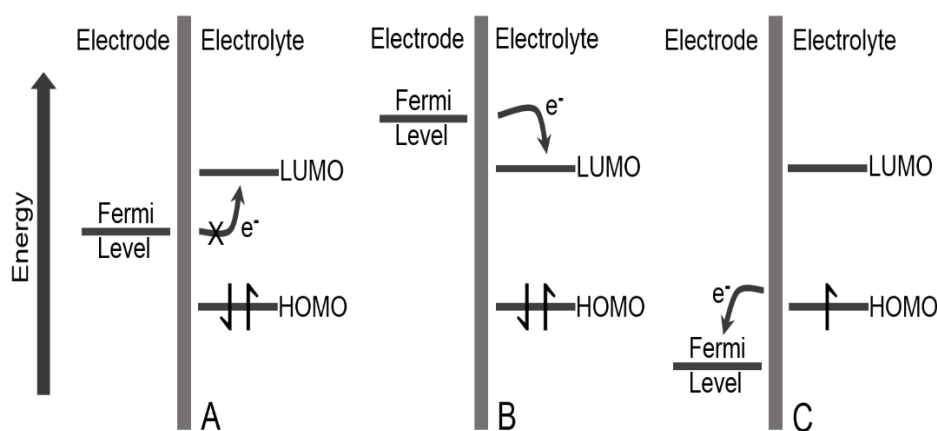


Figure 1.1.1 Schematic representation of the electron transfer processes that occur at solid-electrolyte interfaces. (A) Circumstance without electron transfer, (B) Reduction of electrolyte species and (C) Oxidation of electrolyte species.

In equilibrium, these processes are associated with the standard potential, E^0 , of the redox couple being studied^{1,2,5} and are kinetically or thermodynamically favourable.^{2,6} The electron transfer kinetics relies on the standard heterogeneous rate constant, k^0 .^{1,5} This means that when the value of k^0 is large, equilibrium is achieved quickly, while if it is small, equilibrium is achieved slowly. When k^0 is large for both the forward and the reverse reactions, the concentrations of the oxidized and reduced

species at the surface of the electrode, $C_O(x = 0)$ and $C_R(x = 0)$, are said to be thermodynamically in equilibrium.

Also, the activities of the redox species (O and R in Equations 1.1.1 and 1.1.2) can be linked with the Gibbs free energy of the system, as shown in the following equation.

$$\Delta G = \Delta G^0 + RT \ln \frac{a_O}{a_R} \quad \text{Equation 1.1.3}$$

where ΔG is the Gibbs free energy, and ΔG^0 is the standard free energy (both are in J mol^{-1}), R being the universal gas constant ($8.314 \text{ J mol}^{-1} \text{ K}^{-1}$), while T is the temperature (K). The activities of the oxidized and reduced species respectively are a_O and a_R (both in mol L^{-1}). E^0 can also be derived from the correlation between the redox species' concentration and the standard Gibbs free energy, ΔG^0 as presented in the following equation:

$$\Delta G^0 = -nFE^0 \quad \text{Equation 1.1.4}$$

where ΔG^0 is the standard Gibbs free energy (J mol^{-1}), E^0 as the standard electrode potential (V), n represents the number of moles of electrons while F is Faraday's constant ($96,485 \text{ C mol}^{-1}$). A system where no external voltage or source of current present is used as a reference to the standard potential difference and such relationships form the basis of the Nernst equation.^{1,2,5} This is illustrated in Equation 1.1.5:

$$E = E^0 + \frac{RT}{nF} \ln \frac{a_O}{a_R} \quad \text{Equation 1.1.5}$$

E is the potential difference (V) while the other species are as previously defined. This equation is vital since it describes how the potential of an electrode can be associated to the electroactive species' (O and R) concentrations.

1.1.3 Faradaic and Non-Faradaic Reactions

The phenomena observed in an electrochemical cell can be classified as faradaic or non-faradaic yet both processes adds to the measured current.⁷ Faradaic reactions refer to the occurring chemical reactions (either reduction or oxidation) that produce an electrical signal in the form of a current and this is known as the faradaic current. Such processes obey Faraday's Law,^{1,5} which states that the amount of

chemical change is proportional to the amount of electricity passed into the cell. This relationship is revealed in Equation 1.1.6.

$$Q = nFN \quad \text{Equation 1.1.6}$$

where Q is the total charge (C), n is the number of electrons, while F is Faraday's constant (96,485 C mol⁻¹) then N is the number of moles reacted (mol).

Meanwhile, non-faradaic processes are the remaining processes that do not involve a chemical reaction at the solid electrode-electrolyte interface. Examples would be adsorption and desorption processes that can result to the accumulation of charge at such interface. Also, non-faradaic processes can result to a charging current at the electrode, which was later on explained to be affected by the electrical double layer (as discussed in Section 1.1.5), a structure that is affected by changes in potential and solution composition.^{1,5,7}

1.1.4 Polarisable and Non-Polarisable Electrodes

As the electrode moves away from its equilibrium potential value, E_{eq} , due to the faradaic current, polarisation takes place. This is brought about by its difference from the potential applied, E , and is described as the overpotential, η , shown in the following equation:

$$\eta = E - E_{eq} \quad \text{Equation 1.1.7}$$

By definition, it is described as an ideally polarisable electrode wherein no transfer of charge can take place between the electrode-electrolyte interface despite applying different potentials.^{1,2} Such kind of electrode will display a large change in potential upon application of even a minute current. An illustration for this is shown in Figure 1.1.2 (A) with the ideally polarisable electrode distinguished by the horizontal region of an $i - E$ curve. This is quite impossible yet it is observed at some potential ranges by certain electrode-electrolyte systems.^{1,2} Meanwhile, an ideally non-polarisable electrode is the instance wherein no variance in potential is shown upon the current passage. Simplified, such electrode is of a fixed potential and distinguished as a vertical region on the $i - E$ curve, displayed in Figure 1.1.2B.

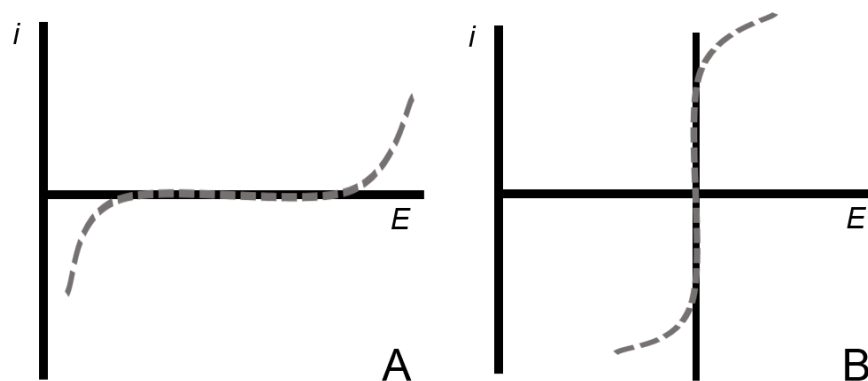


Figure 1.1.2 Schematic illustration for a (A) polarisable and (B) non-polarisable electrode. Solid and dashed lines show theoretical as well as practical plots respectively.

1.1.5 The Electrical Double Layer

As mentioned earlier, faradaic and non-faradaic processes happen simultaneously thus it is vital to consider the contribution made by non-faradaic processes in investigating electrode reactions. As defined, the electrical double layer is made up of the electrical charge at the electrode surface as well as the charge of distributed ions in solution that are within close proximity with the electrode.

Hermann von Helmholtz¹ was first to expound the concept of the electrical double layer to describe the charging current caused by non-faradaic processes at the electrode. In this model, the separation of charges is observed at the electrode-electrolyte interface comprising the electrical double layer itself due to the electrical charge at the electrode surface together with the charge of the ions in solution within its vicinity. This is caused by applying a potential towards the electrode and resulting in a flow of charge (non-faradaic current) through the cell. This behaviour is similar to that of a capacitor, which is shown in Figure 1.1.3

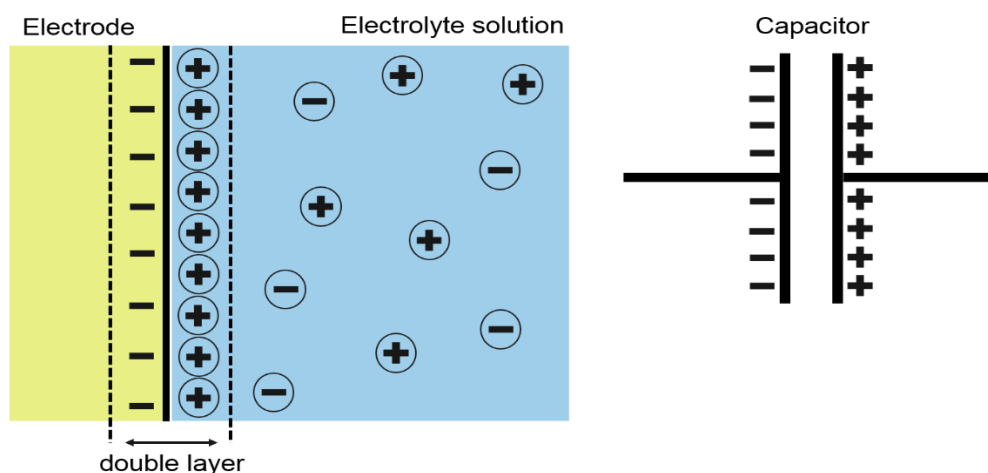


Figure 1.1.3 (Left) Illustration of the electrical double layer according to Helmholtz while (Right) shows a schematic of a capacitor.

A capacitor has two metal electrodes in parallel to each other and is known as an electrical circuit component. As a potential is applied, charge carriers reposition and assemble at the two metal plates as described in the next equation:

$$\frac{Q}{E} = C \quad \text{Equation 1.1.8}$$

where Q is the stored charge on the capacitor (C), E is the applied potential (V) while C represents capacitance (F).¹ This charge will build-up until Q is fulfilled according to Equation 1.1.8. Consequently, charging (non-faradaic) current will flow through it. This shows that the double layer capacitance, C_{dl} , depends on the potential applied thus becoming a characteristic of the electrode-solution interface.¹

Over the years, the concept of the electrical double layer was modified. Gouy and Chapman^{8,9} proposed that the charge in the solution cannot be entirely limited at the surface of the electrode. In solutions with low concentrations, the numbers of charge carriers would also be less. Thus, a wider layer of these charge carriers would be needed to neutralize the electrode surface charge. This layer is known as the diffuse layer and is depicted in Figure 1.1.4

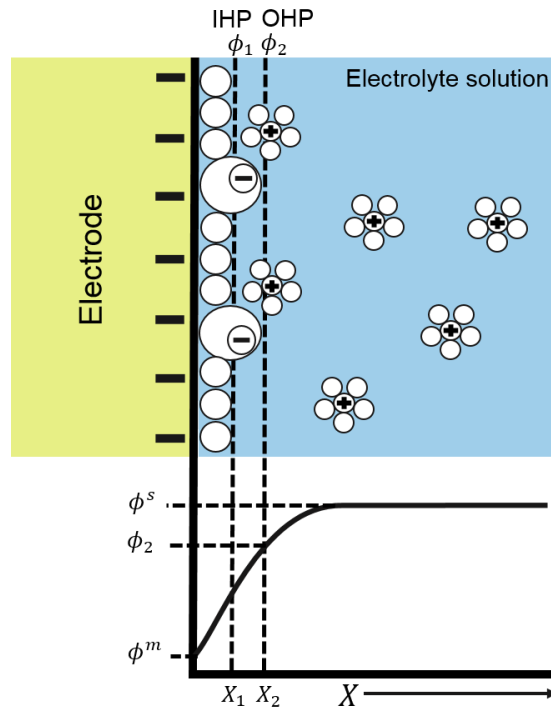


Figure 1.1.4 Schematic representation of electrical double layer showing the inner Helmholtz Plane (IHP) and outer Helmholtz Plane (OHP). ϕ^s , ϕ_2 and ϕ^m depict the Galvani potentials of the electrolyte solution, solvated cation and electrode surface, respectively.

As such, it is near the surface of the electrode where electrostatic attraction is strongest due to higher charge concentration in solution. The concentration difference of counter ions gets reduced as it becomes farther from the surface of the electrode thereby producing a reduction in the electrostatic attraction accordingly. In addition, the applied potential would also affect the thickness of the diffuse layer. A higher applied potential would mean more electrostatic forces thereby reducing the diffuse layer thickness. Moreover, the thickness of the diffuse layer also affects the charging of the electrode surface. At low concentrations, the thicker (more charging current) diffuse layer would hinder the measurement of smaller faradaic currents.^{1,10} Previous models by Helmholtz, Gouy and Chapman regarded ions as point charges that could come arbitrarily close near the surface. However, that is not realistic because ions have finite size and this hinders their approach to the surface if the distance is less than its ionic radius. To address limitations of prior models, Stern¹¹ added the idea of a “plane of closest approach” for centre of ions at a certain distance, x_2 (see Figure 1.1.4). This distance can also be affected when the ion is solvated and/or detached from the electrode surface by an adsorbed layer of electrolyte. In the case of higher concentration of electrolyte, the solution charge would be compressed near to the

distance x_2 , nearing that of Helmholtz's model. Thus, the plane is called the Outer Helmholtz Layer (OHP). The OHP concept is vital for systems where the charge in solution is compressed at the boundary due to large applied potential and high electrolyte concentration.¹

In addition, Grahame¹² added in his contribution to address the concept of counter ions undergoing non-specific adsorption to the surface of the electrode via distant electrostatic effects, as previously discussed by Helmholtz. Grahame explained that specific interactions are normally in short distances, wherein specifically adsorbed species and solvent molecules may be closely bound to the electrode surface. This plane was later called the Inner Helmholtz Layer (IHP) and is defined as the distance x_1 from the electrical centre of the species relative to the electrode surface, as also shown in Figure 1.1.4.

1.1.6 Mass Transport

In a simple electrochemical reaction, wherein no additional physical or chemical processes are present, the reaction is dictated by the electroactive species' mass transport towards the electrode, its electron transfer while at the surface of the electrode and after the reaction, its movement away from the electrode. When the rate of the reaction is controlled by the rate of the movement of the electroactive species, the reaction may be thought of as mass transport limited.^{1,2,5} Thus, mass transport, by definition, is the flow of electroactive species in solution to and from the electrode and can be due to three possible mechanisms: (a) convection – the movement aided by stirring or other mechanical forces like; (b) diffusion – the movement due to a concentration gradient; and (c) migration – the movement due to an applied electric field.^{1,5}

Mass transport is often described as the flux, J ($\text{mol cm}^{-2} \text{s}^{-1}$), of species i , to the electrode and is explained mathematically by the Nernst-Planck equation:

$$J_i(x) = -D_i \frac{\partial C_i(x)}{\partial x} - \frac{Z_i F}{RT} D_i C_i \frac{\partial \phi(x)}{\partial x} + C_i v(x) \quad \text{Equation 1.1.9}$$

where x is the distance from the electrode; while D , C , and Z are the diffusion coefficient ($\text{cm}^2 \text{s}^{-1}$), concentration (mol cm^{-3}) and the electroactive species' charge respectively; Then, $\frac{\partial C_i(x)}{\partial x}$ is the concentration gradient, $\frac{\partial \phi(x)}{\partial x}$ is the potential gradient

along the x -axis and $v(x)$ is the hydrodynamic velocity (cm s^{-1}).^{1,5} For aqueous media, the diffusion coefficient ranges from 10^{-6} to $10^{-5} \text{ cm}^2 \text{ s}^{-1}$ at standard temperature (298 K)^{5,13} and is dependent on several factors, including solvent viscosity, temperature and molecular size of diffusing species.¹⁴

It is important to note that Equation 1.1.9 (right-hand side) represents respectively the elements of mass transport for diffusion, migration, and convection. However, the equation can be simplified by inclusion of an excess inert supporting electrolyte relative to the analyte concentration to control the migration term and by doing the experiment in stationary conditions (no stirring or hydrodynamic support) to control the convection term. This results to diffusion as the major contributor for mass transport.^{15,16} Consequently, a diffusional flux is generated when the reaction happening at the surface of the electrode produces a concentration gradient.⁵ This is mathematically described in Fick's first law which details the direct proportionality of the flux or diffusion rate towards the slope of the concentration gradient with respect to the position x from the electrode at a time t ⁷ and is shown in the equation below:

$$J_i(x, t) = -D_i \frac{\partial C_i(x, t)}{\partial x} \quad \text{Equation 1.1.10}$$

The negative sign in the above equation is due to the tendency of the course of the species to move in the opposite direction with respect to the concentration gradient. Meanwhile, Fick's second law of diffusion (in one dimension) represents the relationship of the diffusional flux with time as revealed in Equation 1.1.11

$$\frac{\partial C_i(x, t)}{\partial t} = D_i \frac{\partial^2 C_i(x, t)}{\partial x^2} \quad \text{Equation. 1.1.11}$$

Also, the current i is directly proportional to the flux indicating that it estimates the rate of charge flow as shown below:

$$i = -nFAJ(x, t) \quad \text{Equation 1.1.12}$$

The combination of equations 1.1.10 and 1.1.12 results to equation 1.1.13, when other modes of mass transport (migration and convection) are suppressed;

$$i = nFAD \frac{\partial C_i(x, t)}{\partial x} \quad \text{Equation 1.1.13}$$

Referring to the equation, n refers to the number of electrons exchanged, F is Faraday's constant and A as the electrode area.

1.2 Electrochemistry at the Interface between Two Immiscible Electrolyte Solutions (ITIES)

1.2.1 Background on the electrochemistry at the ITIES

The interface between two immiscible electrolyte solutions (ITIES) is formed when two solutions of low mutual miscibility are made to contact. Typically, this is between an aqueous phase that contains hydrophilic electrolytes (e.g. LiCl) and an organic phase that has hydrophobic electrolytes (e.g. bis(triphenylphosphoranylidene)ammonium tetrakis(4-chlorophenyl)borate, BTPPATPBCl). The organic solvent used (e.g. 1,6-dichlorohexane (DCH), 1,2-dichloroethane (DCE)) is polar and must have a dielectric permittivity enough to dissociate (or even partially dissociate) the organic electrolyte salt^{17,18}. It is in this polarisable interface where the main interest, electrochemically, happens. Commonly, it involves an ion transfer from one phase to another,¹⁹⁻²² or it could also be a redox reaction at the liquid-liquid interface, though it is less common.^{23,24} The rise in the use of the electrochemistry at the ITIES can be attributed to several advantages. One key advantage is that, unlike the conventional solid electrode redox electrochemistry, analytes that are not redox active or may involve some complications in their redox electrochemistry, can be studied,¹⁸ given that these analytes possess a charge (or can be charged). An example would be by controlling the pH of the solution and observing changes in electrochemical behaviour, which can be beneficial as a label-free detection of biomolecules.²⁵ In addition, the ITIES is quite amenable for miniaturisation, a property that is vital for electrochemical sensing technology, and has been shown by studies performed originally at the macro (millimetre-centimetre) scale,^{19,26} then to the micro scale^{20,27,28} and down to the nano-scale.²⁹⁻³²

Historically, the first electrochemical studies at the ITIES were performed by Nernst and Riesenfeld in 1902³³ wherein they were concerned about the transport number of organic solvents. With the use of coloured inorganic electrolytes, they observed ion transfer across water-phenol-water interfaces. However, the interest for such systems slowed down until in 1963 when Blank and Feig³⁴ suggested that the

ITIES structure can be a representation of half a biological membrane, which by definition is formed by a phospholipid bilayer having the polar heads towards the aqueous intra- and extracellular solutions while the lipophilic chains form the inner layer of the membrane.³⁵ Years later, Gavach and co-workers³⁶ advanced the field when they exhibited that the ITIES can be polarized and that the resulting Galvani potential difference can be used to propel charge transfer reactions. This was followed by Koryta *et al.* when they expanded on the polarizability of the ITIES and proposed that the description of the transport across the ITIES is tantamount to that of the conventional redox processes observed on solid electrodes.²⁶ This allowed the use of many electrochemical methods in investigating reactions of charge transfer at the ITIES. Samec and his group devised a four-electrode cell to offset the ohmic drop that is usually observed and this enabled them to study the kinetics of charge transfer processes at the ITIES.³⁷

Overtime, the interest of examining molecules of biological importance at the ITIES continued to expand.¹⁸ Analytes range in size from small biomolecules like neurotransmitters dopamine,^{38,39} noradrenaline,⁴⁰ choline⁴¹ and acetylcholine^{42,43} as well as drugs like propranolol,⁴⁴ daunorubicin⁴⁵ and metoprolol,⁴⁶ to the biomacromolecules like the proteins insulin,⁴⁷ lysozyme⁴⁸ and haemoglobin,⁴⁹ carbohydrates like heparin,⁵⁰⁻⁵³ as well as DNA.⁵⁴⁻⁵⁶ In addition, the ITIES was also incorporated with other analytical techniques such as capillary electrophoresis (CE),^{57,58} scanning electrochemical microscopy (SECM),⁵⁹ ion chromatography⁶⁰ and flow injection analysis (FIA).^{61,62} Several other works involving ITIES concentrated on different facets of electrochemistry. These include catalysed oxygen reduction,^{63,64} hydrogen evolution by catalysis,⁶⁵⁻⁶⁷ photocurrent analysis⁶⁸ and nanoparticle assembly,⁶⁹⁻⁷¹ amongst others.

1.2.2 Structure of the ITIES

Probing into the interfacial structure formed at the ITIES, Verwey and Niessen⁷² postulated the first theoretical model of it, which is a modification on the Gouy-Chapman theory.⁵ According to them, the interface at the ITIES is described as “back-to-back” diffuse layers, one consisting of excess positive charge while the other has excess negative charge. Later, this was improved by Gavach *et al.*,⁷³ when they introduced the concept of a compact non-ionic layer of dipole molecules in a certain

orientation that separates the “back-to-back” diffuse layers, which is now called as the modified Verwey-Niessen (MVN) model.³⁷

Girault and Schiffrin⁷⁴ studied pure aqueous electrolytes as well as organic solvents and suggested that ions penetrate the interfacial region after the consideration that the excess water surface was less than one monolayer. This brought the conclusion that the interfacial layer can be thought of as a mixed solvent layer.^{74,75} A similar finding on the mixed solvent layer dividing the two diffuse layers was also reported by Samec and his group, which they furthered by suggesting that ions can move into the inner layer over a certain distance.⁷⁶ The scope of ion penetration into the layer was studied by Schiffrin *et al.* as a function of the ionic radii^{74,77} and then Schmickler added that the solubility of the two solvents affects the thickness of the mixed solvent.⁷⁸ A schematic illustration of the mixed solvent layer is shown in Figure 1.2.1

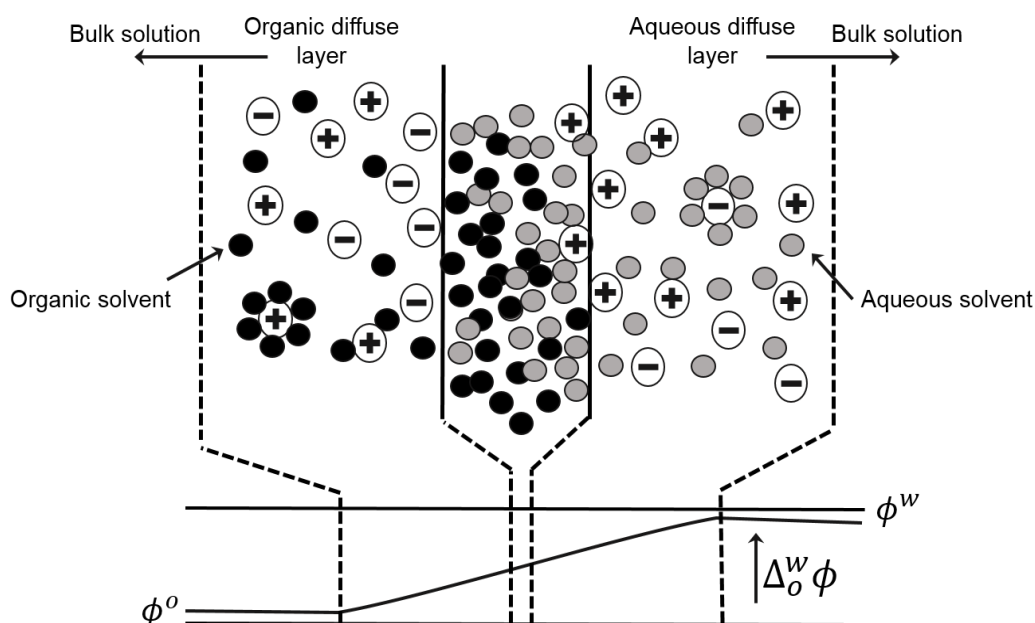


Figure 1.2.1 Illustration of the mixed solvent layer model representing the structure of the ITIES electrical double layer.

The advancement in technology also provided modern experimental means to study the characteristics of this liquid-liquid interface electrical double layer. Schlossman *et al.*⁷⁹ employed synchrotron x-ray reflectivity to examine the width of water-alkane interfaces and found that this evaluation of microscopic interfacial width depended on a method to “straighten” the liquid-liquid interface. Also, it was shown that the microscopic parameter is in concordance to macroscopic interfacial tension

measurements within the context of the capillary wave theory. The same group then utilized molecular dynamics (MD) simulations to estimate ion distributions⁸⁰ and gathered results that agree with their reflectivity studies. Also, the same group revealed the influence of the ion-ion coupling strength on ion distributions at the nanoscale.⁸¹ The combination of these experimental findings and theoretical simulations confirm the possibility to interpret the distribution within the vicinity of the charged interface at a molecular scope, which contrasted with what mean field theory predicted.⁸⁰ An interfacial thickness of 3.5 – 6 Å was measured by Mitrinovic and co-workers⁸² using x-ray reflectivity for water – alkane interfaces while Strutwolf *et al.*⁸³ reported a root mean square roughness of approximately 10 Å for water – dichloroethane interface via neutron reflection and scanning electrochemical microscopy (SECM). Although the interface is described to be molecularly sharp, molecular dynamic (MD) simulations carried out by Benjamin and colleagues⁸⁴ revealed that it has distortions from capillary waves, making the interface rough. Later on, the capillary wave theory included the non-linear polarization of the double layer.⁸⁵ This approach accounts for the influence of the capillary waves on the double layer capacitance. All these findings indicate that consideration should always be made for ion-solvent interactions as well as ion-ion correlations when trying to comprehend the complex interfacial structure as these influences structure and thickness of the ionic double layer.

1.2.3 General Theory of the Electrochemistry at the ITIES

Having two immiscible electrolyte solutions, in contact forms the ITIES. The charge carriers of these conducting liquids separate between two adjacent phases because of their difference in Galvani potential, $\Delta_o^w \phi$. The equilibrium Galvani potential difference is defined in the following equation:^{4,17}

$$\Delta_o^w \phi = \phi^w - \phi^o \quad \text{Equation 1.2.1}$$

where ϕ^w is the aqueous phase (*w*) potential and ϕ^o is that of the organic phase (*o*). Under equilibrium conditions, the electrochemical potential of an ion (*i*) at the ITIES is described as:

$$\bar{\mu}_i^w = \bar{\mu}_i^o \quad \text{Equation 1.2.2}$$

which shows the electrochemical potential of an ion, $\bar{\mu}_i$, in either the water (w) or organic (o) phase. Thermodynamically, the work needed to move a species (i) from a vacuum phase to a liquid phase (α) is known as:

$$\bar{\mu}_i^\alpha = \mu_i^\alpha + z_i F \phi^\alpha \quad \text{Equation 1.2.3}$$

where μ_i^α is the chemical potential of species (i) in phase (α) while z_i is its charge. The term $z_i F \phi^\alpha$ illustrates the electrical contribution in this equation for electrochemical potential. When the species is neutral ($z = 0$), the electrochemical potential equals the chemical potential which is defined as follows:

$$\mu_i^\alpha = \mu_i^{\alpha,0} + RT \ln \alpha_i^\alpha \quad \text{Equation 1.2.4}$$

where $\mu_i^{\alpha,0}$ is the standard chemical potential, α_i^α is the activity of the ion, which depends on solution composition, pressure and temperature. This activity can be represented in terms of concentration with γ_i^α being the activity coefficient, as shown:

$$\alpha_i^\alpha = \gamma_i^\alpha C_i^\alpha \quad \text{Equation 1.2.5}$$

Now, Equation 1.2.3 can be rewritten as:

$$\bar{\mu}_i^\alpha = \mu_i^{\alpha,0} + RT \ln \alpha_i^\alpha + z_i F \phi^\alpha \quad \text{Equation 1.2.6}$$

As mentioned earlier, thermodynamic equilibrium is achieved when the electrochemical potential of species i is equal in both phases (see Equation 1.2.2). Thus, equating Equation 1.2.6 into Equation 1.2.2 produces:

$$\mu_i^{w,0} + RT \ln \alpha_i^w + z_i F \phi^w = \mu_i^{o,0} + RT \ln \alpha_i^o + z_i F \phi^o \quad \text{Equation 1.2.7}$$

Then, re-arrangement of Equation 1.2.7 provides the equation for the Galvani potential difference, formed at the interface between the two phases:

$$\Delta_o^w \phi = \phi^w - \phi^o = \frac{\mu_i^{o,0} - \mu_i^{w,0}}{z_i F} + \frac{RT}{z_i F} \ln \left(\frac{\alpha_i^o}{\alpha_i^w} \right) \quad \text{Equation 1.2.8}$$

This difference in standard chemical potentials can be linked to the standard Gibbs energy of ion transfer, $\Delta G_{transfer,i}^{0,w \rightarrow o}$ which can be described in terms of a standard ion transfer potential, $\Delta_o^w \phi_i^o$ as revealed in the following equation:

$$\Delta_o^w \phi_i^o = \frac{\Delta G_{transfer,i}^{0,w \rightarrow o}}{z_i F} = \frac{\mu_i^{o,0} - \mu_i^{w,0}}{z_i F} \quad \text{Equation 1.2.9}$$

where $\mu_i^{\alpha,0}$ as the standard chemical potential of species i in phase α (can either be organic (o) or aqueous (w)), while z_i is the charge and F is Faraday's constant.

Combining Equation 1.2.8 with Equation 1.2.9, achieves the Nernst-type equation. This is an analogous equation to that at solid electrodes, in this case formulating the distribution of species at the interface. Thus, it is perceived as the Nernst equation for ion transfer at the ITIES.

$$\Delta_o^w \phi = \phi^w - \phi^o = \Delta_o^w \phi_i^o + \frac{RT}{z_i F} \ln \left(\frac{\alpha_i^o}{\alpha_i^w} \right) \quad \text{Equation 1.2.10}$$

When the interfacial potential is altered, $\Delta_o^w \phi_i^o$ remains constant as the ratio $(\alpha_i^o / \alpha_i^w)$ changes accordingly. This results to a movement of a portion of equilibrated ions across the interface thereby translating into an electrical current across the interface as well. Thus, current can be determined as a function of the applied potential and voltammograms are obtained by plotting measured current against the potential applied, like that of the solid electrode – electrolyte interface. Also, altering the activities of a common ion on either side of the interface can be a way to manipulate the potential difference at the liquid-liquid interface.

Equation 1.2.10 (the Nernst-type equation) could also be conveyed in terms of concentration and activity coefficients of species i . Combining Equation 1.2.5 into 1.2.10 results into:

$$\Delta_o^w \phi = \Delta_o^w \phi_i^o + \frac{RT}{z_i F} \ln \left(\frac{\gamma_i^o C_i^o}{\gamma_i^w C_i^w} \right) \quad \text{Equation 1.2.11}$$

Re-arranging Equation 1.2.11 via replacement of the standard Galvani transfer potential and activity coefficients with the formal Galvani transfer potential ($\Delta_o^w \phi_i^{o'}$) gives:

$$\Delta_o^w \phi_i^{o'} = \Delta_o^w \phi_i^o + \frac{RT}{z_i F} \ln \left(\frac{\gamma_i^o}{\gamma_i^w} \right) \quad \text{Equation 1.2.12}$$

Thereby, when expressed individually in terms of concentration of species i in either phase (w or o) results to:

$$\Delta_o^w \phi_i^o = \Delta_o^w \phi_i^{o'} + \frac{RT}{z_i F} \ln \left(\frac{C_i^o}{C_i^w} \right) \quad \text{Equation 1.2.13}$$

1.2.4 Polarizable and Non-polarizable ITIES

Like a solid electrode-electrolyte interface, one can differentiate between a polarizable and non-polarizable ITIES. Generally, polarisation of a liquid-liquid

interface is an ionic process, where one phase exhibits positive charge excess while a negative charge excess is observed on the other.⁸⁶ The interface itself serves as the working electrode and this is where processes of interest occur. The ability of the interface to be polarised relies on the electrolyte ions present in the two immiscible phases.

An ideal polarisable ITIES is observed when electrolyte ions in both phases have infinite Gibbs transfer energies, giving rise to no current flow despite an applied potential. However, the fact is no kind of such system exists since ions will have restricted solubility in any solvent and this is why electrolyte ions present dictate the polarisability of that system. A polarisable interface is observed when a highly hydrophilic electrolyte (A^+B^-) is present in the aqueous phase while a highly hydrophobic electrolyte (C^+D^-) is found on the organic phase. A schematic representation is shown in Figure 1.2.2. It is vital to note that the interface is polarised within a certain potential window and is dictated by the employed supporting electrolytes' formal ion transfer potentials.

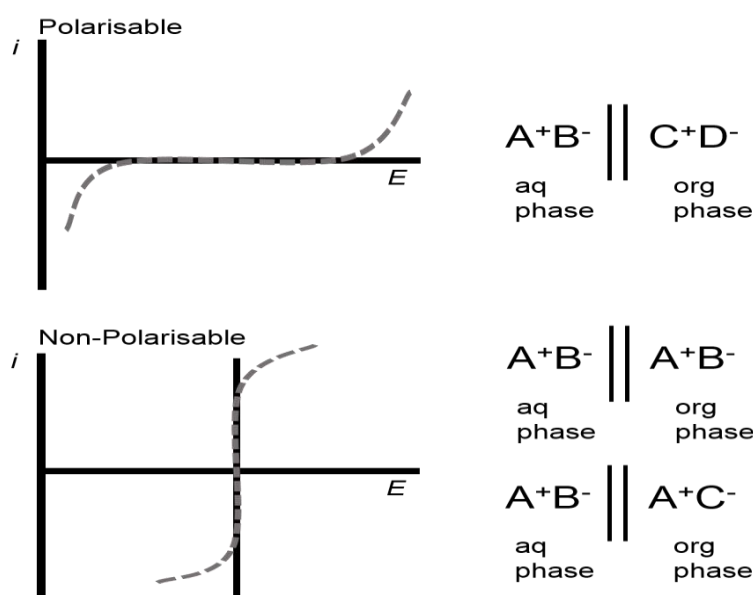


Figure 1.2.2 Schematic representation of an ITIES that is polarisable and non-polarisable. For the polarisable type, A^+B^- is very hydrophilic while C^+D^- is highly hydrophobic. For the non-polarisable type, (top) A^+B^- would be common ions in the two phases or (bottom) A^+ is a common ion while B^- is very hydrophilic and C^- is just amply hydrophobic.

On the other hand, a non-polarisable ITIES is observed in two forms. First is when a single binary electrolyte (A^+B^-) is common in the two phases. The Nernst

equation revealed earlier (see Equation 1.2.10) can be expressed for cation A^+ ($z_{A^+} = +1$) and the anion B^- ($z_{B^-} = -1$) as follows:

$$\Delta_o^w \phi = \Delta_o^w \phi_{A^+}^o + \frac{RT}{z_i F} \ln \left(\frac{\alpha_{A^+}^o}{\alpha_{A^+}^w} \right) \quad \text{Equation 1.2.14}$$

$$\Delta_o^w \phi = \Delta_o^w \phi_{B^-}^o + \frac{RT}{z_i F} \ln \left(\frac{\alpha_{B^-}^o}{\alpha_{B^-}^w} \right) \quad \text{Equation 1.2.15}$$

In this case, there would be a distribution potential initiated across the interface because the solubility of A^+ is different in both phases and this is not affected by the concentration. So, the Nernst equation can be re-written to consider the activity coefficients instead as depicted below:

$$\Delta_o^w \phi = \frac{\Delta_o^w \phi_{A^+}^{o'} + \Delta_o^w \phi_{B^-}^{o'}}{2} + \frac{RT}{2F} \ln \left(\frac{\gamma_{A^+}^o \gamma_{B^-}^o}{\gamma_{A^+}^w \gamma_{B^-}^w} \right) \quad \text{Equation 1.2.16}$$

In the second form, a common ion (A^+) is present in the two phases while B^- is very hydrophilic and C^- is just amply hydrophobic. These two ions remain respectively in the aqueous and organic phase. Consequently, the Galvani potential difference across the interface is controlled by the distribution of the A^+ ions only and the previous equation simplifies into:

$$\Delta_o^w \phi = \Delta_o^w \phi_{A^+}^o + \frac{RT}{F} \ln \left(\frac{\alpha_{A^+}^o}{\alpha_{A^+}^w} \right) \quad \text{Equation 1.2.17}$$

1.2.5 Potential Window for the ITIES

As mentioned previously, the working potential window at the ITIES is dictated by the formal ion transfer potentials of the electrolytes present, so to better demonstrate the generation of the electrochemical signal at the ITIES in creating a polarisable interface, cyclic voltammetry (CV) data acquired using 10 mM lithium chloride (LiCl) as the aqueous electrolyte and 10 mM bis(triphenylphosphoranylidene)ammonium tetrakis(4-chlorophenyl)borate (BTPPATPBCl) as the organic electrolyte is shown in Figure 1.2.3. The aqueous phase used was MilliQ water while the organic phase was 1,6-dichlorohexane (1,6-DCH). In cyclic voltammetry, the applied potential is scanned forward and back within two potential limits and results in the production of measurable current. Typically, the

voltage applied is scanned from a low starting potential to a more positive value on the forward scan and then back to the starting potential. As a common agreement, it is understood that positive currents are formed on the forward scan just as the applied voltage is positive (seen as the right side of the graph) and this indicates cations moving from the aqueous phase towards the organic phase and/or the transfer of anions from the organic towards the aqueous phase. Whereas a negative current on the reverse scan depicts the back transfer of cations from the organic to the aqueous phase and/or the transfer of the anions from the aqueous to the organic phase.

Illustrated in Figure 1.2.3 is a typical CV of a cell having only the background electrolytes. It is divided into three regions as indicated by the dashed lines surrounding that region. At the start, a lower positive potential is applied (from 0.05 to 0.2 V) and this transfers the organic cation (BTPPA⁺) from the organic phase towards the aqueous phase while the aqueous anion (Cl⁻) moves into the organic phase simultaneously. Scanning into a more positive potential (from 0.25 to 0.75 V) gives no transfer of any background electrolytes and this region is known as the polarisation region or the potential window. Then, moving into a more positive potential region (from 0.8 to 1.0 V) reveals the transfer of the aqueous cation (Li⁺) from the aqueous phase into the organic phase as well as the organic anion (TPBCl⁻) moving from the organic phase into the aqueous. As a result, a positive rise in the current is seen on the voltammogram (right side of the graph).

Upon switching the potential and scanning in the reverse direction, the ions previously transferred will transfer back. From 1.0 to 0.8 V, Li⁺ and TPBCl⁻ ions move back into aqueous and organic phases respectively. Scanning into the polarisation region again (from 0.75 to 0.25 V) shows only current registered because of non-faradaic processes. Then, at the next region (from 0.2 to 0.05 V) reveals BTPPA⁺ and Cl⁻ transferring back into the organic and aqueous phases respectively. Thus, it is clear that the potential window is constrained by the transfer of the chosen hydrophilic cation/hydrophobic anion at the positive potential region and by the hydrophilic anion/hydrophobic cation at the negative potential region. The polarisation region is where detection of analytes happens at the ITIES and ideally, the transfer potential of such analyte should fall within that region. Thus, it is desirable to have a broad operating potential window and this can be realized with careful selection of electrolytes to be dissolved in the aqueous and organic phases.⁸⁷

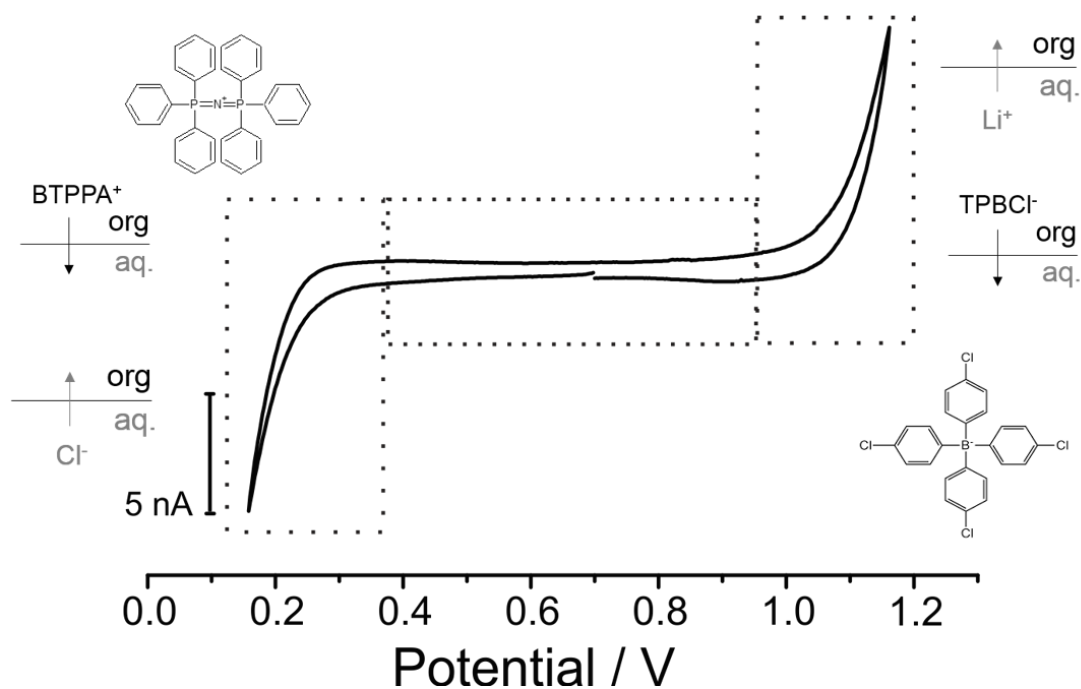


Figure 1.2.3 Cyclic voltammogram of 10 mM LiCl in the aqueous phase and 10 mM BTPPATPBCl in the gellified organic phase (10 % w/v low molecular weight poly(vinyl) chloride (PVC)/1,6-dichlorohexane) using a 30 micropore array silicon membrane. Scan rate of 5 mVs⁻¹

1.2.6 Forms of Charge Transfer at the ITIES

Unlike most electrode-electrolyte electrochemistry that mostly deals with electron transfer (ET), electrochemistry at the liquid-liquid interface can involve different forms of charge transfer (CT). First, ion transfer (IT), being the simplest, involves the movement of ions across the interface before the concentration ratio is reached as defined by the Nernst equation. Remember that this transfer is brought about by the application of an external potential difference across the interface. The ion transfers across the ITIES when the applied potential difference surpasses the Gibbs energy of transfer for that ion.¹⁷ This then can be measured if the required potential is in the working potential window.

Second, facilitated/assisted ion transfer (FIT)¹⁷ is a modified version of IT. This involves the incorporation of a ligand or ionophore in the other phase which is available to interact with the ion to form a complex.⁸⁸ The added reagent lowers the transfer energy needed for the ion as well as take it within the working potential window. FIT can be further classified as a) transfer via interfacial complexation (TIC), b) transfer via interfacial dissociation (TID), c) aqueous complexation followed by transfer (ACT) and d) transfer to the organic phase followed by complexation (TOC).

These ion transfers are categorized on complexation mechanism as well as the charge transfer between the ion and the ionophores. Third, which is more complex than the other two, ET occurs between redox species in each phase. Then, at equilibrium, Equation 1.2.18 is observed:



For such case, the Nernst equation can be re-written as:

$$\Delta_o^w \phi = \Delta_o^w \phi_{ET}^o + \frac{RT}{F} \ln \left(\frac{\alpha_{R_1}^w \alpha_{O_2}^o}{\alpha_{O_1}^w \alpha_{R_2}^o} \right) \quad \text{Equation 1.2.19}$$

The difficulty here is in choosing the redox couples that can thrive within the potential window and whose redox products, ideally, should not transfer across the ITIES because this could possibly mask the currents produced by the actual electron transfer process.³⁷ A summary representation of these charge transfer processes is exemplified in Figure 1.2.4

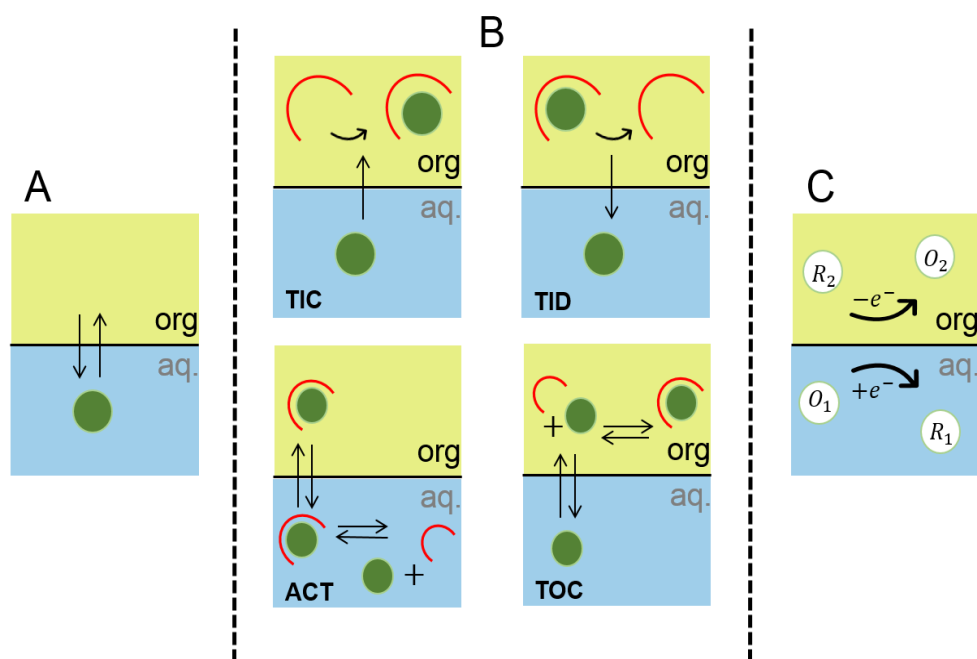


Figure 1.2.4 Schematic illustration of the types of charge transfer phenomena. (A) Simple ion transfer (IT), (B) Facilitated/assisted ion transfer (FIT), (C) Electron transfer (ET).

1.3 Micro-ITIES

1.3.1 Advantages of ITIES miniaturization

Similar to the advancement of solid-liquid electrochemistry upon the introduction of ultramicroelectrodes (UME) as well as nano-electrodes, miniaturization of the interface between two immiscible electrolyte solutions opens several advantages. Obviously, smaller interfaces impart lower currents and consequently reduce iR or Ohmic potential drop, which is due to the resistive organic phase.² In the electrochemical cell for ITIES, R_s is the resistance of the solution. In most experiments, observing the applied potential between the working electrode and the reference electrode, a voltage drop, tantamount to the iR_s , is recorded and is described by Ohm's Law as displayed in Equation 1.3.1. Recalling Ohm's Law, current (i) that goes through two points in a conductor is proportional to the potential difference (V) among those two points and resistance (R) is the proportionality constant.

$$i = \frac{V}{R} \quad \text{Equation 1.3.1}$$

Likewise, the greater contribution of the R_s in the ITIES would be that of the hydrophobic organic phase, which usually involves an organic solvent having low permittivity values, versus the aqueous phase that offers a better capacity to carry current. In a reduced surface area, R_s is of small value, the voltage drop (iR_s) is also low (*ca.* 1-2 mV), then a two-electrode cell can be utilized.² Moreover, other advantages of downsizing the interface size includes an increase in the mass transport flux due to the smaller surface area, portability, lower cost as well as integration into compatible techniques.^{89,90}

As defined, microelectrodes should have at least one dimension that is less than 50 μm , which is known as the critical dimension, and is smaller than the thickness of the diffusion layer. This generates steady state voltammetry due to radial diffusion at the interface.^{21,91} The first reported micrometre sized ITIES was by Taylor and Girault²⁰ when they showed the use of glass pipette tips to hold the organic electrolyte and upon immersing into the aqueous phase, produced a radial diffusion type of

response for a simple ion, which is similar to that observed at a solid-state microelectrode.⁹¹

This then led to several explorations with the aim to further develop the micro-ITIES. Shao and colleagues²¹ discovered asymmetric diffusion schemes at the micro-ITIES – spherical for transfer of ions into the micropipette while linear for the opposite direction. Beattie *et al.*⁹² introduced an advanced pipette puller with borosilicate glass or quartz materials that provided hydrophilic properties ensuring only the aqueous phase is inside the micropipette. In contrast, Shao and Mirkin⁹³ reversed that process by using silanization of the glass pipette tips, producing hydrophobic conditions. However, single or dual microITIES, despite overcoming the Ohmic drop issue, still faced the problem of low current levels, which is not desired for some applications. This directed the field into the development of microarrays (microholes or micropores).^{94,95} Different materials have been explored like silicon wafers,^{96,97} silicon nitride,⁹⁸ polymers⁹⁵ and glass.^{90,99}

From the micrometre scale, research has then eventually ventured into the nanometre size. Investigations on nano-ITIES supported by glass pipettes were introduced.^{29,100} This was followed by reports on fabrication of nano-ITIES arrays utilizing track etched membranes,^{94,101} alumina membranes,¹⁰² and silicon nitride membranes.^{32,98,103,104} As more studies are being done to further this field, several reviews have been published to highlight achievements so far.^{105,106}

1.3.2 Gellification of the miniaturized ITIES

One problem when investigating the interface between two immiscible electrolyte solutions is its mechanical instability. Aiming to answer this problem, Senda *et al.*¹⁰⁷ initiated the gellification of the organic phase. However, at regular-sized ITIES, gellification also gives rise in some unwanted increase in the system resistance but miniaturization of the ITIES surpasses the issue and has been continuously used. A common gellifying agent for the organic phase is low molecular weight PVC. Studies reported include the use of PVC-nitrobenzene (NB),¹⁰⁸ PVC-nitrophenyl octyl ether (NPOE),¹⁰⁹ PVC-1,2-dichloroethane (DCE)¹¹⁰ and PVC-1,6-dichlorohexane (DCH). However, research has also been reported where the aqueous phase was gellified using agarose¹¹¹ and exposing it to freezing conditions.¹¹²

1.3.3 Effect of Interface Arrangement

As discussed in the previous section, the interface size plays a vital role on the electrochemical signal observed at the ITIES. For the solid-liquid electrochemistry, a difference in the voltammetric response would be observed depending on the surface feature of the disc electrode and the common ones include recessed disc,¹¹³ inlaid disc,¹¹⁴ and the hemispherical. Illustrations of these are displayed in Figure 1.3.1.

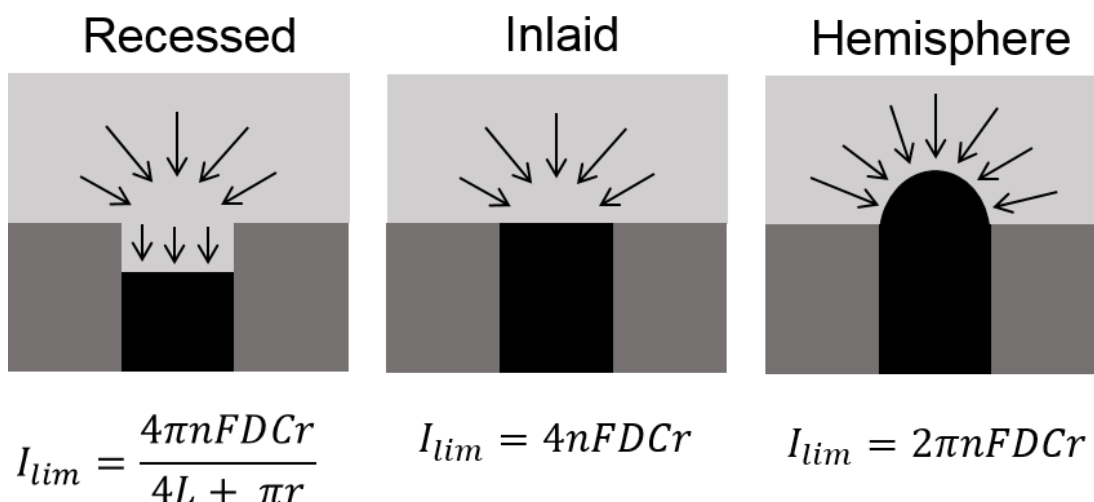


Figure 1.3.1 Different geometries of a disc electrode with corresponding diffusion modes associated with it. The limiting current equation for each geometry is also shown. I_{lim} is the limiting current, n refers to number of electrons, F is Faraday's constant, D as the diffusion coefficient, C refers to the concentration, r is the radius of the electrode and L refers to the recessed depth when applicable.

Expectedly, soft polarized interfaces produced amongst micropores behave like a microdisc and the same equations (as presented in Figure 1.3.1) for the limiting current can be utilized especially for characterization. For the micro-ITIES, n becomes the overall charge of the ion being studied when applicable. In this study, microporous membranes were used for the experiments at the ITIES. Generally, electrochemical characterization of such micro-arrays by simple ion transfer reveals that the organic phase fills the pores and forms an inlaid disc arrangement. This is indicated by a radial diffusion as the ion is moved from the aqueous into the organic phase while a planar or linear diffusion as the ion moves back into the aqueous phase.⁹⁷ Displayed in Figure 1.3.2 are schematic representations of such diffusion profiles for an inlaid disc microinterface showing a single micropore filled with the organic phase.

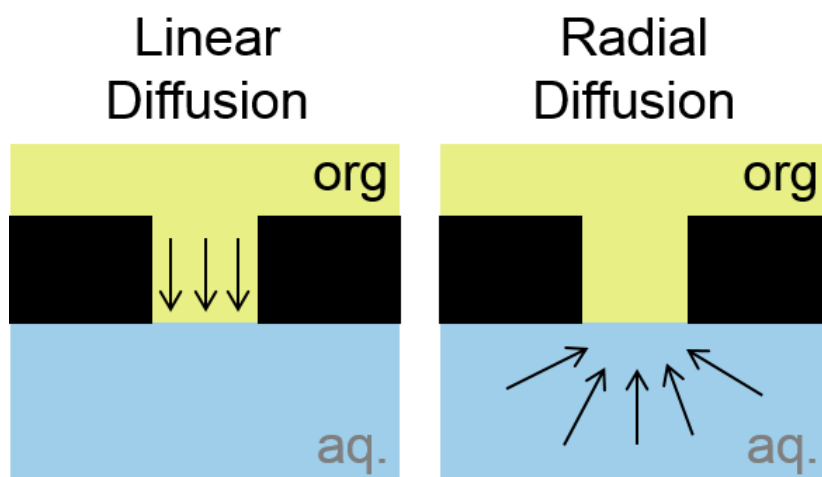


Figure 1.3.2 Illustration of a single, filled microinterface showing different diffusion profiles. *Left:* Linear or Planar diffusion demonstrating movement of simple ion from organic to aqueous phase. *Right:* Radial diffusion showing transfer of simple ion from aqueous into the organic phase.

Given that each electrode in an array works at a similar potential, the overall electrochemical signal relies on the dimensions of the microelectrode as well as the electrode distribution density.⁹¹ For example, when interfaces in an array are too near to each other, a possible overlap of diffusion zones can result and decrease the measured current. Aside from the geometry, other factors that impact diffusion characteristics in an array of micropores include pore centre-to-centre separation, actual pore dimensions (depth and radius of pore), diffusion coefficient of analyte as well as other experimental parameters like time scale.⁹⁷

For an ideal voltammetric response, center-to-center separation in microinterfaces, just like in microdisc electrode arrays, demands to be in a distance enough to evade overlapping of diffusion zones. Experimental¹¹⁵ and theoretical¹¹⁶ distance values for a cubic, hexagonal, and random arrangement for microelectrode arrays were published by Davies *et al.* For this thesis, a hexagonal arrangement is utilized as it provides minimal overlapping of diffusion zones.⁹⁷ Figure 1.3.3 shows a representation of a cubic and a hexagonal arrangement for microdisc arrays.

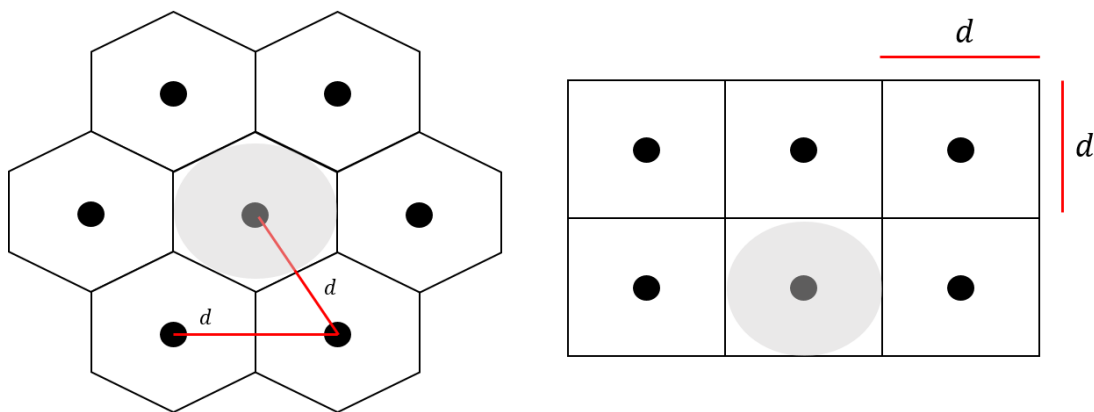


Figure 1.3.3 Representation of a cubic (left) and hexagonal (right) arrangement of microdisc arrays. d refers to the distance amongst pores while r is the pore radius. The greyed part depicts a diffusion zone for a single microelectrode.

Thus, it is vital to ensure sufficient distance between micropores is observed when designing arrays so that independence of individual diffusion zones is maintained for optimal signal. In terms of diffusion profiles at the microinterfaces, Figure 1.3.4 details various forms observed. First, (A) shows that of a radial diffusion created by ion transfer from aqueous phase to organic, then (B) displays the overlapping of diffusion zones, also known as shielding effect. Next is (C) which represents that of a linear diffusion as the ion moves from organic to the aqueous phase and (D) reveals that case when overlapping is so extensive that it results in an overall linear diffusion from the organic phase to the aqueous.⁹⁷

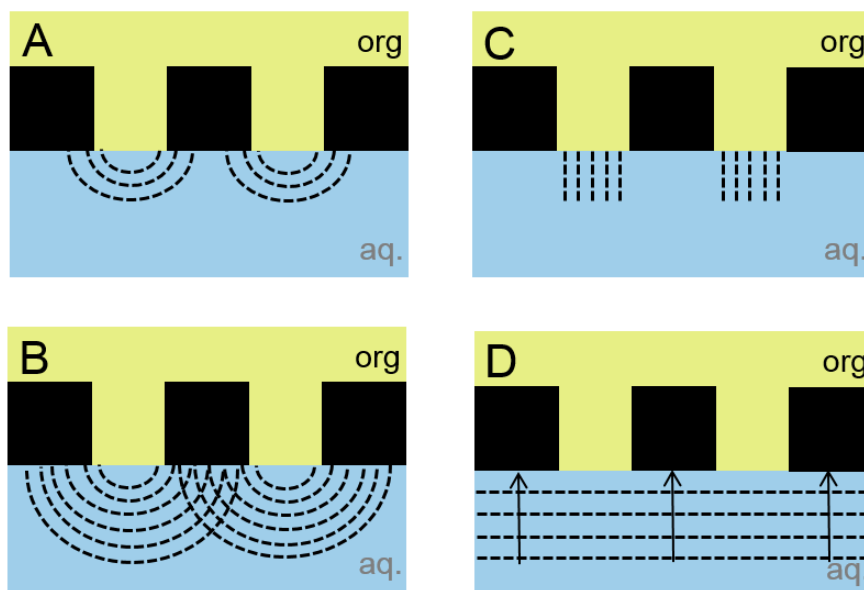


Figure 1.3.4 Representation of diffusion profiles at the microinterface: (A) radial diffusion from aqueous to organic; (B) diffusion overlap (shielding effect); (C) linear diffusion from organic to aqueous and (D) extensive diffusion overlap inducing a linear diffusion from organic to aqueous phase.

A number of studies were done to find that optimal distance in between micropores or microdiscs to avoid overlapping of single diffusion layers. Saito¹¹⁷ investigated this overlapping of diffusion zones at a microdisc electrode. Based on the findings and the assumption that only steady-state response is observed at microelectrodes and that it is independent of sweep rates, he proposed an expression shown in Equation 1.3.2. This expression reveals that shielding happens when the microdisc centre-to-centre distance (d) is lower than 12 times the electrode radius (r).

$$d > 12r \quad \text{Equation 1.3.2}$$

This was modified by research done by Alfred and Oldham¹¹⁸ as well as Fletcher and Horne¹¹⁹ using their approximation and suggested the following equation instead:

$$d \geq 20r \quad \text{Equation 1.3.3}$$

Another related work was done by Davies and Compton¹¹⁶ where they postulated a way to estimate the diffusion zone at microelectrode arrays. This equation is shown below:

$$\delta > \sqrt{2D_i \frac{\Delta(\Delta_{\beta}^{\alpha}\phi)}{v}} \quad \text{Equation 1.3.4}$$

where δ is the diffusion zone, D is the diffusion coefficient of the species i , v is the sweep rate and $\Delta (\Delta_{\beta}^{\alpha} \phi)$ refers to the potential range from the current (faradaic) onset up to the steady-state current or when a peak is observed. This equation reveals the dependence of how the diffusion zone expands relative to the time given according to the scan rate and is independent of the individual pore radius in contrast to the previous equations (Equation 1.3.2 and 1.3.3). This is because Equation 1.3.4 was derived with the assumption that diffusion is one-dimensional.

In terms of the time scale, the microinterface will observe non-linear diffusion if the diffusion zone is less than half of the pore centre-to-centre separation (r_c ; $\delta < 0.5r_c$). The overall voltammetric response is determined by multiplying the single interface response with the total number of interfaces in the array design. However, when $\delta > 0.5r_c$, diffusion zones overlap and linear diffusion is observed. This is because neighbouring pores exhaust a similar region in the solution producing a decreased flux to a single pore/interface as compared to a well-distanced pore/interface.^{97,116} All the prior equations and assumptions are acceptable when $r > 1\mu\text{m}$, and can be easily applied to micro-ITIES experiments as outlined in this thesis. Although, as researchers move into smaller interfaces like nano-ITIES, the challenge is using these equations and the assumptions would not be suitable since $r < 1\mu\text{m}$.¹¹⁶

A previous investigation on silicon micropore arrays detailed the effect of varying the pore arrangement and pore size. Strutwolf and co-workers⁹⁷ reported the agreement of their experimental values using aqueous-gelled 1,6-DCH microinterfaces with their simulation values using COMSOL. These results provided a way to pinpoint the interface within the pores and an insight into the possible overlapping of diffusion zones in the membrane array. A number of the designs showed diffusion zone overlap when Equation 1.3.1 was not satisfied while some designs exhibited diffusion overlap that generated a peak-shape response when Equation 1.3.3 was unfulfilled.

For this thesis, two designs of micropore arrays were utilized. One was made up of 8 micropores, having a radius of *ca.* 11 μm with a pore centre-to-pore centre distance of 400 μm , while the other was composed of 30 micropores having a *ca.* 11.2 μm radius, with a pore centre-to-pore centre distance of 200 μm . Both designs have a 100 μm depth and both types of micropore arrays were in a hexagonal arrangement that satisfies Equations 1.3.1 as well as 1.3.2 as $d \geq 20r$.

1.4 Electroanalysis of Biological Molecules at the ITIES

One of the earliest work on the electroanalysis of biologically important molecules at the interface between two immiscible electrolyte solutions was by Vanysek *et al.*¹²⁰ when they reported the adsorption of proteins bovine serum albumin (BSA), colicine E₃ and ovalbumin that affected Cs⁺ transfer across an aqueous-nitrobenzene interface. In this case, the proteins were indirectly observed because the working potential window for the simple ion was shortened in the presence of such proteins. The same group extended the study by focusing mostly on BSA with impedance, voltammetric and capacitance techniques and found that the protein bulk concentration affects the adsorbed monolayer and then influenced the ion distribution at the interface.¹²¹ Numerous studies then followed involving a range of discoveries about the behaviour and detection of biological and bioactive molecules.

Small molecules that play a role in biological processes have been investigated. Ohde *et al.*¹²² studied redox reactions between nicotinamide adenine dinucleotide (NADH) and quinone derivatives, a process vital for energy collection in mitochondria, via a liquid-liquid interface. The mechanistic aspects related to the oxidation of L-ascorbic acid was studied at a water/1,2-DCE interface¹²³ by Osakai and group. Another group of small biomolecules that are of interest at the ITIES is neurotransmitters. Dopamine is one common example and has been detected at the ITIES via a facilitated transfer via incorporation of an ionophore, dibenzo-18-crown-6 (DB18C6)³⁸. Beni and colleagues¹²⁴ studied the effect of interfering species (e.g. ascorbate) on the detection of dopamine with DB18C6 in the organic phase. Background-subtracted differential pulse voltammetry (DPV) afforded a detection limit of 2 μM dopamine for their study. A lower detection limit of 0.5 μM for dopamine was achieved by using microinterfaces.³⁹ Pereira *et al.*⁴⁰ employed DB18C6 at an aqueous/1,6-DCH interface to probe the behaviour of noradrenaline, another dopamine-related neurotransmitter, at low millimolar concentrations. In addition, choline and acetylcholine were also studied in different ITIES arrangements like a hanging electrolyte drop format⁴² that afforded *ca.* 2.7 μM lowest detected concentration, and then a μITIES formed at the mouth of a glass pipette¹²⁵ as well as a microhole array in a polymer film with a gelled-NPOE as the organic phase that achieved a detection limit of 5 μM for choline.^{95,126} In a more recent work by Ortuño and colleagues¹²⁷ 2-phenylethylamine (PEA) was investigated based on its protonated

form transfer facilitated by DB18C6 via square wave voltammetry (SWV), chronoamperometry (CA) and chronocoulometry (CC).

Amino acids and simple peptides were studied as model molecules for their larger counterparts. Among the earlier reports were by Chen *et al.*¹²⁸ who used DB18C6 to assist the transfer of amino acids across micro- and nano-ITIES. Other studies reported cationic or anionic simple peptides^{129,130} and found that the overall lipophilicity of the peptide depends on the composing amino acids and its position on the peptide chain. Scanlon and co-workers reported the detection of a range of di-, tri-, and tetrapeptides at a gelled microITIES array formed at microporous silicon membrane.⁹⁶

The study of ionizable drug molecules at the ITIES has also been a rising interest in pharmacokinetics studies.¹⁸ Heading this kind of studies, Bouchard and group reported the effect of aqueous pH on the behaviour of several zwitterionic drug molecules¹³¹ at an aqueous/1,2-DCE system. Ortuno *et al.* incorporated the ITIES into a flow injection analysis system to detect a range of cationic drugs.¹³² The combination of stripping voltammetry and microITIES afforded a detection limit of 20 nM propranolol in synthetic saliva¹³³ and 50 nM in the presence of serum albumen⁴⁴ as reported by Collins *et al.* In more recent years, the use of a rotating liquid-liquid interface allowed the detection of warfarin with propranolol¹³⁴ and chiral discrimination for propranolol was achieved via interaction with α 1-acid-glycoprotein.¹³⁵ It was found that S-propranolol binds more to the glycoprotein than its R enantiomer. The type of drugs being investigated at the ITIES have expanded to include anthracycline derivatives like daunorubicin,⁴⁵ and doxorubicin¹³⁶ as well as anti-hypertensive drugs such as metoprolol.⁴⁶

After discovering the use of the ITIES to investigate the smaller biomolecules, the interest expectedly included larger biomolecules. Carbohydrates have been in that spotlight especially heparin, a known anti-coagulant that interacts with antithrombin III. The detection of heparin at a polarized aqueous-organic interface was first published by Samec and members.¹³⁷ They utilized poly(vinyl) chloride (PVC) – 1,6-dichlorohexane membranes based on earlier studies by Meyerhoff *et al.*^{138,139} using equilibrium potentiometry with ion selective electrodes (ISE). The same group of Langmaier^{140,141} furthered the research by using different

solvents and electrolytes in the membrane phase. They discovered that the optimal composition for heparin detection involved the cation tridodecylmethylammonium (TDMA⁺), that produced a detection limit of 0.2 units per millilitre even in human blood plasma. Amemiya and co-workers⁵⁰ used 1,2-dichloroethane and discovered that complexation and interfacial adsorption was vital for the detection of heparin concentrations down to 0.012 units per millilitre in buffered electrolyte and 0.13 units per millilitre in sheep blood plasma. Rodgers *et al.*¹⁴² expanded the research with a heparin mimetic, *Arixtra* using micropipette interfaces. The ionophore used affected the transfer potential and rate constant of the heparin mimetic. A more recent publication reported the employment of room temperature ionic liquids (RTILs) to advance heparin extraction.⁵³

Aside from heparin, which is a sulfated polysaccharide and can be also classified as a polyelectrolyte, other polyelectrolytes were also the interest of several studies at the ITIES. Yudi *et al.*¹⁴³ investigated a number of polyelectrolytes at a polarized aqueous-1,2-dichloroethane interface and discovered relationships between polyelectrolyte structure and their propensity to adsorb at the polarized interfaces. The interaction of chitosan with anions in the aqueous phase was examined by Riva and co-workers¹⁴⁴ and found that a higher negative charge of the anion leads to more electrostatic interactions with cationic polyelectrolytes.

Electrochemistry at the ITIES is also used for modelling cell membranes. Mendez *et al.*¹⁴⁵ studied the formation of a lipid monolayer at the aqueous/1,2-dichloroethane interface. This set-up was then utilized to examine a cell membrane peptide, melittin, which was perceived to undergo adsorption at the interfaces thereby damaging the phospholipid layer.¹⁴⁶ A study by Lillie and colleagues²³ evaluated the charge transfer properties of a 1,1-dimethylferrocene (DMFcP₂)-mediated cytochrome C at the polarized interfaces. It was detailed that the CV response was due to the oxidised protein undergoing a heterogeneous electron transfer with the mediator (DMFcP₂) resembling charge transfer processes that occur *in vivo*, similar to biological membranes.

Ultimately, the ITIES was then exploited to examine biomacromolecules. Since the first report by Vanysek *et al.* in 1984,¹²⁰ numerous advances have been made in probing large proteins at the ITIES. The first published electrochemically induced

movement of protein across the ITIES was by the group of Karyakin¹⁴⁷. The protein, α -chymotrypsin, was non-redox active but when made soluble in reversed micelles at the organic phase, an increase in current was recorded that is associated to the transfer of cations from the aqueous phase to the formed reverse micelles. Amemiya and co-workers¹⁴⁸ studied the electrochemical behaviour of protamine, an arginine-rich protein giving it a highly positive charge, at the polarized interface. The same group improved on that study by examining the effect of adding anionic surfactants such as dinonylnaphthalenesulfonate (DNNS) as well as various organic electrolytes.¹⁴⁹ The proposed mechanism was that DNNS adsorbs at the interface and then forms a complex with the charged protamine after which the complex is transported into the organic phase. Succeeding this, Vagin *et al.*¹⁴⁷ characterized the impact of various surfactants in the organic phase with proteins like α -chymotrypsin, lysozyme, and soybean trypsin inhibitor. When neutral surfactants polyoxyethylen(4)-lauryl ether (Brij-30) and polyoxyethylen(2)-cetyl ether (Brij-52) were present, no protein-surfactant interaction was observed yet micelles formation was noted when bis(2-ethylhexyl) sulfosuccinate (AOT) and cetyltrimethylammonium bromide (CTAB) were utilized. A similar observation was reported by Shinshi and colleagues when AOT was added into the organic phase of an aqueous-1,2-dichloroethane interface in the presence of cytochrome C, ribonuclease, and protamines.¹⁵⁰ Additional work about protamines at the ITIES was conducted by Trojanek and colleagues¹⁵¹ by applying cyclic voltammetry, conductometry and quasi-elastic light scattering (QELS). The study confirmed that ion pairing between protamine and the organic anion supports the facilitated transfer of protamine into the organic phase.

More recent work involving protein-surfactant interaction was published by O'Sullivan *et al.*^{152,153} involving the complex formed between cytochrome C, haemoglobin, and myoglobin with AOT. The signal was known to be increased by 17-folds in terms of the interfacial coverage. This protein-surfactant interaction was also employed in a flow cell to detect albumin in a synthetic urine environment. Matsui and co-workers¹⁵⁴ used DNNS and was able to attain a detection limit of 1.2 μM .

The use of the electrochemistry at the ITIES continued to expand as the years progressed. Herzog *et al.*¹⁵⁵ applied the technique in analysing protein digests with enzymes at the micro-ITIES. Findings indicate that proteins gave unique responses after digestion and the enzyme preference influenced the response of the digested

protein. Following that, the same group investigated the effect of the protein tertiary structure with its electroactivity at the ITIES.⁴⁹ With haemoglobin as the model analyte, the research suggested that denaturation of the protein diminished its electrochemistry response. More work was done in probing protein structures at the polarized soft interfaces. Using synchrotron radiation circular dichroism spectroscopy (SRCD), dual polarisation interferometry (DPI) and front-face tryptophan fluorescence spectroscopy (FFTFS), Zhai and colleagues¹⁵⁶ revealed that a new non-native secondary structure is present after the hydrophobic core becomes unfolded. The interaction between hydrophobic regions of the protein and the hydrophobic electrolyte was pointed as the mechanism for its detection and this agreed with a previous study for facilitated ion transfer mechanism for a protein at the ITIES.¹⁵⁷ A different aspect of probing adsorbed proteins at the ITIES was reported by Jensen *et al.* when they investigated the formation of dielectric layers and charge regulation¹⁵⁸. The main result of the study was a model to assess the net charge of an adsorbed protein and compare it with that of the bulk solution.

With the aim to lower the detection limit of proteins to a level of biochemical relevance, Alvarez and colleagues employed an adsorptive stripping approach¹⁵⁹ at a polarized soft interface and attained limits of detection at *ca.* 30 nM. The approach utilized a pre-concentration step by application of an optimized adsorption potential for lysozyme. In a more recent work, Alvarez *et al.*¹⁶⁰ have shown that cytochrome C oligomer formation can be induced at an aqueous-gelled organic interface after an electroadsorption step. This opened another avenue for the use of the electrochemistry of the ITIES for protein investigation.

As can be deduced from the literature presented so far, several parameters like the aqueous/organic electrolytes, organic phase solvent, interface dimensions, presence of ionophores/surfactants and the electrochemical technique employed greatly influence the behaviour of the biomolecule at the liquid-liquid interface. In addition, the charge on the biomolecule, size and hydrophobic components dictate its Gibbs energy of transfer. A highlight on the organic solvent was also seen as studies move from the traditional higher dielectric constant nitrobenzene ($\epsilon = 34.8$),¹⁶¹ to the more common solvents 1,2-dichloroethane ($\epsilon = 10.45$), 1,6-dichlorohexane ($\epsilon = 8.83$) and gelled-1,6-dichlorohexane aiming to boost the hydrophobicity of the organic solvent thereby widening the working potential window. The choice of the ionophore

or the organic electrolyte, since it influences the behaviour of the biomolecule at the polarized soft interfaces, is mechanistically crucial as it may form a complex with the biomolecule and that can be further studied in order to fully comprehend the biomolecule's behaviour.

It is also important to consider complimentary techniques for the ITIES. One example was reported by Mendez *et al.*¹⁴⁵ that employed a biphasic electrospray ionisation mass spectrometry (BESI-MS). Results reveal the strong interactions between the protein and organic electrolyte once a chemically-imposed potential difference was applied. This has been used to illustrate complexes of proteins at various charge states like DPPC-angiotensin III,¹⁴⁵ DPPC-mellitin,¹⁴⁶ and lysozyme-TPBCl or TPFB.¹⁶² With the clamour to improve sensitivity and selectivity at the polarised soft interfaces as well as across the electrochemistry field, more integrations of techniques or methodologies are possible and this has been one of the aims of the thesis.

1.5 Aims of this Work

The general aim of this work is to expand the exploration of the electrochemical characteristics of biomolecules at the interface between two immiscible electrolyte solutions. The advancement of this information may add to the knowledge in developing technologies for biosensing. There are two major themes in this thesis: 1) Examination of methods to enhance sensitivity and selectivity of biomolecular detection via electrochemistry at polarized liquid-liquid interfaces, and 2) Investigation of the electrochemical behaviour of biologically important molecules at the interface between two immiscible electrolyte solutions.

Probing the use of solvent-casting as an alternative way of organic phase gellification process was analysed and is discussed in Chapter 3. In contrast to the usual method that involves heat-treatment to dissolve the gellifying agent – PVC - tetrahydrofuran (THF) was utilized and allowed to evaporate over time. The efficiency of this method was tested by lysozyme detection at these liquid-organogel interfaces.

In expanding the application of the electrochemistry at the ITIES for carbohydrate detection, fucoidan – a sulfated polysaccharide derived mostly from brown seaweeds - was studied and is reported in Chapter 4. A similar behaviour to

heparin, another sulfated polysaccharide, was observed using CV and AdSV. Detection in a synthetic urine sample was also tested.

After discovering the electrochemical behaviour of fucoidan, the focus of the study then moved into probing smaller carbohydrates – sulfated disaccharides - to explore their electrochemical behaviour at the polarized soft interfaces. These analytes were studied in almost similar conditions to the fucoidans using CV and AdSV as well as detection in a complex matrix (synthetic urine). Results are detailed in Chapter 5. In addition, infrared spectroscopic analysis of these electrochemically adsorbed biomolecules (sulfated disaccharides and proteins) were also performed and is also discussed in Chapter 5.

As an extension of the previous biomolecules studied so far, uncovering the electrochemical behaviour of aptamers, which are synthetic oligonucleotides that bind to specific targets, at the ITIES was investigated. The effect of having a surfactant and a target protein was also explored. Details of this investigation is revealed in Chapter 6.

Lastly, general conclusions for all the work done and then suggestions or recommendations for future work is discussed in Chapter 7.

Chapter 2. Experimental Materials and Methods

2.1 Electrochemical Set-up (ITIES)

2.1.1 Electrochemical Cell

The general electrochemical set-up used to study electrochemistry at the interface between two immiscible electrolyte solutions will be presented in this section. Samec and colleagues.^{19,163} introduced the four-electrode electrochemical cell system to achieve the polarisation of the ITIES. This arrangement allows for real-time monitoring of the Galvani potential difference, $\Delta_o^w \phi$, while measuring the current.

A typical glass electrochemical cell used for measurements at a liquid-liquid interface is illustrated in Figure 2.1.1.

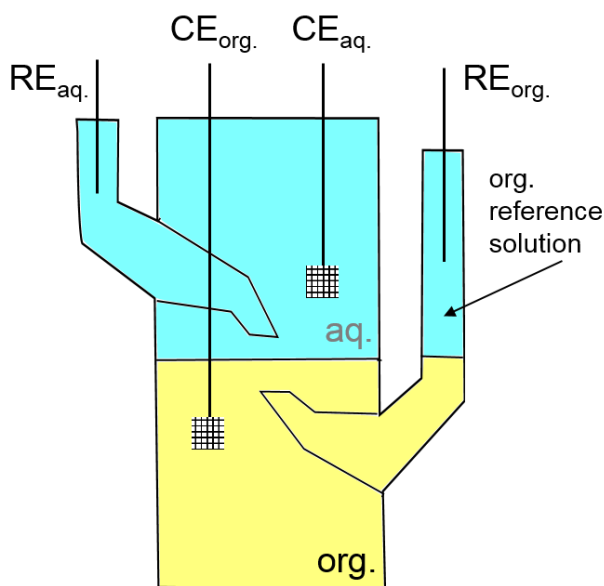


Figure 2.1.1 Schematic illustration of a typical four-electrode cell set-up for an ITIES. RE is the reference electrode and CE is the counter electrode. Aq. refers to the aqueous phase while org. refers to the organic phase.

The cell is composed as a 4-electrode set-up having two reference and two counter electrodes with one of each at the two phases.² The counter electrodes usually used are platinum (Pt) mesh and the reference electrodes silver/silver chloride (Ag/AgCl). This set-up is mostly employed for centimetre or millimetre sized ITIES since it is known to address the issue of the Ohmic drop caused by the organic solution

resistance. On the other hand, all experiments reported in this thesis were with a two-electrode cell. This means two Ag/AgCl electrodes were used and these served as both the reference and counter electrodes, having one in each phase. This is possible because the magnitude of generated current at these micro interfaces are within the nano Ampere (nA) region, which is decreased massively in comparison to its macro-sized counterpart. This means a reduced Ohmic drop, in line with Ohm's Law.

All voltammograms displayed in this thesis, unless otherwise stated, correspond to the responses observed at the micro-ITIES array when utilizing a silicon microporous membrane sealed onto a cylindrical glass. Generally, the organic phase is placed inside the glass cylinder and then topped with the organic reference solution. The resulting set-up is then immersed into a small beaker containing the aqueous solution.⁹⁶ As a result, the microinterfaces are formed at the pores of the membrane when both phases (aqueous and organic) come into contact with each other. Shown in Figure 2.1.2 is a schematic representation of a two-electrode electrochemical cell when using the microporous membrane to establish the micro-ITIES array.

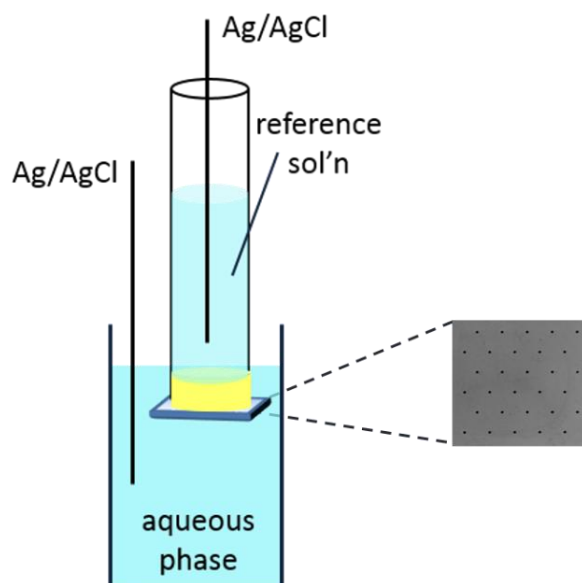


Figure 2.1.2 A schematic representation of a two-electrode electrochemical cell with a micropore array membrane.

The reference solution, wherein the Ag/AgCl is immersed, as well as the organic phase both contain BTPPA⁺ as a common ion making this interface between the reference solution and the organic phase as non-polarisable. Meanwhile, the aqueous phase – organic phase interface is polarisable and the potential difference at

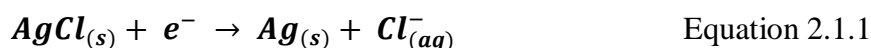
this interface is regulated via an external voltage application along the two reference (Ag/AgCl) electrodes that are linked to the potentiostat. For this thesis, measurements were performed using an Autolab PGSTAT302N electrochemical analyser (Metrohm Autolab, The Netherlands). All experiments with the electrochemical cell were done inside a Faraday cage to minimize effect of external charges and these electrochemical experiments were conducted in unstirred solutions at room temperature.

Furthermore, the mechanical stability of the organic phase during electrochemical characterisations is reported to be enhanced when it is gellified.^{157,164} This is done via the addition of low-molecular weight poly(vinyl) chloride (PVC) to the organic phase solution. For this thesis, 10% w/v gel is optimal while also maintaining the organic electrolyte concentration at 10 mM. The organic electrolyte salt used in the organic phase was synthesized via a metathesis reaction as reported previously.⁹⁵ The outline of the preparation of the organic electrolyte salt is presented in details in Appendix A.

2.1.2 Electrodes and Electrolytes

The working electrode (WE) in a typical solid-liquid electrochemical system is the electrode where the redox reaction of interest happens. Mostly, this electrode is made from conducting materials such as carbon, platinum, or gold. In earlier days, mercury, a liquid conductor, was used as the working electrode but due to health and environmental concerns, it is now modified or replaced.^{5,7} For the ITIES, the actual interface is considered as the working electrode since it is where the charge transfer processes are observed. Unlike solid electrodes, no mechanical or electrical cleaning is required for such working electrode. Meanwhile, electrode size modification can also be achieved in the ITIES as discussed in the previous chapter, just like the solid electrode and alteration of the electrode surface in solid electrodes also has a version for the ITIES where studies have been done in the presence of nanoparticles¹⁶⁵⁻¹⁶⁷ and meso-porous silica^{168,169} at the liquid-liquid interface. In a recent review, Poltorak and colleagues revealed three main methods of decorating the polarized soft interface that was developed in the last four decades. These are via a) electrochemically induced/self-assembly, b) in situ generation of materials at the interface and c) ex situ modification by solid supports.¹⁷⁰

On the other hand, the reference electrode (RE) in a typical solid-liquid electrochemical system offers a reference potential that is stable and reproducible, against which the WE potential is quantified. A common example of this electrode is the silver-silver chloride (Ag/AgCl/Cl⁻) and the standard half-cell reaction is:



Its standard potential is, E^0 , +0.222 Volts against the standard hydrogen electrode (SHE) as provided by the definition of the International Union of Pure and Applied Chemistry (IUPAC).¹⁷¹ Another common reference electrode is the saturated calomel electrode (SCE) (Hg/Hg₂Cl₂/Cl⁻) and just like the Ag/AgCl electrode, stability is achieved once the ratio of the redox species is constant.^{2,172} Looking at the Nernst expression for the Ag/AgCl, shown below in Equation 2.1.2, it is revealed that its potential relies on the activity of chloride (Cl⁻) ions.

$$\mathbf{E}_{Ag/AgCl} = \mathbf{E}^0_{Ag/AgCl} - \frac{\mathbf{RT}}{\mathbf{F}} \ln \mathbf{a}_{Cl^{-}} \quad \text{Equation 2.1.2}$$

The typical source of chloride ions in the aqueous solution phase for solid-liquid electrochemical cells are KCl or NaCl from 1.0 mM to saturated concentrations.¹ For the liquid-liquid systems, the aqueous phase contains a chloride salt electrolyte like lithium chloride (LiCl) and forms a non-polarisable interface with the Ag/AgCl electrode immersed in it. As for the other Ag/AgCl electrode, it is placed in the organic reference solution, which contains, normally, the chloride salt of the organic phase electrolyte cation such as bis(triphenyl)phosphoranylidene ammonium chloride (BTTPACl). This results in another non-polarisable interface and ensures that only one polarisable interface is formed. This polarisable interface is between the aqueous phase and the organic phase solutions.

Meanwhile, the interface between the organic reference solution and the actual organic phase is known as the reference interface¹⁷³ wherein the common cation BTTPA⁺ reaches equilibrium between the two solutions thereby resulting in an interfacial potential difference, as expressed in Equation 1.2.13. However, the applied potential via the potentiostat normally varies from the Galvani ion transfer standard potential, $\Delta_{\sigma}^w \phi_i^o$ so it is vital to consider that the potential difference applied refers to the total of the potential differences between the two Ag/AgCl electrodes¹⁷³ together with the potential of the reference interface. Under those circumstances, when an

experiment is conducted, a suitable reference ion like tetrapropylammonium (TPrA^+) is spiked into the aqueous phase to estimate the half-wave potentials, $E_{1/2}$, of the species under study relative to that of the tetrapropylammonium (TPrA^+), $E_{1/2, \text{TPrA}^+}$ and to the Galvani potential scale.

2.2 Micro ITIES

In this thesis, the microinterfaces were created utilizing a silicon membrane composed of either eight or thirty micropores, arranged in a hexagonal pattern. The diameters were 22 and 22.4 μm while the pore-to-pore separations were 400 and 200 μm respectively. A scanning electron microscopy (SEM) image of the micropore array is displayed below. The dimensions provide a total geometric area of $3.04 \times 10^{-5} \text{ cm}^2$ and $1.18 \times 10^{-4} \text{ cm}^2$ for the eight and thirty micropore array.

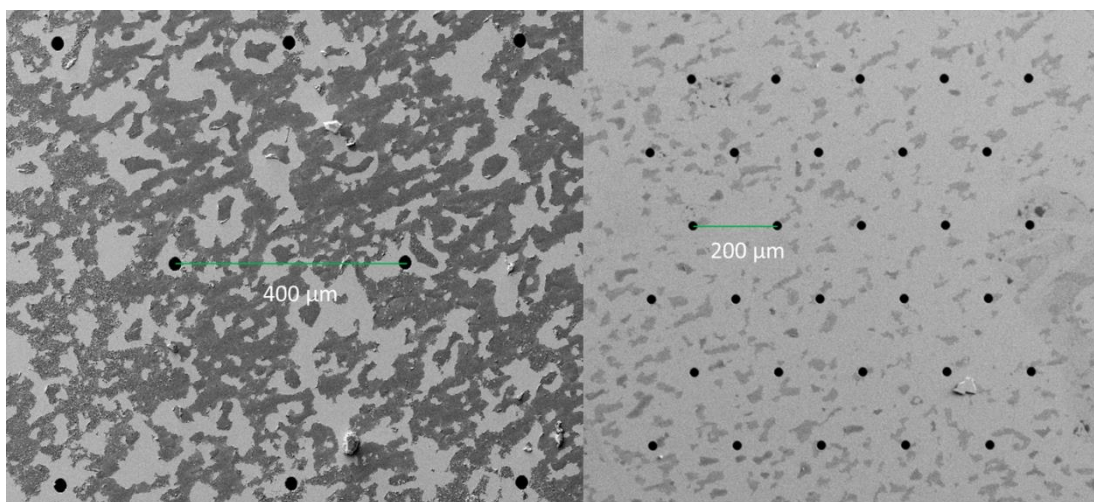


Figure 2.2.1 Scanning Electron Microscopy (SEM) of the micropore arrays (silicon membrane). Images taken by Dr. Yang Liu and Dr. Eva Alvarez de Eulate using a Zeiss Neon 40 EsB FIBSEM microscope (Carl Zeiss Nanotechnology Systems).

The thirty micropore array was fabricated via a consolidated dry and wet etching processes that include deep reactive ion etching (DRIE), wherein the inner part of the pores was overlaid with fluorocarbon film to make it sufficiently hydrophobic.^{97,174} As a result, this design, along with the filling of the pores influences the shape of the voltammogram with the response as it affects mass transport. In addition, the design chosen, if not prevents the overlap of diffusion zones and is

optimal for the system with the pore-to-pore separation twenty times that of the pore radius (as discussed in Section 1.3).

The microITIES set-up was prepared by affixing the silicon micropore membrane to the end of a capillary glass cylinder using silicone rubber (acetic acid curing Selley's glass silicone). The gellified organic phase (see Appendix B for the organogel preparation procedure) was then placed into the silicon micropore membrane via the opening of the glass cylinder using a pre-warmed glass Pasteur pipette. The resulting set-up was allowed to set for at least one hour before use. After that, the organic reference solution (composition is specified in the corresponding chapters) was then added on top of the organogel. The whole gellified organic phase/micropore membrane assembly was then submerged into the aqueous phase (composition is specified in the corresponding chapters). Then, electrochemical experiments were done.

2.3 Electrochemical Techniques

2.3.1 Cyclic Voltammetry

Cyclic voltammetry (CV) is one of the more familiar electrochemical techniques as it can be utilized to gain information about the kinetics and thermodynamics of the reactions of interest. Also, it can provide deeper insight into other analyte characteristics such as adsorption, diffusion, and number of electrons transferred in charge transfer reaction.^{5,172}

CV starts with a forward linear scan from E_1 , a starting (initial) potential to E_2 , a different (switching) potential and then back into the starting potential, E_1 , as the potential is reversed scan at a fixed scan rate, v . The resulting current is measured as a function of the applied potential and this is represented as a cyclic voltammogram. The potential cycle obeys a triangular waveform as displayed in Figure 2.3.1.

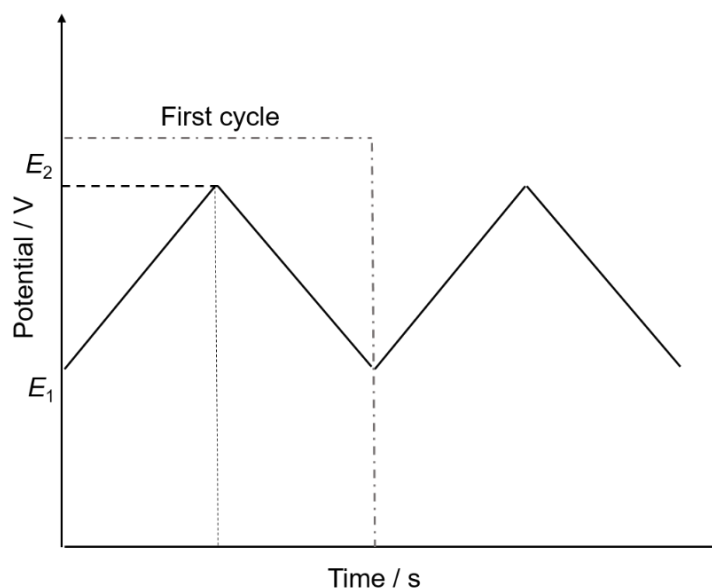


Figure 2.3.1 Applied potential against time waveform for cyclic voltammetry.

The usual first information that can be derived from a cyclic voltammogram is related to the peak current, i_p , and the peak potential, E_p . In the case of the electrochemistry between two immiscible electrolyte solutions, the initial and final applied potential, which is E_1 and E_2 , will be dictated by the background electrolytes in both the aqueous and organic phases as previously discussed in Chapter 1. To recall, these background electrolytes restrict the working potential window wherein charge transfer reactions are exposed because when scanning is conducted at these potentials where background electrolyte transfers, the analyte response may be masked by the background electrolyte current.

Additionally, Figure 2.3.2 displays two cyclic voltammograms showing different cases of cation (A^+) transfer at the ITIES. Shown in (A) is the reversible transfer of the cation via an entirely linear diffusion at a millimetre-sized ITIES while (B) reveals the asymmetric diffusion of A^+ across the polarized micrometre-sized interface.

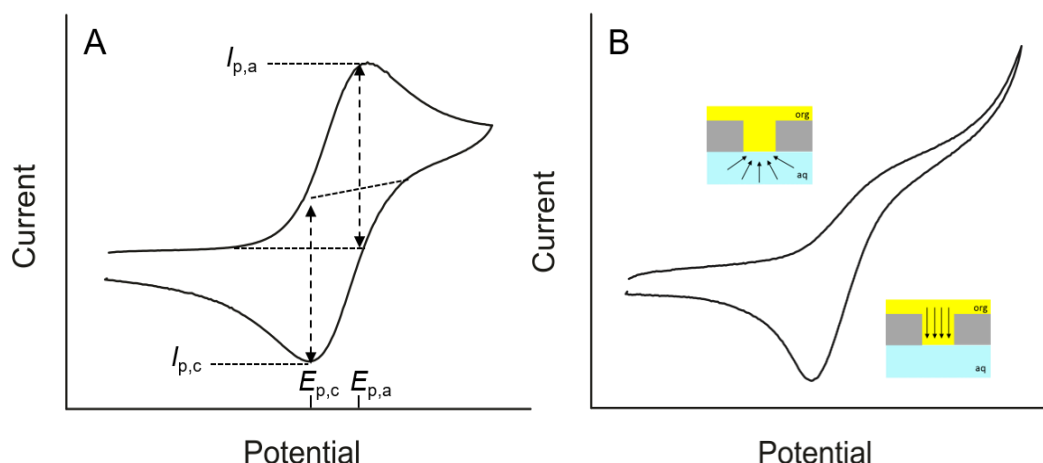


Figure 2.3.2 Cyclic voltammogram of (A) cation transfer at the ITIES and (B) at the microinterface. Inset in (B) show (top) radial diffusion as cation transfer from aq. to org. phase while (bottom) linear diffusion as it back transfers from org. to aq. phase.

As mentioned, details about the species being studied can be derived from the parameters measured using cyclic voltammetry such as the peak current, I_p , which can indicate the transfer of the species from the aqueous to the organic phase during the forward scan or the back transfer from the organic to the aqueous phase during the reverse scan, as displayed in Figure 2.3.2 (A). Also, the peak potential, E_p , can be a characteristic of the species under study. For such a case (linear diffusion), the peak current is described by the Randles-Sevcik equation shown:

$$I_p = (2.69 \times 10^5) z_i^{3/2} A D_i^{1/2} C_i v^{1/2} \quad \text{Equation 2.3.1}$$

where I_p is the peak current, z_i is the charge of the ion i , D_i as the diffusion coefficient of the species i , then C_i as the concentration of species i , and A is the interface area. Also, as can be seen in the equation, peak current is proportional to $v^{1/2}$, the square root of the scan rate under the assumptions that the diffusion is one-dimensional, the interface is flat and the background electrolyte is in excess.¹

One way to test the reversibility of the system is to plot the I_p against the $v^{1/2}$. In this case, the ratio between $I_{p,w \rightarrow o} / I_{p,o \rightarrow w}$ should be *ca.* 1 and show that the I_p for both forward and reverse scans is proportional to $v^{1/2}$. Also, the peak-to-peak separation, $E_{p,w \rightarrow o} - E_{p,o \rightarrow w}$, should be approximately 59 mV/ z_i at 25° C. Using the same equation (see Equation 2.3.1), information about the transferring species' diffusion coefficient can also be determined.²⁷

For the quasi-reversible systems, the peak-to-peak separation deviates from $59/z$ mV and relies on the scan rate, v . Also, the process can be expressed in an equation similar to Equation 2.3.1, where the transfer coefficient, α and the charge for the charge transfer step, z_a is introduced. Note that $\alpha = nFv/RT$.

$$I_p = (2.99 \times 10^5) z (\alpha z_i)^{1/2} A D_i^{1/2} C_i v^{1/2} \quad \text{Equation 2.3.2}$$

In the case where no reverse peak is observed, the system is considered to be irreversible. Generally, when peak currents, I_p are proportional to the scan rate, v , this may represent non-faradaic charge transfer that includes adsorption processes. For adsorption processes, a proportional relationship exists between the scan rate, v , and the peak current, I_p and this is shown below:

$$I_p = \frac{z_i^2 F^2 \Gamma A v}{4RT} \quad \text{Equation 2.3.3}$$

where z is the charge transferred, F is Faraday's constant then Γ is the surface coverage while R is the universal gas constant and T being the temperature. In an experiment, the charge in Coulombs (C) is calculated by integrating the measured peak when current is plotted against time. The calculated charge can then render more details about the adsorption process. Equation 2.3.4 reveals that the charge, Q is directly proportional to the surface area, A , and the surface coverage, Γ along with the charge of the species, z_i .

$$Q = z_i F A \Gamma \quad \text{Equation 2.3.4}$$

In the microITIES, a characteristic steady state current is observed indicating a radial diffusion (see Figure 2.3.2 B) at the interface and this can be described similar to that of an inlaid disc electrode as shown in the next equation:

$$I_{lim} = n z_i F D C r \quad \text{Equation 2.3.5}$$

where the limiting current, I_{lim} is directly related to the number of microinterfaces, n and their radii r ; the number of charge of species, z_i as well as its concentration C ; and the diffusion coefficient, D . In the instance when the organic phase does not completely fill in the micropore or it has become recessed at a certain L distance from the pore opening, the previous equation is re-written as follows:

$$I_{lim} = n \frac{4\pi z_i F D C r}{4L + \pi r} \quad \text{Equation 2.3.6}$$

Additionally, when the organic phase overfills the micropore, it is described as a hemispherical electrode wherein the limiting current can be reported as in the equation:

$$I_{lim} = n 2\pi z_i F D C r \quad \text{Equation 2.3.7}$$

Most, if not all cyclic voltammograms reported in this dissertation were conducted with a sweep rate of 5 mV s⁻¹ to consider the size of the interface and the processes therein. Higher sweep rates were utilized when investigations on the mechanism were needed and is specified in the corresponding sections.

2.3.2 Linear Sweep Voltammetry

Linear sweep voltammetry (LSV) uses similar principles with cyclic voltammetry except that it represents half of the cycle when the potential is scanned through a single direction only. This means the potential is scanned linearly from a starting potential, E_1 where no electron flows to a final potential, E_2 where a charge transfer process can occur. The applied potential is a function of the scan rate, ν and the scan time, t . Figure 2.3.3 (A) illustrates a potential-time excitation signal for LSV. The voltammetric response produced is equivalent to half of a typical cyclic voltammogram where only the forward or the reverse peak is seen considering the initial potential as well as the scan direction. For a linear diffusion at the ITIES, a peak-shaped voltammogram is observed with LSV. The maximum current or the peak current, I_p is directly proportional with the concentration of the transferring species and is affected by the scan rate.⁸⁶ Shown in Figure 2.3.3(B) is a voltammogram for the transfer of a cation from the aqueous phase to the organic phase.

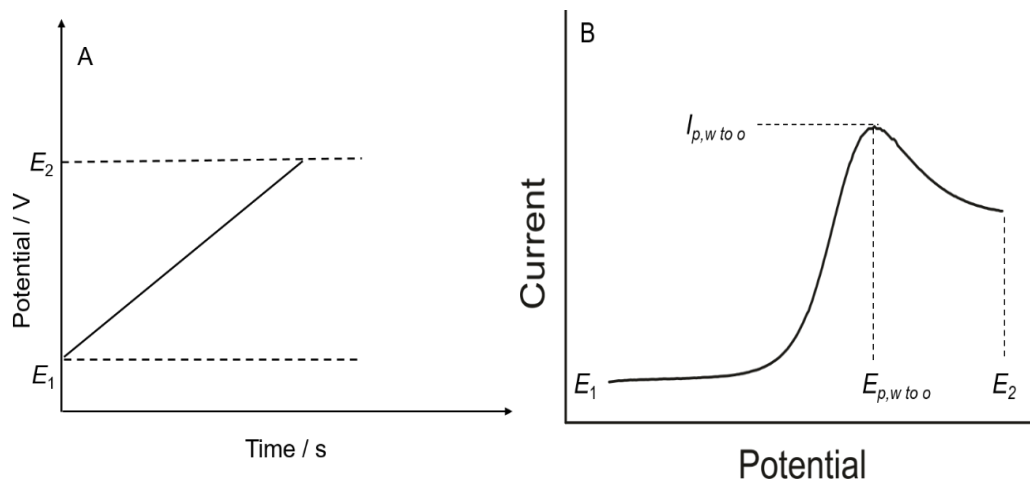


Figure 2.3.3 (A) LSV potential-time excitation signal (B) LSV cation transfer from aq. to org. phase.

2.3.3 Differential Pulse Voltammetry

Differential pulse voltammetry (DPV) is an electrochemical method that results to a considerable increase on the sensitivity by reducing the contribution of the charging current to the analytical signal. This means the ratio of the faradaic current, i_f as compared to the charging current, i_c is maximized. This is because i_f usually decreases with $1/t^{1/2}$, while i_c decreases much faster¹⁷⁵ as depicted in Figure 2.3.4 (A). Using a pulsed-potential waveform, as shown in Figure 2.3.4 (B), current sampling is carried out over a period of time: before the pulse application (i_1) and at the end of pulse application (i_2), whereby i_c should be significantly decreased. Consequently, the difference between the two current values, $\Delta i = i_2 - i_1$, is calculated and is plotted against the Galvani potential difference across the interface, $\Delta_o^w \phi$.

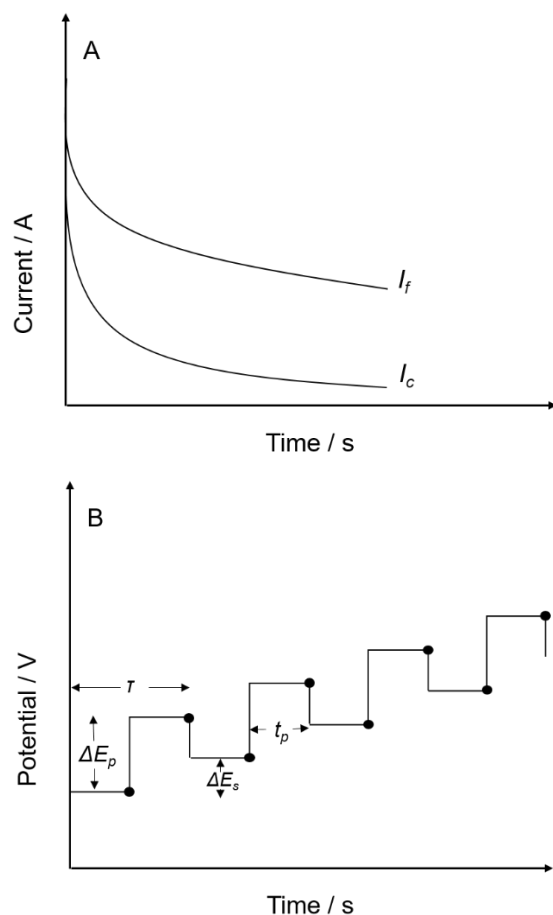


Figure 2.3.4 (A) Plot of faradaic current, i_f and the charging current, i_c over time after potential application; (B) Potential-time waveform for differential pulse voltammetry

In DPV, the changes in potential are limited to small pulses, $\Delta(\Delta_o^w \phi)$ as illustrated in Figure 2.3.5 (A). When $\Delta(\Delta_o^w \phi)$ creates the most substantial changes in the faradaic current, this is shown as the rising part of the curve where Δi also has the higher values. The $i - \Delta_o^w \phi$ response resembles a sigmoidal curve, as shown in Figure 2.3.5 (A), because the potential excitation signals are short for DPV and the diffusion-limited transient commonly noted for LSV once $\Delta_o^w \phi > \Delta_o^w \phi'$ is not seen. Consequently, the $\Delta i - \Delta_o^w \phi$ curve looks like a derivative of $i - \Delta_o^w \phi$ and is displayed in Figure 2.3.5 (B).

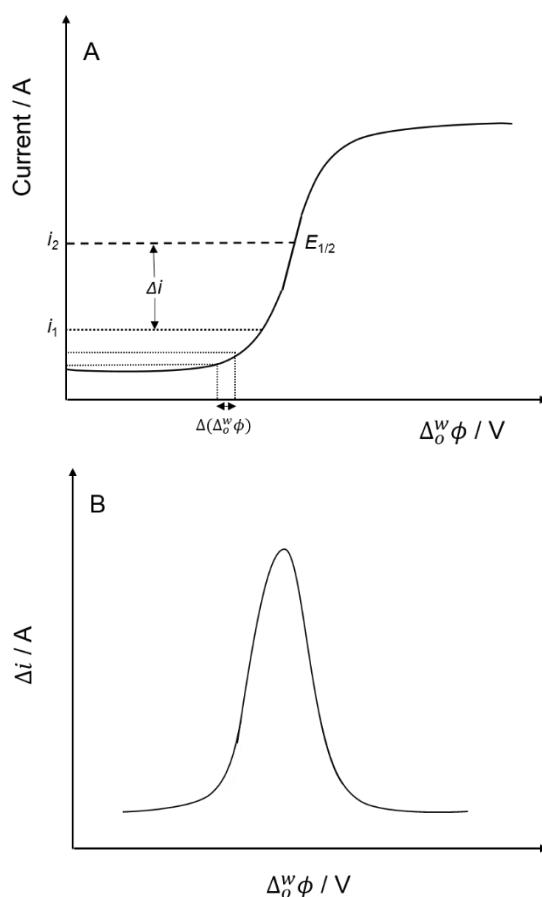


Figure 2.3.5 (A) Sigmoidal curve of $i - \Delta_0^w \phi$. Δi is higher at the rising part of the curve since $\Delta(\Delta_0^w \phi)$ is inducing more changes in i_f (B) DPV voltammogram showing a cation transfer from aq. to org. phase.

Moreover, Δi will be at maximum on the point where changes in current with potential occur swiftly.¹⁷⁶ No faradaic processes are observed when $\Delta_0^w \phi$ is greatly more negative than $\Delta_0^w \phi'$. This means Δi will approach zero with the exception of minute i_c contributions. During the application of a pulse where $\Delta_0^w \phi > \Delta_0^w \phi'$, Δi would be miniscule because the applied $\Delta(\Delta_0^w \phi)$ is positive enough to make the maximum faradaic current flow from the onset (i_1) to end of pulse (i_2).

Then, for Figure 2.3.5 (C), as the potential difference becomes more positive, i_f also increases accordingly. In this part, the current at the base potential (i_1), will be always smaller than that at the end of the pulse (i_2) because i_f has also already increased from the time current sampling was done at the base to the end. This results to an increase in Δi but then reaches a maximum at $E_{1/2}$, which corresponds to the peak shown in Figure 2.3.5 (B).

2.3.4 Stripping Voltammetry

Stripping voltammetry (SV) is an electroanalytical technique usually utilized to improve detection limits^{177,178} and is commonly associated with trace metal detection.¹⁷⁹ It involves a two-step process: (1) a pre-concentration and (2) a stripping or detection step. The pre-concentration step entails holding the applied potential for a certain span of time which induces the adsorption or extraction of the species of interest causing its accumulation. This is then followed by the stripping step, wherein the potential is scanned towards the positive or negative direction resulting to the release or stripping of the species of interest and consequently, its detection. Figure 2.3.6 illustrates the two-step process of the SV via waveform.

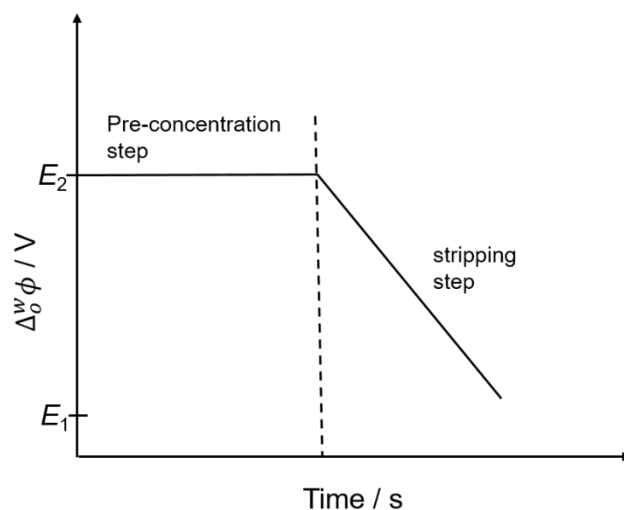


Figure 2.3.6 Potential-time waveform depicting the steps in a stripping voltammetry

For the ITIES, the pre-concentration step involves the extraction of the analyte from the aqueous phase and its accumulation at the interface. Then, the - extracted analyte is transferred back into the aqueous phase as the potential is scanned either on the positive or negative direction. The stripping process produces a peak current as the analytical signal and is proportional to the concentration of the analyte.¹⁷⁷

Other types of SV include anodic stripping voltammetry (ASV) and cathodic stripping voltammetry (CSV), both techniques involve the deposition of the analyte as the first step and then a detection step follows by application of an oxidizing potential or reducing potential, respectively. A related SV technique is adsorptive stripping

voltammetry (AdSV) which is based on the accumulation of the surface-active analyte for a certain period of time and then followed by scanning of the potential that serves as the detection step. The recorded response is directly attributed to the concentration of the analyte or to the surface concentration for AdSV.⁵

For this thesis, the applied potential and pre-concentration times were optimised for each set of experiments when AdSV was used and more details of which are discussed in the corresponding chapters.

Chapter 3. Electrochemical Detection of Lysozyme at a Liquid | Solvent-Cast Organogel Microinterface Array¹

3.1 Introduction

Biomolecules, such as proteins, play a vital role in maintaining the functionalities of every activity within living species. Hence, understanding and detecting protein behaviour can be beneficial for a number of biomedical applications.³⁵ One of the commonly studied model proteins is lysozyme, a protein found in mammals that is responsible for the cleavage of an acetal group located in the polysaccharide walls of bacteria.¹⁸⁰ Composed mainly of 129 amino acids residues held together by cysteine disulphide bonds¹⁸¹, it is usually available as hen-egg-white-lysozyme (HEWL) since it comprises 3.5% of egg white protein.¹⁸² Its molecular weight is *ca.* 14,600 g mol⁻¹¹⁸⁰ and isoelectric point is 11.35, making it positively charged at physiological pH.¹⁸³ Aside from being a model protein analyte, the investigation of lysozyme was propelled by its use as an indicator for several diseases.¹⁸⁴⁻¹⁸⁶

For the past 45 years, the study of electrochemistry at the interface between two immiscible electrolyte solutions (ITIES) has been rapidly increasing.^{17,86,173} One of the main themes of research in this area in recent years has been the electrochemistry of proteins, since protein detection at the ITIES offers advantages for bioanalytical applications such as label-free detection, due to charge transfer processes at the ITIES, and amenability to miniaturization.^{187,188} Amongst several biomolecules of interest at the ITIES or μ ITIES, dopamine⁴⁰, heparin⁵², and cytochrome *c*¹⁸⁹ have been investigated in addition to HEWL. Scanlon *et al.*^{48,157} examined the electrochemical behaviour of HEWL at the ITIES and showed its adsorption at both all-liquid ITIES and gellified μ ITIES. The proposed mechanism for its detection included adsorption of the cationic protein at the interface and the protein-facilitated transfer of the organic

¹ This material was published as: Felisilda, Bren Mark B., Eva Alvarez de Eulate, and Damien WM Arrigan. "Investigation of a solvent-cast organogel to form a liquid-gel microinterface array for electrochemical detection of lysozyme." *Analytica Chimica Acta* 893 (2015): 34-40. <https://doi.org/10.1016/j.aca.2015.08.024>

electrolyte anion across the interface, resulting in a protein-anion complex.^{48,157} This proposed complexation between the lysozyme and the organic electrolyte anion (hydrophobic) was demonstrated by Hartvig *et al.*¹⁹⁰ using an online mass spectrometry method to reveal this complexation. Subsequent mass spectrometry studies revealed partial unfolding of lysozyme following its electroadsorption at the aqueous-organogel interface.¹⁶² Similar detection mechanisms were suggested for other biomacromolecules, including insulin⁴⁷ and haemoglobin.^{49,191}

In terms of detection limits for HEWL at the ITIES, reports have been within the low micromolar range, such as that based on background-subtracted cyclic voltammetry at a μ ITIES array that detected 0.5 μ M.⁴⁸ However, lower detection limits are required for protein detection when applied in clinical diagnostics.¹⁹² One common method that is utilized by researchers to address such concerns for low detection limits is in the form of pre-concentration. In voltammetric analysis, this entails pre-concentrating the analyte into or onto the electrochemical interface before application of the voltammetric analysis. This is referred to as stripping voltammetry and a recent review by Herzog and Beni¹⁷⁷ highlighted how this technique has been applied to μ ITIES arrays. In particular, its application to exploiting protein adsorption at the μ ITIES array has enabled lysozyme detection at 30 nM¹⁵⁹ as well as haemoglobin at \sim 40 nM¹⁹³ and insulin at 10 nM.¹⁹⁴ In all such methods, however, the organic phase was prepared using a high temperature process that involves pouring the hot gel mixture into the micro-interface-forming membrane and allowing it to cool.^{48,96,157,159,193,194} However, alternative methods for organogel preparation, such as the solvent-casting methods widely used in potentiometric ion-selective electrode research,^{195,196} may offer a more convenient method for the preparation of the gelled organic phase.

The purpose of the work reported here was to examine whether the solvent-casting organogel preparation method was a viable approach for the development of a gelled μ ITIES array for protein detection. The combination of this method with adsorptive stripping voltammetry and differential pulse voltammetry will be described in the following sections, with a low detection limit of 10 nM achieved.

3.2 Experimental Method

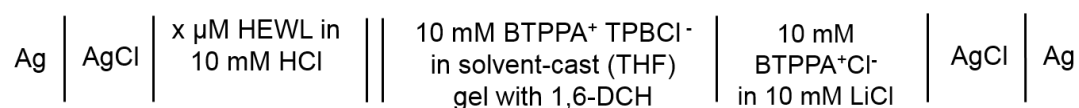
3.2.1 Reagents

All reagents were obtained from Sigma-Aldrich Australia Ltd. and were used as received unless otherwise stated. The organic phase was prepared by dissolving bis(triphenylphosphoranylidene) tetrakis(4-chlorophenyl)borate (BTPPA⁺TPBCl⁻, 10 mM) in 1,6-dichlorohexane (1,6-DCH). It was then gelled by the addition of 10% w/v low molecular weight poly(vinyl chloride) (PVC).^{157,164} A maximum equal volume of tetrahydrofuran (THF) was then added dropwise, with continued stirring for *ca.* 15-20 min, to complete the gel formation. The resulting solution was set aside for 48 hours to evaporate excess solvent before being used.¹⁹⁶ The organic electrolyte salt (BTPPA⁺TPBCl⁻) was prepared by metathesis of bis(triphenylphosphoranylidene) ammonium chloride (BTPPA⁺ Cl⁻) and potassium tetrakis(4-chlorophenyl)borate (K⁺TPBCl⁻) following the published procedure.⁹⁵ The HEWL stock solutions were prepared fresh in 10 mM HCl and then stored at 4°C. Similarly, tetraethylammonium (TEA⁺) chloride was dissolved in 10 mM HCl. All aqueous solutions used were made with MilliQ water from a USF Purelab plus UV, having 18.2 MΩ*cm resistivity.

3.2.2 Apparatus

All electrochemical experiments were performed on an AUTOLAB PGSTAT302N electrochemical station (Metrohm, The Netherlands) through a NOVA 1.9 software interface. The μITIES array employed was defined by a micropore array silicon membrane, previously described.^{97,174} The membrane employed in this study consisted of eight micropores in a hexagonal arrangement, each having a diameter of 22 μm and a pore centre-to-pore centre distance of 400 μm. These microporous silicon membranes were sealed onto the lower orifice of a glass cylinder using silicone rubber (acetic acid curing Selley's glass silicone). The solvent-cast organogel mixture was introduced into the silicon micropore arrays via the glass cylinder with the aid of a pre-warmed glass Pasteur pipette. The set-up was then set aside for at least one hour before use. When ready, the organic reference solution (composition: 10 mM BTPPA⁺Cl⁻ in 10 mM LiCl) was then placed on top of the solvent-cast organic phase. The solvent-cast organogel/silicon membrane assembly was then immersed into the aqueous phase (10 mM HCl, HEWL in 10 mM HCl, and/or TEA⁺ in 10 mM HCl) and voltammetric

experiments were implemented. Scheme 3.2.1 summarizes the electrochemical cell employed.



Scheme 3.2.1 Schematic representation of the electrochemical cell employed. *x* represents the various HEWL concentrations used in the study.

3.2.3 Electrochemical Measurements

A pair of Ag/AgCl electrodes were used for all measurements. The geometric area of the microinterface array was $3.04 \times 10^{-5} \text{ cm}^2$. Cyclic voltammetry (CV) and adsorptive stripping voltammetry (AdSV) were carried out at a scan rate of 5 mV s^{-1} , unless noted otherwise. Optimal parameters for differential pulse voltammetry were found to be 75 mV as the modulation amplitude, 200 ms for the modulation time and 500 ms for the interval time, which resulted in a scan rate of 10 mV s^{-1} . Other parameters such as protein concentration, applied potential, and duration of the pre-concentration step were varied accordingly. In order to compare all techniques utilized, all the calculated limits of detection were based on three times the standard deviation of the blank ($n=3$) divided by the slope of the straight line. In the case of the AdDPSV, when semi-logarithmic curves were observed, the slope of the straight line was for the lower concentrations (0.02, 0.06 and $0.12 \mu\text{M}$ HEWL) only.

3.3 Results and Discussions

3.3.1 Cyclic Voltammetry

One approach to study the adsorption of a biomacromolecule at microITIES is via CV. This can also be used to compare the voltammetric response for an ion transfer process in the presence and absence of the target biomacromolecule.^{157,197} In this latter approach, the CV shape for an ion transfer will be affected if the biomacromolecule is adsorbed at the microITIES. Figure 3.3.1 shows CVs of HEWL at the solvent-cast aqueous-organogel microinterface array. Figure 3.3.1 (A) is the CV (grey line) obtained when $15 \mu\text{M TEA}^+$ was present in the aqueous phase. Figure 3.3.1

(A) also shows the CV (dashed line) that was recorded when only background electrolytes were present. The background electrolyte transfer across the ITIES is indicated by the increase of current at the more positive potential end.¹⁵⁷ Meanwhile, the CV in the presence of TEA⁺ shows the typical CV shape at a micro-interface array formed at silicon micropore array membranes, showing a steady-state voltammogram on the forward (going to positive direction) scan, indicative of radial diffusion, and a peak-shaped voltammogram on the reverse (going to negative direction) scan, indicative of linear diffusion control.

These mass transport phenomena dominate the ion transfer of TEA⁺ at the microITIES array and are concordant with previous reports in which the micropores were filled with gelled organic phase.^{97,174} However, the case is different when HEWL is added to the aqueous electrolyte phase. Figure 3.3.1(B) displays the CV (grey line) observed when 15 μM of HEWL was present and Figure 3.3.1 (C) shows the CV when 15 μM TEA⁺ and 15 μM HEWL were present in the aqueous phase. Overlaid in both is the background CV response (dashed line). The CV obtained in the absence and presence of HEWL is distinguishable primarily by the reverse scan peak, indicating that HEWL is detected. This peak can be attributed to the desorption of HEWL from the interface, following its electroadsorption there during the forward scan.

Previous studies have discussed that the HEWL response at the liquid-liquid interface is complex and is usually a mixture of HEWL adsorption at the interface and its participation in the facilitated transfer of the background electrolyte anion from the organic to the aqueous phase and the formation of a complex.^{48,157,190} This complexity was exhibited as the presence of HEWL changed the shape of the TEA⁺ CV, as shown in Figure 3.3.1 (C). The steady-state response of the TEA⁺ transfer at the forward scan is less defined in comparison to the absence of HEWL (see Figure 3.3.1 A).

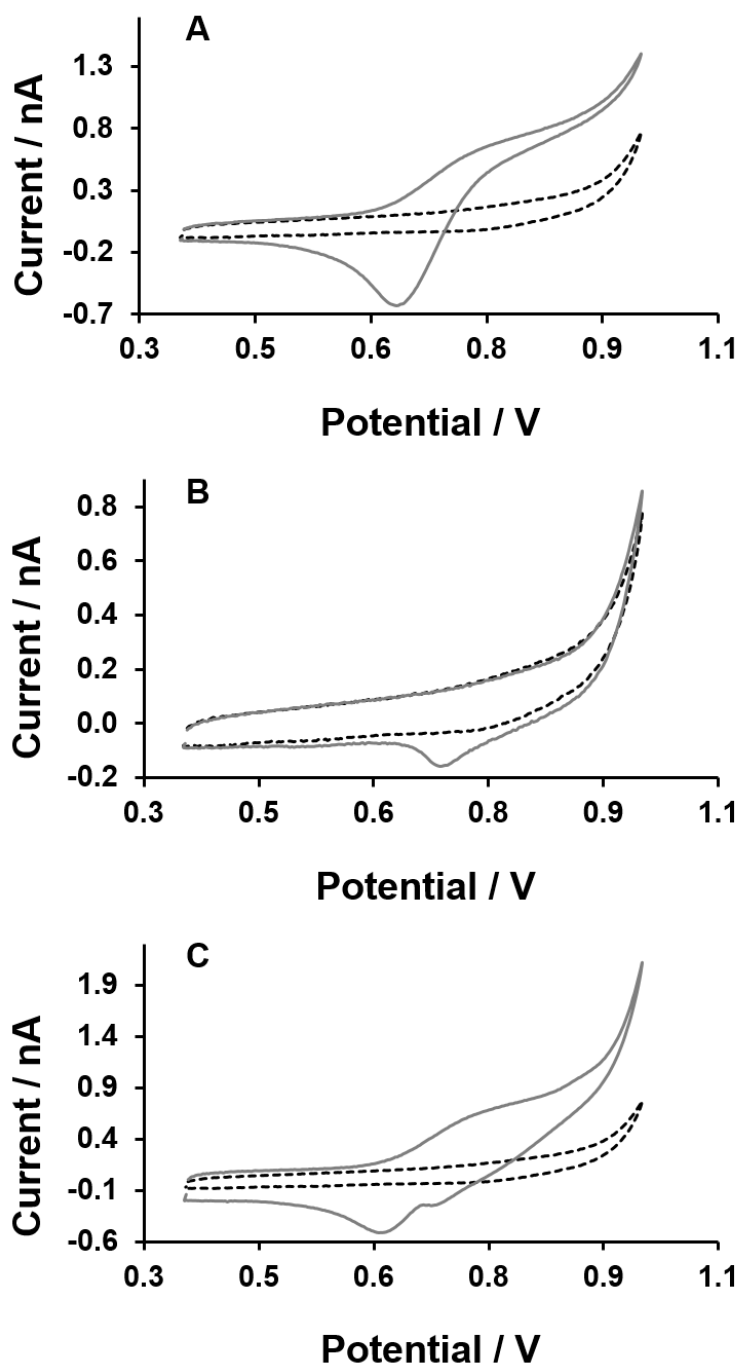


Figure 3.3.1 Cyclic voltammograms observed with the solvent-cast aqueous-organogel μ ITIES array (Scheme 1) in the absence and presence of TEA^+ and HEWL in the aqueous phase: a) $15 \mu\text{M TEA}^+$; b) $15 \mu\text{M HEWL}$ and c) $15 \mu\text{M TEA}^+ + 15 \mu\text{M HEWL}$. The blank experiment is shown as the dashed line. Scan rate: 5 mV s^{-1}

The intensity of the peak-shaped response of TEA^+ on the reverse scan was also less-defined, as well as the existence of the additional peak due to the desorption of HEWL. The peak for the TEA^+ transfer can be seen at *ca.* 0.62 V while that for desorption of HEWL is at a more positive potential of *ca.* 0.68 V. The formation of an

adsorbed protein layer was shown by how the presence of HEWL transformed the shape of the expected steady-state response for TEA⁺ as it transfers from the aqueous into the organic phase. This was also observed in a previous report¹⁵⁹ where a heat-treated gellification of the organic phase was employed. The presence of HEWL has also affected the reverse scan peak as shown by the slight shifting of the TEA⁺ transfer peak potential and its decreased intensity. This can be attributed to the presence of adsorbed HEWL that diminishes the area of the interface for TEA⁺ transfer. In addition, the theoretical limiting current was also determined to characterize the mass transport behaviour at the solvent-cast aqueous-organogel μ ITIES array. Using the inlaid disc model¹⁷⁴, the limiting current was calculated to be 4.3×10^{-10} A, while using the hemisphere model¹⁰⁵, it was found to be 6.7×10^{-10} A. When compared to the experimental limiting current of 5.9×10^{-10} A for a 15 μ M TEA⁺ aqueous concentration, it is suggested that the formed interface is in between that of an inlaid disc and hemispherical model.

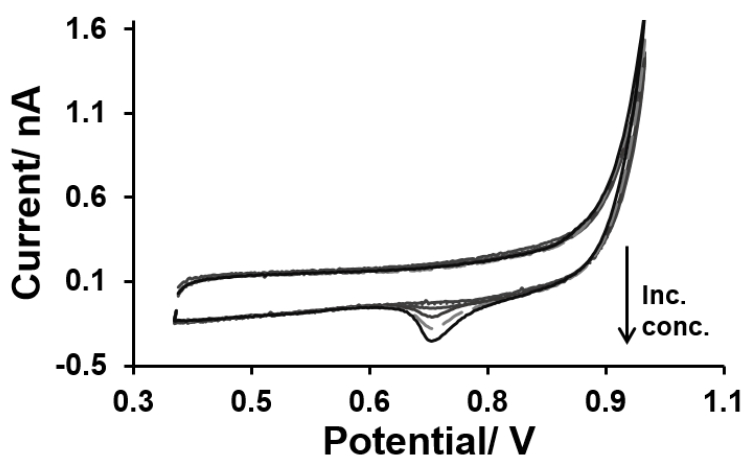


Figure 3.3.2 Cyclic voltammograms observed with the solvent-cast aqueous-organogel μ ITIES array (Scheme 1) in the presence of increasing concentrations of HEWL, as indicated by the arrow direction (5, 10, 15, 20 and 25 μ M), in the aqueous phase. Scan rate: 5 mV s^{-1} .

CVs of increasing HEWL concentrations, in the range 5-25 μ M, at the solvent-cast aqueous-organogel μ ITIES array are illustrated in Figure 3.3.2. Despite the added HEWL concentrations, a similar broad, indistinct rise in current for the forward sweep was observed at every concentration. This can be related to the adsorption of HEWL at the interface, in agreement with previous reports.^{48,159} However, the reverse scan was more revealing, as the desorption peak increased with increasing HEWL concentration. This can be explained by a desorption process

following the complexation of the organic electrolyte anion with the cationic protein. It was also shown in previous studies that multilayer formation^{48,162,191} occurs at the interface in the presence of increasing biomacromolecule concentrations, which supports the idea that the reverse sweep current increases in proportion to the adsorbed amount.

3.3.2 Adsorptive Stripping Voltammetry

The utilization of adsorptive stripping voltammetry (AdSV) for analytical detection purposes at the μ ITIES has been studied for different model proteins.^{159,193,194} AdSV involves application of a constant potential, for a defined and controlled time, during which adsorption occurs at the interface. This is then followed by the detection step, via a voltammetric scan to lower potentials that desorbs the protein from the interface and produces a peak current that is concentration- and adsorption time-dependent. In order to optimize the parameters for HEWL adsorption at the solvent-cast aqueous-organogel microinterface array, the effect of applied potential during the adsorption step was examined. The applied potential was held at chosen values for various times, after which the potential was scanned to lower potentials so as to desorb HEWL from the interface and yield a stripping voltammogram. The effect of varying applied potentials on HEWL adsorption at the solvent-cast aqueous-organogel μ ITIES is displayed in Figure 3.3.3.

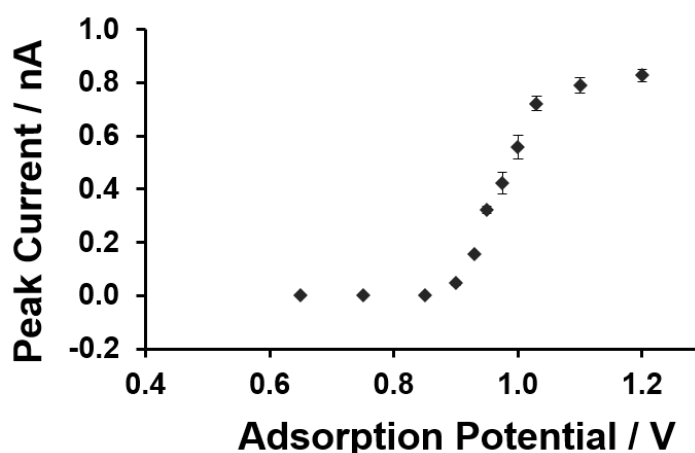


Figure 3.3.3 Plot showing the effect on the peak current of varying the interfacial potential on the adsorption step. Aqueous phase contains: 10 mM HCl + 10 μ M HEWL. Adsorption time was 60 s, without stirring. The solvent-cast organogel was used as the organic phase (Scheme 1). Scan rate: 5 mV s^{-1} .

In consideration of the effect of the adsorption potential on the peak current, the optimum potential chosen must not only maximise the stripping signal but also minimise the background (electrolyte transfer) signal which occurs in the region of HEWL adsorption. The best compromise was determined to be at 0.95 V for HEWL, in agreement with the results for the heat-treated organogel.¹⁵⁹ Above this potential, the peak current starts to display a shoulder and the increasing current may be mostly due to background electrolyte transfer contributions.

In order to examine whether the peak on the AdSV scan was indeed adsorption/desorption related, voltammograms were recorded at different scan rates, to test whether linear behaviour between peak current and scan rate was present, as predicted for an adsorption process by the equation:

$$i_p = \frac{z_i^2 F^2 \Gamma A v}{4RT} \quad \text{Equation 3.3.1}$$

where i_p is the peak current, z_i refers to the number charges each molecule transfers, F is the Faraday constant, R is the universal gas constant, T is the temperature and A is the total interfacial area. Figure 3.3.4 illustrates the recorded voltammograms following application of a constant potential and constant time for protein adsorption.

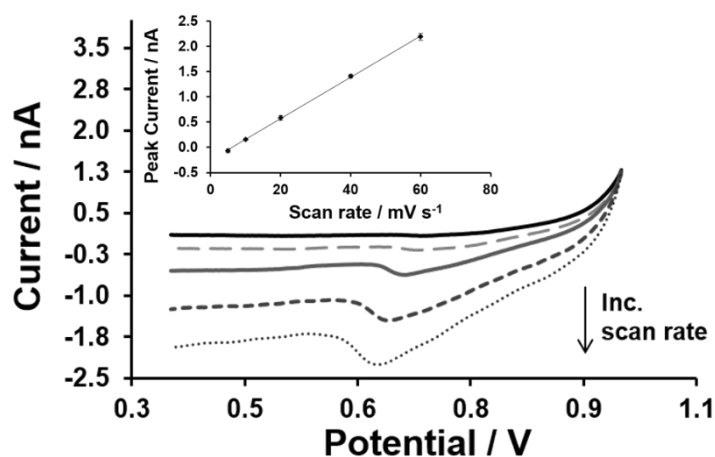


Figure 3.3.4 AdSV of 0.5 μM HEWL + 10 mM HCl at various scan rates: 5 mV s^{-1} (black bold line) to 60 mV s^{-1} (black dotted line). Inset shows plot of peak current against scan rate. The solvent-cast organogel was used as the organic phase (Scheme 1). Pre-concentration time and potential were 60 s and 0.950 V respectively.

The inset displays the linear relationship between the peak current and the scan rate, verifying that the peak is associated with desorption from the interface. Using the temperature of 21 °C, together with the assumption that the number of ions transferred per molecule is equal to the charge of the protein, +17¹⁹⁸, and that the formed interface follows that of an almost hemispherical model, the surface coverage for a 0.5 μM HEWL concentration adsorbed for 60 s was obtained from the slope of the line of the inset graph, giving the value of 2.5 pmol cm⁻², which is in good agreement with previously reported value, 4 pmol cm⁻² ¹⁵⁹.

In addition, the effect of varying the adsorption time was investigated and the resulting voltammograms are shown in Figure 3.3.5. Without any pre-concentration (0 s adsorption time), no stripping peak was observed for an HEWL concentration of 0.5 μM. However, LSV following adsorption times of more than 60 s produced stripping peaks and the peak current continued to rise as adsorption time was increased. To ensure that there was no carryover of HEWL between experiments, a blank analysis was performed between all voltammograms; no peaks were evident on these blank analyses.

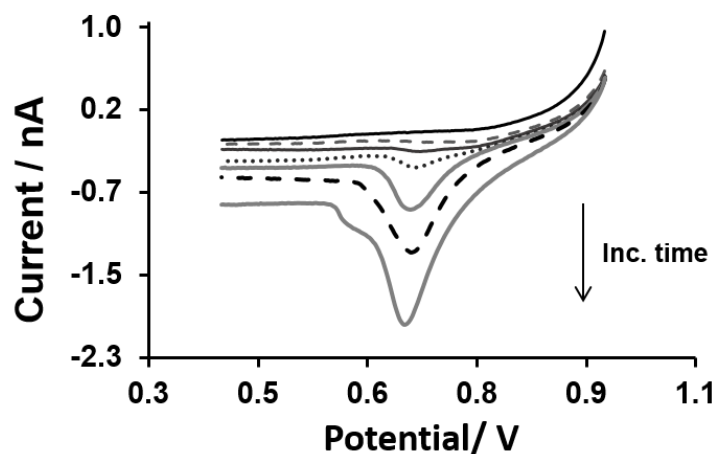


Figure 3.3.5 AdSV of 0.5 μM HEWL + 10 mM HCl at various pre-concentration times from 5 (black bold line) to 1800 (grey bold line) s. The solvent-cast organogel was used as the organic phase (Scheme 1). Scan rate: 5 mV s⁻¹.

Furthermore, increasing concentrations of HEWL (0-1.0 μM) were examined under different adsorption times of 60, 120 and 300 s. The idea was to see how solution concentration and adsorption time can be utilized to control HEWL adsorption and to maximise the detection signal (current). Figure 3.3.6 compares the AdSV obtained for (A) 60 s and (B) 300 s pre-concentration times at increasing (0 - 1.0 μM) HEWL

concentration. It can be seen that the peak currents increased with adsorption time, indicating that longer adsorption times can improve the sensitivity. This agrees with previous reports¹⁵⁹ on the kinetics of HEWL adsorption at the μ ITIES, where it was suggested that long pre-concentration times were required for saturation or equilibrium surface coverage.

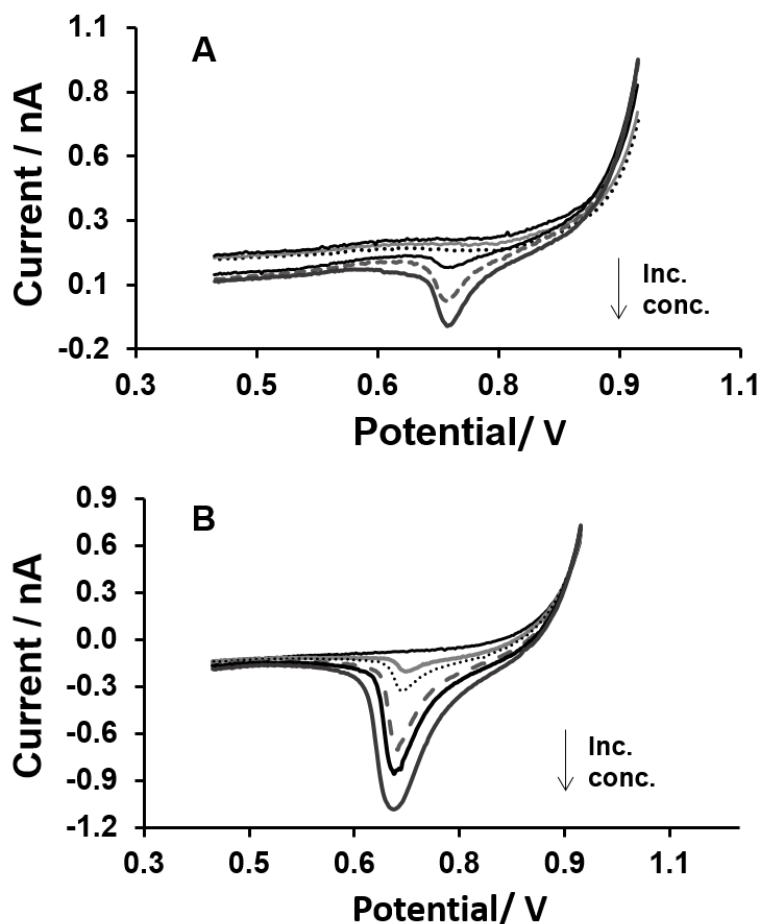


Figure 3.3.6 AdSV of various HEWL concentration for different adsorption times: (A) 60 s and (B) 300 s at an applied potential of 0.950 V. Aqueous phases contain (0 – 1.0) μ M HEWL in 10 mM HCl. The solvent-cast organogel was used as the organic phase (Scheme 1). Scan rate: 5 mV s^{-1} .

In terms of analytical performance, higher slopes from increased peak currents indicate better sensitivity and so 300 s was used to investigate the analytical characteristic for AdSV at the solvent-cast aqueous-organogel μ ITIES array. Figure 3.3.7 shows the voltammograms obtained when increasing concentrations of HEWL were added (0.02 – 0.84 μ M) to the aqueous phase. Concentrations of 0.04 μ M were detected and the calculated limit of detection was 0.03 μ M. This value agrees with a previous report on a heat-treated aqueous-organogel μ ITIES array¹⁵⁹, but is

magnitudes better than the reported value of 0.5 μM for CV detection at a heat-treated aqueous-organogel μITIES array¹⁵⁷, and even more so for other ITIES studies on HEWL.⁴⁸

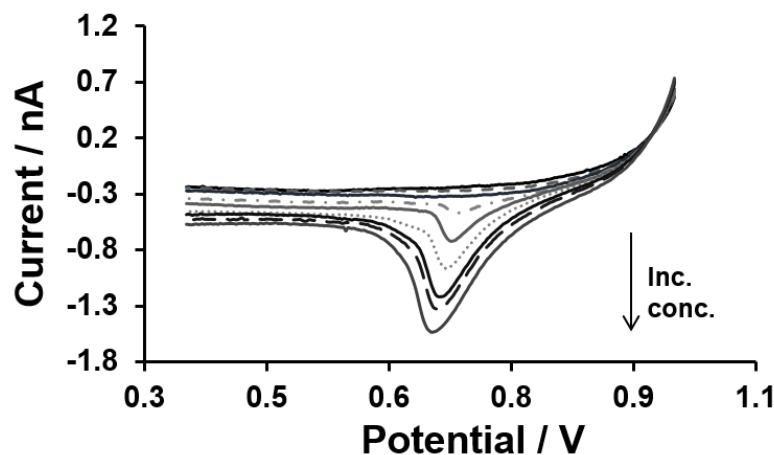


Figure 3.3.7 AdSV of increasing aqueous phase HEWL concentrations, as indicated by the direction of the arrow (0.02 to 0.84 μM) at the solvent-cast aqueous-organogel μITIES (Scheme 1). The adsorption time and potential were 300 s and 0.950 V respectively. Scan rate: 5 mV s^{-1} .

3.3.3 Adsorptive Differential Pulse Stripping Voltammetry

With the aim to further improve the detection limit of HEWL at a solvent-cast aqueous-organogel μITIES array, differential pulse voltammetry (DPV) was employed following the HEWL adsorption, since DPV is a well-known method that achieves lower detection limits^{5,199}. Similar to the major steps involved in AdSV, adsorptive differential pulse stripping voltammetry (AdDPSV) employs a pre-concentration step followed by a voltammetric scan. Background-subtraction was also utilized to further improve the sensitivity. Background subtraction was performed by recording a blank experiment (0 μM HEWL) at the beginning of the run. Then this blank response was subtracted from each of the pulse voltammetric responses to HEWL subsequently recorded. Figure 3.3.8 shows the background-subtracted voltammograms obtained at various HEWL concentrations.

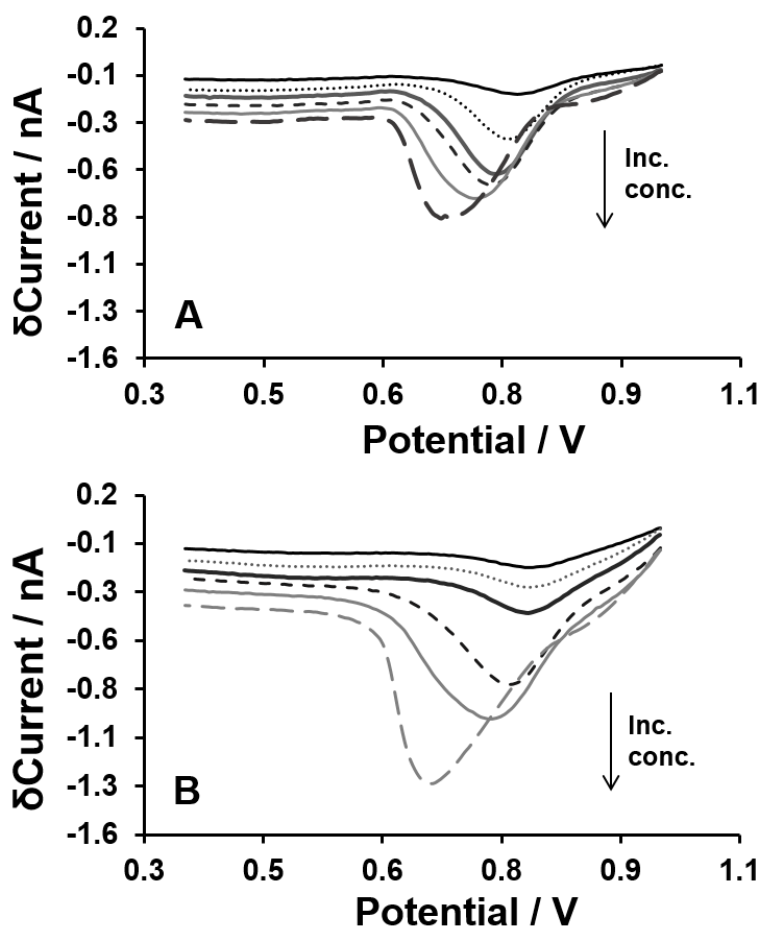


Figure 3.3.8 AdDPSV of HEWL (0.02 to 0.60 μM , increasing as directed by the arrow direction) for (A) 60 s, (B) 120 s, pre-concentration times prior to voltammetric desorption. Solutions contained increasing (0.02 - 0.60 μM) HEWL + 10 mM HCl in the aqueous phase (Scheme 1).

Voltammetric scans of a blank experiment were performed in between runs to ensure that the solvent-cast aqueous-organogel was clean prior to the next run.⁴⁴ The voltammograms correspond to 60 s (Figure 3.3.8 A) and 120 s (Figure 3.3.8 B) adsorptive pre-concentration times. It is observed that as more HEWL was added, the resulting desorption peak increased but also shifted to a less positive potential. This produced a semi-logarithmic curve when plotted with HEWL concentration and has been observed in other previous studies using pulse voltammetry.^{38,39} This may be attributed to kinetic effects in the DPV detection mechanism, which is supported by the observed broadening of peaks at the higher concentrations. Nevertheless, a linear increase of peak current with concentration was observed at low concentrations, in the range of 0.02 to 0.12 μM HEWL.

Table 3.3.1 shows the summary of analytical characteristics of the various voltammetric techniques employed in this study of a solvent-cast aqueous-organogel μ ITIES array for HEWL detection. In order to compare all techniques utilized, all the calculated limits of detection were based on three times the standard deviation of the blank (n=3) divided by the slope of the straight-line calibration plots. It is seen that from 4.5 μ M for CV, the LOD has improved to 0.030 μ M for AdSV, mainly due to the additional 300 s pre-concentration step. For the AdDPSV, which produced semi-logarithmic curves, the linearity observed on the lower concentrations were used to determine the sensitivity of the calibration (n=3).

Table 3.3.1 Summary of analytical performance of the solvent-casted organogel microarray for different voltammetric techniques used.

Detection Method	Pre-concentration time / s	Sensitivity (calibration graph) / nA μ M ⁻¹	Number [†] of Points (n)	Limit of Detection (LOD) / μ M	Concentration Range / μ M	Correlation Coefficient (R)
CV	0	0.0109	6	4.5	5-25	0.985
AdSV	300	1.62	9	0.030	0.02-0.84	0.993
AdDPSV	60	4.57	7 (3)	0.017	0.02-0.60	0.990
AdDPSV	120	3.55	7 (3)	0.014	0.02-0.60	0.992
AdDPSV	300	3.42	7 (3)	0.010	0.02-0.60	0.998

[†]Corresponds to the number of HEWL concentrations used providing the data points fitted for the linear regression. Since AdDPSV resulted in semi-logarithmic curves, the slope across the lowest three (3) concentrations was used.

Overall, longer pre-concentration times for the AdDPSV has further enhanced the limit of detection from 0.017 μ M with only 60 s pre-concentration time, to 0.014 μ M after 120 s pre-concentration time, and to 0.010 μ M following 300 s pre-concentration time. However, the desorption peaks for the 300 s pre-concentration time were already broadened. In terms of precision, the relative standard deviation was 3.8% for CV (n=4, 15 μ M HEWL), 7.6% for AdSV (n=10, 0.30 μ M HEWL) at 300 s pre-concentration, while it was 3.2%, 7.4% and 5.8% (n=6, 0.02 μ M HEWL) for AdDPSV at 60, 120 and 300 s pre-concentration times, respectively.

Furthermore, a comparison of the heat-treated organogel versus the solvent-casting organogel was done using AdDPSV with 400 s pre-concentration time. The results (not shown) produced fairly similar response. Hence, the improved limit of

detection and enhanced sensitivity due to improved signal-to-noise ratio, are all attributed to the detection method used that combines the benefits of pre-concentration, stripping voltammetry and differential pulse voltammetry.

3.4 Conclusions

Solvent-casting of PVC with THF was investigated as an alternative method to gel the organic phase in the formation of a μ ITIES array for protein detection. The behaviour was examined by cyclic voltammetry, adsorptive stripping voltammetry and adsorptive differential pulse stripping voltammetry for its application to HEWL detection. CV results indicate that HEWL is identified with a distinct peak on the reverse scan at *ca.* 0.68 V. Investigation of the optimal adsorption potential for HEWL at this type of organogel shows that maximum protein adsorption happens at a positive potential just below the potential range where background electrolytes are transferred. With a pre-concentration time of 300 s for AdSV, a detection limit of 0.03 μ M was achieved. Differential pulse voltammetry was also utilized to further improve the limit of detection for this solvent-cast aqueous-organogel system. The use of AdDPSV enabled the same (0.017 μ M) detection limit with only 60 s pre-concentration and still better limits were obtained following 120 s (0.014 μ M) and 300 s (0.010 μ M) pre-concentration. This work further supports the capacity of the use of electrochemistry at the μ ITIES array as a label-free bioanalytical tool. However, studies on selectivity and sample matrix effects remain as challenges currently being addressed.

Chapter 4. Electrochemical Behaviour of Fucoidan at Polarized Liquid-Organogel Microinterfaces¹

4.1 Introduction

Fucoidan is a class of sulfated polysaccharide derived from a variety of brown algae and some marine invertebrates, including sea cucumber and sea urchins.²⁰⁰ They primarily contain either $\alpha(1-3)$ - or alternating $\alpha(1-3)$ - and $\alpha(1-4)$ -linked L-fucose components, with acetyl groups, sulfates or various branch points present at different locations along the polymer chain.²⁰¹ Aside from L-fucose monomers, small amounts of other monosaccharides, such as galactose, glucose, mannose and xylose, are also present in the polymer backbone of most fucoidans.²⁰² In addition, the method of extraction, the source and even the species of algae can affect the composition and properties of the isolated fucoidan, such as molecular weight distribution, charge density and degree of branching.²⁰³⁻²⁰⁵ However, despite such differences, they are all negatively charged polyelectrolytes.²⁰⁶

The uses of fucoidan are diverse and have been the focus of several studies, ranging from biological and biomedical activities to food and nutraceutical applications. For instance, fucoidan was found to have higher antioxidant capacity and higher dietary fibre content than some commercial non-fucoidan nutraceutical counterparts,²⁰⁷ as discussed in a recent review.²⁰⁸ Fucoidan was found to induce apoptosis of some human cancer cells (colon, urinary bladder, and lymphoma cancer cells²⁰⁹⁻²¹¹) and was also investigated for other cancer therapies.^{212,213} Moreover, fucoidan was reported to help minimize osteoarthritis,²¹⁴ to have immunomodulatory effects²¹⁵ and to inhibit retroviruses such as the herpes simplex virus and the human immunovirus (HIV).²¹⁶⁻²¹⁸ Given its range of practical applications, a simple and direct detection method for measuring the presence of fucoidan is desirable. In order to establish fucoidan's bioactivity, quantitative measurements are required in blood or

¹ This material was published as: Felisilda, Bren Mark B., Eva Alvarez de Eulate, Damien N. Stringer, J. Helen Fitton, and Damien WM Arrigan. "Electrochemical behaviour at a liquid-organogel microinterface array of fucoidan extracted from algae." *Analyst* 142, no. 17 (2017): 3194-3202. DOI: 10.1039/C7AN00761B and is available via open access (CC BY-NC).

urine samples to elucidate its metabolic pathway.²⁰⁸ Techniques currently used for fucoidan detection include electrophoresis coupled with infra-red and Raman spectroscopies,^{219,220} fluorometric assays^{221,222} and enzyme-linked immunosorbent assay (ELISA) using anti-fucoidan antibodies.^{223,224} However, the spectroscopic studies mentioned did not report any detection limit while the ELISA approach afforded 4.00 mg L⁻¹ and 12.98 mg L⁻¹ in serum for a 10% and 75% pure fucoidan supplements²²³ while the sandwich ELISA reported 97-98% recovery of 20-80 ng mL⁻¹ of *Cladosiphon okanuramus* fucoidan in human serum and urine.²²⁴ Generally, ELISA need sample pre-treatment, several washing steps and several hours of incubation. The more recent fluorescent assays reported a detection limit of 0.025 ng μ L⁻¹ with a cationic nucleic acid dye in a buffer solution²²¹ while the other one made use of Heparin Red as the fluorescent probe and detect 0.5 – 20 μ g mL⁻¹ of fucoidan as well as test it in human plasma.²²²

The need for fast, low-cost and sensitive methods has focused attention on electrochemical detection platforms. Potentiometric ion-selective electrodes (ISEs) employing a polymer membrane doped with tridodecylmethylammonium (TDMA⁺) have been explored to detect negatively charged macromolecules like carrageenan,²²⁵ DNA,²²⁶ heparin^{53,227} and pentosan polysulfate.²²⁸ Kim *et al.*²²⁹ investigated several species of fucoidan using polyion-sensitive ISEs. They found that the species of algae and the extraction method used influenced the charge density and polymer backbone composition of fucoidan, and consequently the ISE response. Detection at concentrations as low as *ca.* 2.5 μ g mL⁻¹ fucoidan using titrimetry was reported.²²⁹

In recent decades, there has been an increased interest in the electrochemistry of the interface between two immiscible electrolyte solutions (ITIES) as the basis for new analytical strategies.^{188,230} Since electrochemistry at the ITIES offers advantages such as label-free detection and amenability to miniaturization,⁹⁰ it has been employed in the study of biological macromolecules such as proteins^{189, 231} and carbohydrates.²³² A range of polysaccharides has been studied by this approach. The sulphated polysaccharide heparin has been studied by a number of groups.^{50-52,137} It was found that adsorption at the interface depended on binding with an ionophore,⁵² which can be the organic electrolyte cation.¹³⁷ Guo *et al.* studied several hydrophobic quaternary ammonium cations as heparin selective ionophores and found that heparin adsorption was facilitated via complexation with such cations.⁵⁰ Yudi and colleagues evaluated

several cationic polysaccharides (chitosan, polyquaternium-4, diethylaminoethyl dextran, polyquaternium-10) at the ITIES and found relationships between the polymer structure and adsorption at the interface.¹⁴³ They observed no transfer processes at the interface when the charged groups were directly connected to the monomers; however when attached via flexible linkers, charge transfer processes consistent with enhanced counterion interactions were observed¹⁴³. This group also explored complex formation between cationic cellulosic polymers and anionic fluorinated surfactants at the ITIES, finding that the binding was dominated by electrostatic and hydrophobic interactions.¹⁴⁴ Moreover, it was revealed that cationic polysaccharides adsorption at the interface included interaction with the organic phase electrolyte anion.²³³

The present work explores the electrochemistry of fucoidan at the ITIES and examines whether this is a viable approach for its quantitative detection. Fucoidan from two species of brown algae were investigated, *Fucus vesiculosus* (bladderwrack) and *Undaria pinnatifida* (wakame), using a liquid-organogel microinterface array (i.e. μ ITIES array) for voltammetric characterization and detection. The results reveal that adsorption and counter-ion interactions are important in the electrochemical behaviour. Using the discovered behaviour, a detection limit of $1.8 \mu\text{g mL}^{-1}$ was achieved for fucoidan from *Undaria p.* in 10 mM NaOH and $2.3 \mu\text{g mL}^{-1}$ for this fucoidan in pH-adjusted synthetic urine.

4.2 Experimental Method

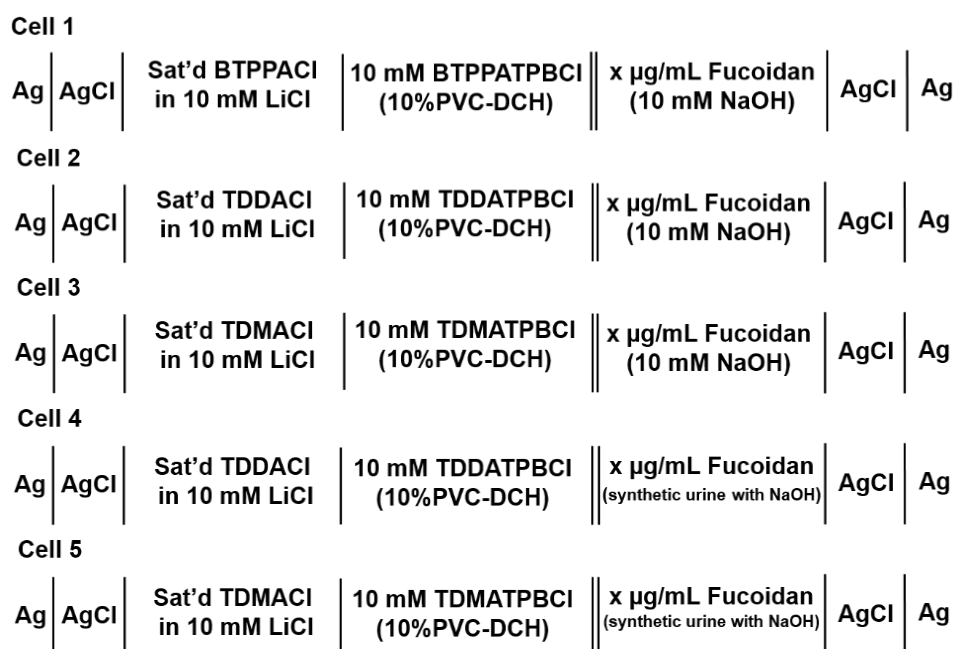
4.2.1 Reagents

All reagents were obtained from Sigma-Aldrich Australia Ltd and were used as received, unless stated otherwise. The organic phase was prepared by dissolving bis(triphenylphosphoranylidene) tetrakis(4-chlorophenyl) borate (BTPPATPBCl), tetradodecylammonium tetrakis(4-chlorophenyl) borate (TDDATPBCl) or tridodecylmethylammonium tetrakis(4-chlorophenyl) borate (TDMATPBCl) in 1,6-dichlorohexane (1,6-DCH). This electrolyte solution (10 mM) was then gelled by the addition of 10% w/v low molecular weight poly(vinylchloride) (PVC).¹⁵⁷ The organic electrolyte salt BTPPATPBCl was prepared by metathesis of bis(triphenylphosphoranylidene)ammonium chloride (BTPPACl) and potassium

tetrakis(4-chlorophenyl)borate (KTPBCl).¹⁶⁴ The organic electrolyte salt TDMATPBCl was also prepared by metathesis of equimolar tridodecylmethylammonium chloride (TDMACl) and potassium tetrakis(4-chlorophenyl)borate (KTPBCl). Fucoidans extracted from two brown algae species, *Undaria pinnatifida* and *Fucus vesiculosus*, were provided by Marinova Pty Ltd., with purities of 96% and 98%, respectively (both pharma-grade, de-acetylated). These were stored at 4 °C. Fucoidan stock solutions were prepared weekly in aqueous 10 mM NaOH and stored at 4 °C. Likewise, tetrapentylammonium (TPenA⁺) chloride was prepared in 10 mM NaOH. A synthetic urine mixture²³⁴ containing ammonium chloride (1.00 g L⁻¹), calcium chloride dihydrate (1.103 g L⁻¹), creatinine (1.10 g L⁻¹), potassium chloride (1.60 g L⁻¹), potassium dihydrogen phosphate (1.40 g L⁻¹), sodium chloride (2.295 g L⁻¹), sodium sulfate (2.25 g L⁻¹) and urea (25 g L⁻¹) was prepared and modified to pH 12 with NaOH solution as needed. All aqueous solutions were prepared with de-ionised water from a USF Purelab plus UV system (resistivity: 18.2 MΩcm).

4.2.2 Apparatus

Electrochemical experiments were performed with an AUTOLAB PGSTAT302N electrochemical station (Metrohm, The Netherlands) with its NOVA software interface. The μ ITIES array used was defined by a micropore array silicon membrane,¹⁷⁴ which consisted of thirty micropores in a hexagonal arrangement, each pore having a diameter of 22.4 μ m, a pore centre-to-pore centre distance of 200 μ m and membrane thickness of 100 μ m. The geometric area of the microinterface array (i.e. total cross-sectional area of the micropores) was 1.18×10^{-4} cm². These microporous silicon membranes were sealed onto the lower orifice of a glass cylinder using silicone rubber (acetic acid curing Selley's glass silicone). The organogel was introduced into the silicon micropore arrays via the glass cylinder with the aid of a pre-warmed glass Pasteur pipette. The set-up was then set aside for at least 1 hour before use. When ready, the organic reference solution (composition: saturated BTTPACl, TDDACl or TDMACl in 10 mM LiCl) was placed into the glass cylinder so as to sit on top of the gelled organic phase. The organogel/silicon membrane assembly was then immersed into the aqueous phase (10 mM NaOH, fucoidan in 10 mM NaOH, and/or TPenA⁺ in 10 mM NaOH) and voltammetric experiments were implemented. Scheme 1 summarizes the electrochemical cells employed.



Scheme 4.2.1 Schematic representation of the electrochemical cells employed, where x represents the fucoidan concentrations employed in the study.

4.2.3 Electrochemical Measurements

A pair of Ag/AgCl electrodes, one in each phase, were used for all measurements. Cyclic voltammetry (CV) and adsorptive stripping voltammetry (AdSV) were carried out at a scan rate of 5 mV s^{-1} unless noted otherwise. Other parameters such as fucoidan concentration, applied potential, and duration of the pre-concentration step were varied accordingly. The calculated limits of detection were based on three times the standard deviation of the blank ($n=3$) divided by the slope of the best-fit linear calibration line. All potentials were transposed to the Galvani potential scale based on the experimental mid-point transfer potential of TPenA⁺ and its formal transfer potential (-0.35 V) in the water | 1,6-dichlorohexane system.²³⁵

4.3 Results and Discussions

4.3.1 Cyclic Voltammetry

Initial studies to probe the electrochemical behaviour at the µITIES array of the fucoidans extracted from *Undaria pinnatifida* and *Fucus vesiculosus* were conducted using cyclic voltammetry (CV). Various aqueous phase pH values were surveyed initially and it was found that the best response for analytical performance was observed at pH 12 (10 mM NaOH). Figure 4.3.1 shows CVs of *Undaria p.*

fucoidan studied using Cells 1-3 (see Scheme 1). Figure 4.3.1 (A) (black line) illustrates the CV obtained when 1 mg mL^{-1} *Undaria p.* fucoidan was present in the aqueous phase, while inset (top right) is that of 1 mg mL^{-1} *Fucus v.* fucoidan. Both figures also show the voltammograms obtained when only the background electrolytes (dashed grey line) were present. On scanning from positive toward more negative potentials, the transfer of background electrolytes across the ITIES was indicated by the decrease of negative current going towards more negative potentials. This process at the negative potentials corresponds to the transfer of the anions (OH^-) from the aqueous phase to the organogel and the cations (BTPPA^+) from the organic to the aqueous phase, whilst at the positive end of the voltammograms the increase in current is due to the opposite effect, i.e. Na^+ ($\text{aq} \rightarrow \text{org}$) and TPBCl^- ($\text{org} \rightarrow \text{aq}$) transfers. A sharp peak response was observed at *ca.* -0.50 V on the reverse scan of the CV for *Undaria p.* fucoidan (Figure 4.3.1 A), while an insignificant broad wave was observed for *Fucus v.* fucoidan at *ca.* -0.45 V (Figure 4.3.1 A inset top right). The different responses obtained may be attributed to the structural differences of the two fucoidan species.²³⁶ *Undaria p.* fucoidan contains more galactose and has a higher peak molecular weight distribution. This may introduce a conformational flexibility of *Undaria p.* fucoidan that enables a higher affinity for the organic cation of the organogel electrolyte phase. This also bears some resemblance to the behaviour of proteins at the ITIES, which can alter their conformation upon interaction with the organic phase.^{162,191,237}

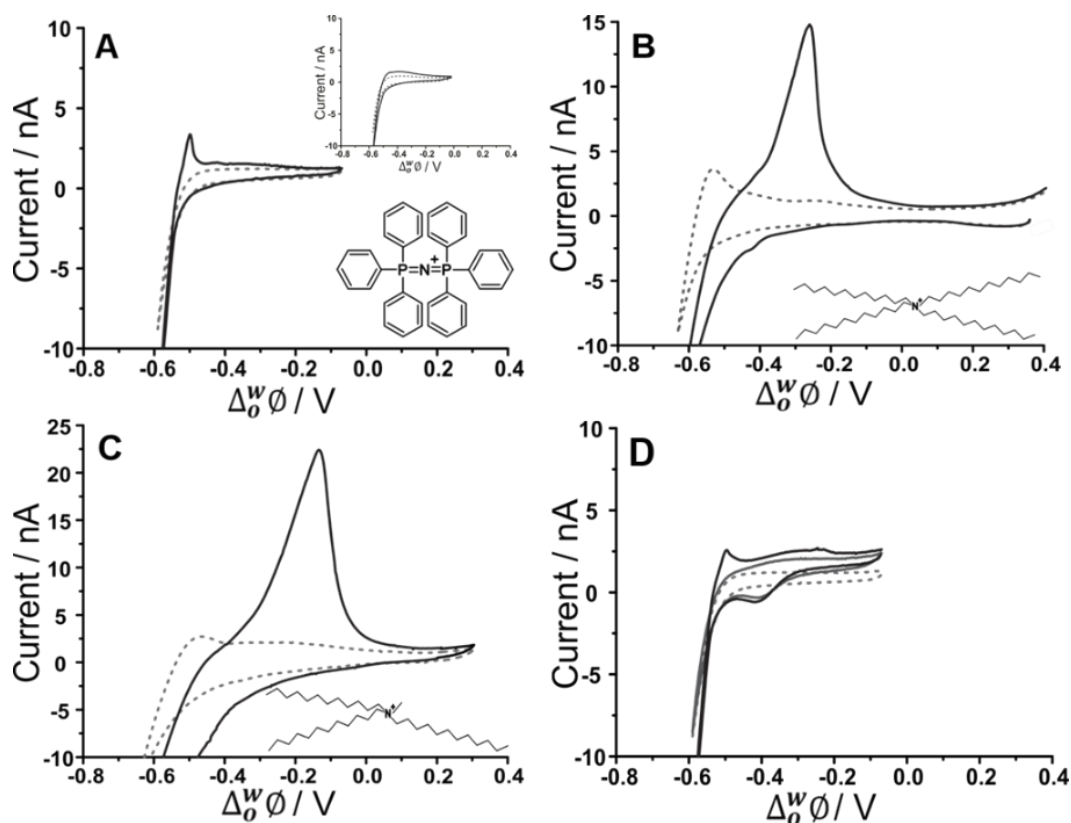


Figure 4.3.1 Cyclic voltammograms of 10 mM NaOH (pH 12) in the absence (grey dashed line) and presence (black line) of 1 mg mL^{-1} *Undaria p. fucoidan* using (A) Cell 1 and (top inset) *Fucus v.*; (B) Cell 2 and (C) Cell 3 all in Scheme 1. (D) CVs recorded in the absence (grey dashed line) and the presence of $10 \text{ }\mu\text{M}$ TPenA⁺ (grey bold line) and with added 1 mg mL^{-1} *Undaria p. fucoidan* (black line) using Cell 1. Scan rate: 5 mV s^{-1} . Scan direction: towards negative potential; species transferred at the negative potential limit: ($\text{OH}^- \text{ aq} \rightarrow \text{org}$), (BTPPA⁺/ TDDA⁺/ TDMA⁺ org \rightarrow aq). Bottom inset: Chemical structures of (A) BTPPA⁺; (B) TDDA⁺; (C) TDMA⁺.

To further investigate counterion-polyion interaction, two alternative organic phase electrolyte cations, as described in Cells 2 and 3 (see Scheme 4.2.1) were used in order to determine whether this influences the behaviour of the fucoidan polyelectrolyte at the polarized aqueous-organogel interface. Tetradodecylammonium (TDDA⁺) and tridodecylmethylammonium (TDMA⁺) replaced the commonly used organic cation bis(triphenyl)phosphoranylidene (BTPPA⁺). Figure 4.3.1 (B) illustrates the CV obtained when 1 mg mL^{-1} *Undaria p. fucoidan* was present in the aqueous phase and 10 mM TDDATPBCl in the organic phase, while Figure 4.3.1 (C) shows the CV when 1 mg mL^{-1} *Undaria p. fucoidan* was present in the aqueous phase and 10mM TDMATPBCl was in the organic phase. With the use of these alkylammonium

cations in the organic phase, the observed potential window was extended on the negative potential side. This can be attributed to the fact that TDDA⁺ transfers at a more negative potential²³⁸ than BTPPA⁺ and, since it is structurally similar, TDMA⁺ was expected to do the same. However, the major difference observed was the intensity of the *Undaria p. fucoidan* response in the presence of TDDA⁺ (Figure 4.3.1 B) and TDMA⁺ (Figure 4.3.1 C) relative to BTPPA⁺ (Figure 4.3.1 A). In the presence of *Undaria p. fucoidan* (Figure 4.3.1 A-C), the distinct peaks observed on the reverse scans signify that *Undaria p. fucoidan* is electrochemically active at the μ ITIES array. A similar response was observed by Samec's group¹³⁷ for another sulfated polysaccharide, heparin. The peaks exhibit a rapid decrease in current to the background levels, consistent with consumption of a finite amount of material at the interface. This behaviour is typical of an adsorption/desorption process.¹ This reverse scan peak is therefore proposed to be the desorption of *Undaria p. fucoidan* from the interface which, in turn, suggests that it undergoes electroadsorption during the forward scan. On the other hand, Figure 4.3.1 (D) shows a voltammogram when 10 μ M TPenA⁺ (grey solid line) was present in the aqueous phase. It shows a steady-state voltammogram on the scan towards the positive potentials, indicative of radial diffusion,²⁷ and a peak-shaped voltammogram on the scan towards negative potentials, representative of linear diffusion. This voltammogram indicates the mass transport-controlled transfer of TPenA⁺ at the μ ITIES array formed by the silicon micropore array membranes, in agreement with previous work⁹⁷ as well as that the fucoidan is not adsorbed in the potential region where TPenA⁺ transfers across the ITIES.

CVs of increasing *Undaria p. fucoidan* concentration (10-1000 μ g mL⁻¹ for BTPPA⁺ and TDDA⁺; 5-25 μ g mL⁻¹ for TDMA⁺) are shown in Figure 4.3.2. Figure 4.3.2 (A) shows the experiment with an organic phase containing 10 mM BTPPA⁺. On the forward scan (towards negative potential), the previously-seen (Figure 4.3.1 A) increase in negative current is observed despite the added *Undaria p. fucoidan*. Meanwhile, on the reverse scan, the peak height increased with increasing concentrations. Once again, the peak shapes are suggestive of a desorption process rather than a diffusion-controlled process. As a result, it is suggested that the response mechanism involves adsorption of *Undaria p. fucoidan* at the interface during the negative-going forward scan, possibly combined with the interaction of the polyanion with the cation of the organic phase electrolyte (BTPPA⁺), as discussed⁵² for heparin.

The peak on the reverse scan (toward positive potential) is then attributed to a desorption process encompassing the dissociation of the complex formed between the polyanionic *Undaria p. fucoidan* and the organic electrolyte cation. Counterion-polyion interactions have been observed in several polyelectrolyte systems at the ITIES,^{144,151,233} and may reflect a generic mechanism for the electrochemical detection of polyionic analytes.

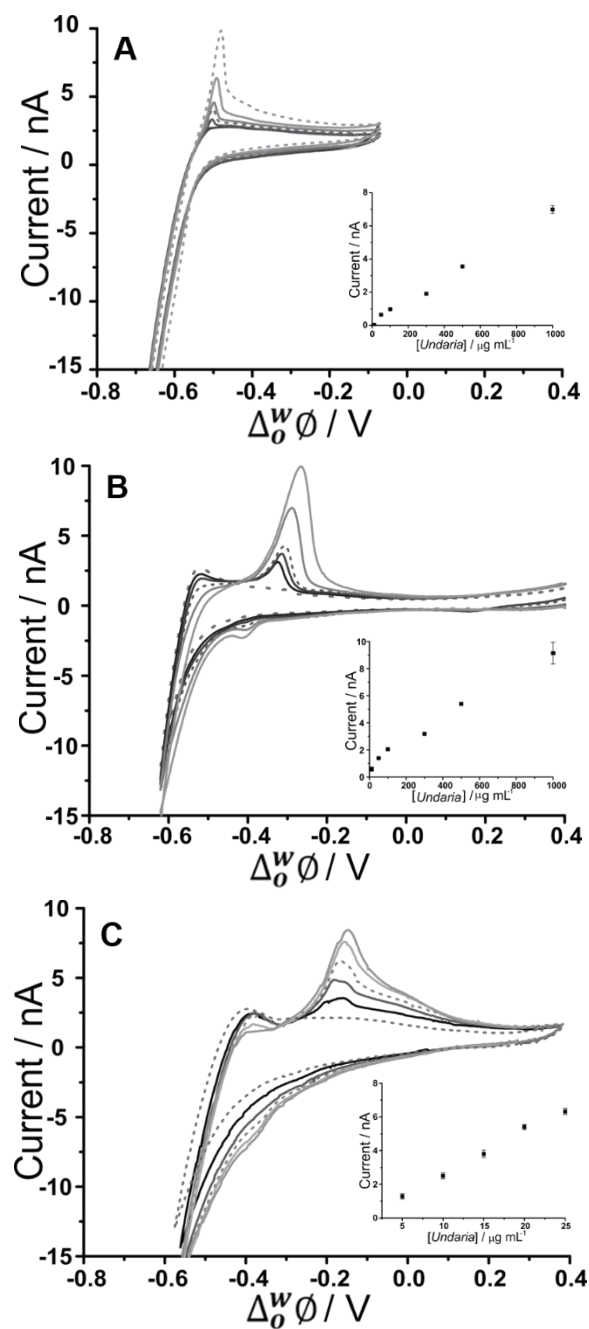


Figure 4.3.2 Cyclic voltammograms of different *Undaria p. fucoidan* concentrations (10-1000 $\mu\text{g mL}^{-1}$ for A&B; 5-25 $\mu\text{g mL}^{-1}$ for C in 10mM NaOH (pH 12). Cell 1, 2 and 3 respectively (Scheme 1). Scan rate: 5 mV s^{-1} . Inset: Plot of peak current against *Undaria p. fucoidan* concentration. Scan direction: towards negative potential; species transferred at the negative potential limit: ($\text{OH}^- \text{aq} \rightarrow \text{org}$), ($\text{BTPPA}^+ / \text{TDDA}^+ / \text{TDMA}^+ \text{org} \rightarrow \text{aq}$).

CVs of increasing concentrations (10-1000 $\mu\text{g mL}^{-1}$) of *Undaria p. fucoidan* in contact with organic phases containing 10 mM TDDA⁺ and (5-25 $\mu\text{g mL}^{-1}$) 10 mM TDMA⁺ are shown in Figure 4.3.2 (B) and 4.3.2 (C), respectively. A peak was observed at *ca.* -0.30 V for 10 $\mu\text{g mL}^{-1}$ *Undaria p. fucoidan* with TDDA⁺ and at *ca.* -

0.15 V for $5 \mu\text{g mL}^{-1}$ *Undaria p. fucoidan* with TDMA^+ whereas in the presence of organic phase BTPPA^+ , a peak was observed only at the higher concentration of $50 \mu\text{g mL}^{-1}$ (Figure 4.3.2 A). In the presence of the alkylammonium organic phase cations, the improvement in response might be attributed to a stronger interaction between *Undaria p. fucoidan* with TDMA^+ or TDDA^+ than with BTPPA^+ . Sulfated polysaccharides, like heparin,¹³⁷ are known to form complexes with cations that serve as ionophores;^{51,137} such studies have determined that weak heparin-cation interactions were observed when BTPPA^+ was used in the organic phase but an improved interaction was seen when hexadecyltrimethylammonium was used. Structurally, it was suggested there was more flexibility for the heparin to interact with hexadecyltrimethylammonium than with BTPPA^+ due to steric hindrance from the phenyl rings in the latter which surround and shield the cationic centre.¹³⁷ Another study, by Guo *et al.*,⁵⁰ found that heparin adsorption at the ITIES was favourable when there was less steric hindrance within the ionophore so that the positive charge of the quaternary ammonium nitrogen was more accessible for electrostatic binding with heparin's negative charges.

A similar phenomenon may be responsible for the observed enhanced electrochemical signal for fucoidan when TDDA^+ is employed in the organic phase, and more so with TDMA^+ , since there are structural similarities amongst the three cations hexadecyltrimethylammonium, TDDA^+ and TDMA^+ . This was also the case when Meyerhoff and co-workers²²⁸ used TDMA^+ based polyion-sensitive potentiometric electrodes to detect pentosan polysulfate and they found out that the more available charge density in TDMA^+ improves the strength of the ion-pairing interaction with the target polyion. These results indicate that fucoidan interaction becomes more favourable in the order of $\text{BTPPA}^+ < \text{TDDA}^+ < \text{TDMA}^+$ as the organic electrolyte cation. The interaction at the ITIES is therefore suggested to be the complexation of *Undaria p. fucoidan* with TDDA^+ or TDMA^+ at the microinterface, followed by adsorption of the complex during the forward scan (in the negative direction); this adsorbed complex is subsequently desorbed during the reverse scan (in the positive direction).

4.3.2 Adsorptive Stripping Voltammetry

Adsorptive stripping voltammetry (AdSV) has been implemented at the microITIES as a detection tool for several polyelectrolytes.^{50,148,159} This technique entails the application of a constant potential to drive adsorption for a defined time, which serves to pre-concentrate the analyte at the interface; a subsequent voltammetric scan, the detection step, desorbs the analyte from the interface and produces a current peak as the analytical signal. In the case of fucoidan, pre-concentration at a suitable negative potential, to promote adsorption, followed by scanning to more positive potentials, to desorb it from the interface, can produce a peak current that is dependent on concentration and adsorption time. For optimization of the fucoidan adsorption parameters, the effect of applied potential during the adsorption step was first examined. Chosen potential values were applied for a certain time and were followed with a voltammetric scan towards positive potentials in order to desorb the fucoidan and produce a stripping voltammogram.

Figure 4.3.3 displays the effect of changing the adsorption potential on the detection of *Undaria p.* fucoidan in conjunction with the three different organic phase cations. In the presence of organic phase BTPPA⁺, at less negative adsorption potentials, the stripping voltammograms display no clear peak, but at adsorption potentials ≤ -0.55 V (Figure 4.3.3 A), a well-defined stripping peak is present, illustrating the influence of potential on the adsorption process. In a similar way, defined stripping peaks were observed when the organic phase cation BTPPA⁺ was replaced with TDDA⁺ or TDMA⁺, although in these cases the peaks started to appear following adsorption at a more positive potential (≤ -0.50 V for TDDA⁺ and ≤ -0.40 V for TDMA⁺, Figure 4.3.3 (B) and 4.3.3 (C, respectively). This difference can be attributed to the degree of interaction between the fucoidan and the organic electrolyte cation, as already discussed in the CV studies section.

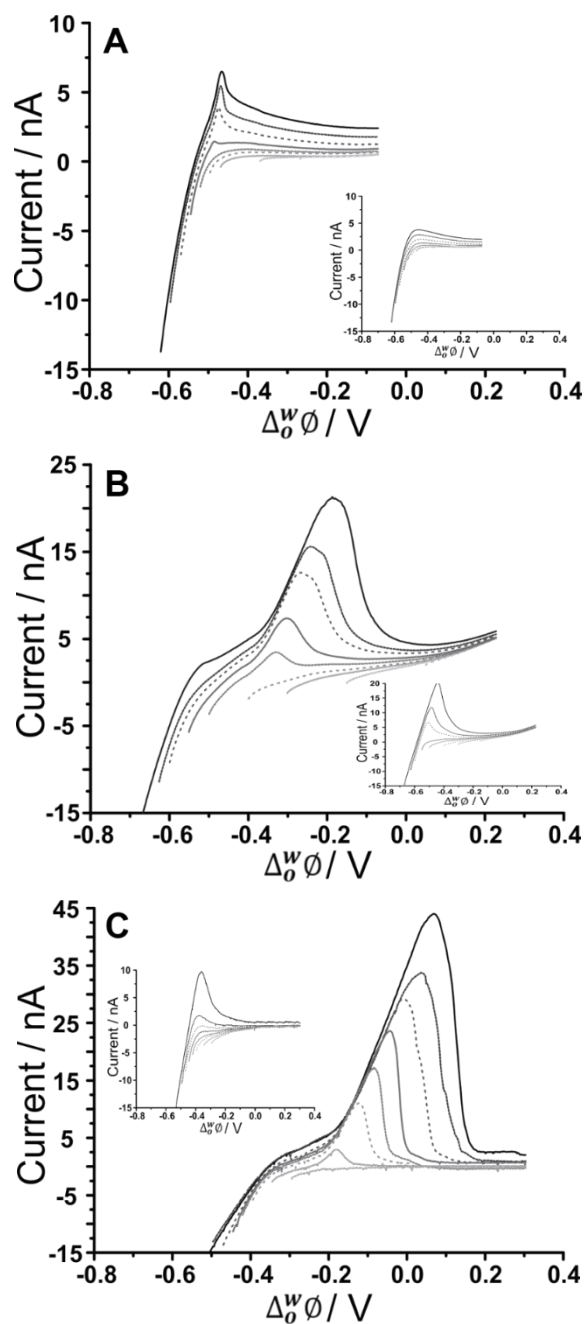


Figure 4.3.3 AdSV in the presence and absence (inset) of $500 \mu\text{g mL}^{-1}$ *Undaria p. fucoïdan*, in aqueous phase of 10 mM NaOH (pH 12) following adsorption at different potentials. Adsorption time: 60 s, (A) Cell 1, (B) Cell 2, and (C) Cell 3 (Scheme 1). Scan rate: 5 mV s^{-1} .

As seen in the CV experiments, the AdSV peaks exhibit the shape of a surface-confined process, consistent with adsorption/desorption at the interface. One important point to consider in optimizing the applied potential for adsorption is that the background electrolyte signal, which occurs near the *Undaria p. fucoïdan* adsorption region, can also be minimised. Thus, the adsorption potential is crucial to both maximising the analytical signal and minimising the background signal. From the

data in Figure 4.3.3 (A), the optimised adsorption potential was determined to be -0.59 V for *Undaria p.* fucoidan in the presence of organic phase BTPPA^+ ; the same value was found for *Fucus v.* fucoidan (data not shown). AdSV following pre-concentration at more negative potentials resulted in a stripping peak with a shoulder, which is due to background electrolyte transfer free of fucoidan interactions (Figure 4.3.3 A inset). In the presence of organic phase TDDA^+ or TDMA^+ , the best adsorption potentials, a compromise between the fucoidan desorption peak and the background electrolyte contribution, were found to be -0.62 V for *Undaria p.* fucoidan (Figure 4.3.3 B) and *Fucus v.* fucoidan (Cell 2, Scheme 4.2.1) as well as -0.47 V (Figure 4.3.3C) for *Undaria p.* fucoidan (Cell 3, Scheme 4.2.1). These optimised adsorption potentials were utilized to determine the effect of varying adsorption time on the peak currents.

Moreover, the effect of varying the adsorption time was investigated for the different organic cations. No stripping peak was observed for $20 \mu\text{g mL}^{-1}$ *Undaria p.* fucoidan when 5 s adsorption time was employed with BTPPA^+ organic phase cation. However, AdSV with 60 s adsorption time at the same concentration produced a small peak which increased with the adsorption time. A similar trend was observed for *Fucus v.* fucoidan when $300 \mu\text{g mL}^{-1}$ was present in the aqueous phase. Note that a blank analysis was performed after each AdSV to check if any carryover of fucoidan was present; no peaks indicating such carryover were observed. In comparison to the previous experiment with BTPPA^+ as the organic electrolyte cation, longer pre-concentration times with TDDA^+ revealed no significant current increase in the blank AdSVs. Accordingly, the chosen adsorption times were 5, 60 and 180 s for both TDDA^+ and TDMA^+ organic phase cations. A current peak at *ca.* -0.30 V was observed when $20 \mu\text{g mL}^{-1}$ *Undaria p.* fucoidan was present in the aqueous phase following 60 s pre-concentration in combination with organic phase TDDA^+ . However, for a 5 s pre-concentration time, a current peak at *ca.* -0.20 V was observed for the same concentration of *Undaria p.* fucoidan with TDMA^+ in the organic phase. This peak current increased with the pre-concentration time. Based on these experiments, an adsorption time of 180 s was chosen for subsequent studies.

Furthermore, increasing fucoidan concentrations were investigated using the adsorption parameters. Figure 4.3.4 shows the peak current versus *Undaria p.* fucoidan concentration plots with the different organic phase cations. The slope of the calibration plots becomes steeper in the order $\text{BTPPA}^+ < \text{TDDA}^+ < \text{TDMA}^+$, which

indicates that sensitivity is improved with TDMA⁺ as the organic cation. This is in agreement with the same observation from the CV studies in terms of the interaction between the fucoidan and the corresponding organic cations. The lowest detected *Undaria p.* fucoidan concentrations using AdSV were 10, 5 and 3 $\mu\text{g mL}^{-1}$ with BTPPA⁺, TDDA⁺, and TDMA⁺ cations, respectively. Combined AdSV with organic phase TDMA⁺ afforded a calculated detection limit of 1.8 $\mu\text{g mL}^{-1}$ for *Undaria p.* fucoidan.

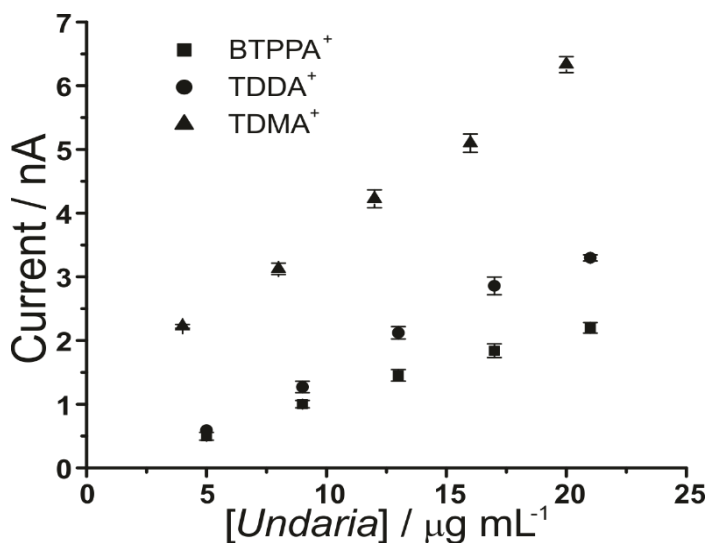


Figure 4.3.4 Plot of peak current versus *Undaria p.* fucoidan concentrations using the optimized adsorption potential for each organic cation. Adsorption time: 180 s. Cells 1, 2 and 3 (Scheme 1).

4.3.3 Matrix Effects

As fucoidan is commonly used as an ingredient in nutritional supplements,²⁰⁸ detection in physiological matrices, such as blood serum or urine, has been the subject of study.²²⁴ In the present study, synthetic urine was evaluated as a matrix for the detection of fucoidan. Synthetic urine was prepared as described elsewhere²³⁴ and was used as the aqueous phase of the electrochemical cell (see Cell 4 and 5, Scheme 4.2.1). It was found that some components of the synthetic urine decreased the potential window when they were added individually to the 10 mM NaOH aqueous phase; specifically, the cations (NH_4^+ , K^+ , Ca^{2+}) were found to transfer at lower potentials. Figure 4.3.5 (A) shows a CV of the prepared pH-adjusted (pH 12) synthetic urine (black solid line) overlaid on the CV recorded when 10 mM NaOH (grey dashed line) was the aqueous phase. This shows that the potential window was shorter when the synthetic urine was present, due to the easier transfer of some of its component

ions. Despite the decreased potential window, it was found that, on spiking *Undaria p. fucoidan* into the synthetic urine aqueous phase (pH adjusted with NaOH), detection of $100 \mu\text{g mL}^{-1}$ *Undaria p. fucoidan* was possible using AdSV with 10 mM TDDA⁺ in the organic phase. This is higher than achieved using a pure electrolyte aqueous phase so the other alternative organic phase cation, TDMA⁺ was utilized based on the above observations of better interaction with *Undaria p. Fucoidan* (see Cell 5, Scheme 4.2.1).

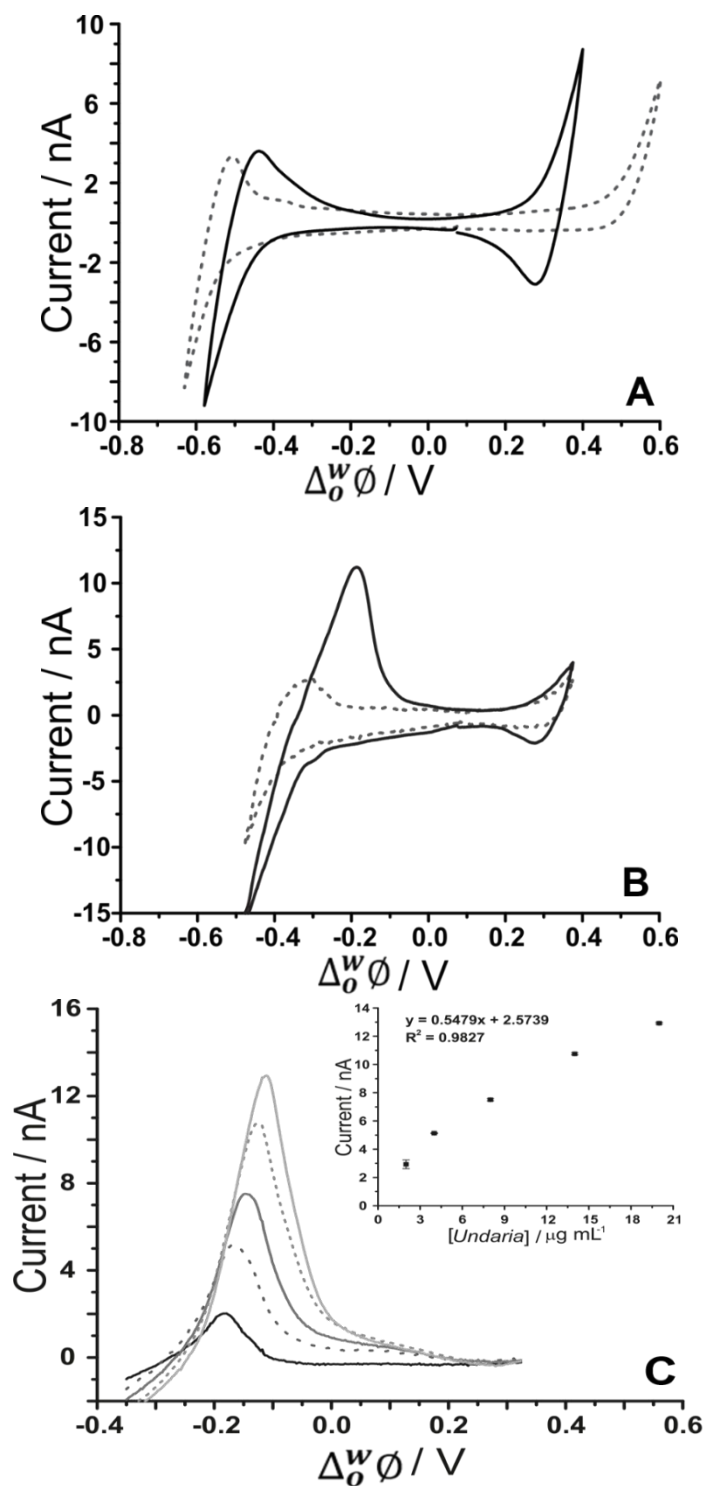


Figure 4.3.5 (A) Cyclic voltammograms of pH-adjusted synthetic urine (black line) in comparison to 10 mM NaOH (pH 12) (grey dashed line) as the aqueous phase. (B) CV in the absence (grey dashed line) and presence of 1 mg mL⁻¹ *Undaria p.* (black line) (Cell 5, Scheme1). (C) AdSV of increasing (background subtracted) *Undaria p. fucoidan* concentration (2-20 µg mL⁻¹). Adsorption potential: -0.35 V, pre-concentration time: 180 s, Cell 5 (Scheme 1), scan rate: 5 mV s⁻¹.

Figure 4.3.5 (B) shows the CV obtained with synthetic urine as the aqueous phase (dashed grey line) and with added 1 mg mL^{-1} *Undaria p. fucoidan* (black line). A peak at *ca.* -0.20 V on the reverse scan (going positive) reveals the detection of the fucoidan in the biomimetic matrix. The sharp peak shape of the CV is indicative of an adsorption/desorption process, as discussed above. The intensity of the peak was more pronounced in comparison to the same fucoidan concentration studied using the TDDA^+ cation in this matrix. This is attributed to the structural flexibility of TDMA^+ that better exposes the positive charge of the nitrogen centre for electrostatic interaction with the negatively charged fucoidan. This was also observed by other groups for sulfated polyelectrolytes in biological matrices.^{50,228} AdSV with optimised parameters (-0.35 V adsorption potential, 180 s pre-concentration time) was used to improve the detection limit. Voltammograms of increasing ($2\text{-}20 \text{ }\mu\text{g mL}^{-1}$) *Undaria p. fucoidan* concentration are displayed in Figure 4.3.5 (C). With the combined AdSV and enhanced interaction with TDMA^+ , a detection limit of $2.3 \text{ }\mu\text{g mL}^{-1}$ for *Undaria p. fucoidan* in the pH-adjusted synthetic urine matrix was achieved, which is comparable to the literature value of $2.5 \text{ }\mu\text{g mL}^{-1}$ achieved with potentiometric titrimetry²²⁹.

It is worthy to note that the presence of additional surface-active species, like proteins, would be detrimental to possible applications in real biological matrix analyses. The presence of additional surface-active species might compete with the target analyte for adsorption to the interface. This could alter the desorption voltammogram if its adsorption potential is near that of the fucoidan and consequently, this could lower the sensitivity. However, careful optimisation of the electrolyte and adsorption potential conditions might help to alleviate this problem as reported previously for insulin detection in the presence of serum albumin.¹⁹⁴

4.4 Conclusions

The electrochemical behaviour of fucoidan was investigated using voltammetry at a μITIES array. The CV of *Undaria p. fucoidan* presented a distinct peak on the reverse scan at *ca.* -0.50 V when the organic phase cation was BTPPA^+ . However, this potential shifted to *ca.* -0.30 V when the organic phase cation was replaced with TDDA^+ and to -0.175 V with TDMA^+ , as a result of the increasing binding strength between these organic phase cations and *Undaria p.* The peak shape

suggested it was a desorption process, consistent with adsorption during the forward scan to negative potentials. Investigation of the optimal adsorption potential for fucoidan at the interface revealed that maximum adsorption occurred at a potential just prior to the background electrolyte transfer. Using AdSV, the combination of TDMA⁺ in the organic phase and pre-concentration for 180 s afforded a limit of detection of 1.8 $\mu\text{g mL}^{-1}$ for *Undaria p.* fucoidan in 10 mM NaOH and 2.3 $\mu\text{g mL}^{-1}$ in a pH-adjusted synthetic urine solution. The behaviour identified here indicates the viability of using electrochemistry at the μITIES array as a label-free bioanalytical tool for the detection of fucoidan. Selectivity (i.e. differentiation between fucoidan species), targeting better cationic receptors in the organic phase and improving conditions with matrix effects are challenges that require further studies.

Chapter 5. Investigation of Sulfated Carbohydrates at a Liquid-Organogel Micro-Array

5.1 Introduction

Polysulfated carbohydrates are considered to be pharmaceutically important molecules because of their known biological activity.^{239,240} A good example of these substances are glycosaminoglycans (GAGs) which manage several biological processes by interacting with their protein binding counterparts via the latter's basic amino acid residues.^{239,241} Moreover, these highly sulfated and mostly negatively charged polysaccharides are major constituents in extracellular matrices of several tissues but they are also located inside as well as on the surfaces of cells.²⁴⁰ A number of these polysulfated carbohydrates are known for their biological activities. Specifically, heparan sulfate is known for signal transduction²⁴² while heparin is used for preventing blood coagulation.²⁴³ Synthetic counterparts are also known to be useful in the pharmaceutical industry as excipients or drug products.^{244,245} One of these synthetic sulfated carbohydrates is sucrose octasulfate or SOS and its structure is shown in Figure 5.1.1.

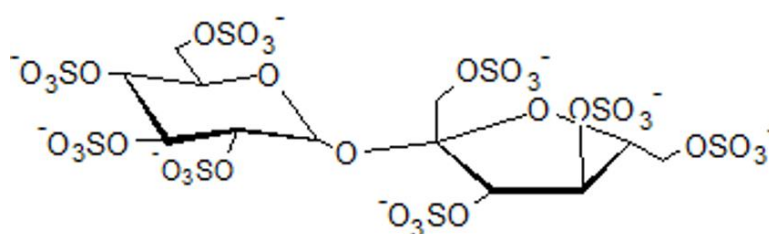


Figure 5.1.1 Chemical structure of sucrose octasulfate (SOS).

A form of SOS, specifically its aluminium salt, is famously called Sucralfate and is commonly utilized as treatment for duodenal ulcer.²⁴⁶ The heightened research interest for SOS can be traced from the proposition that it can promote wound healing²⁴⁷ by its role in the stabilization of fibroblast growth factor (FGF). Other studies report the new application of SOS and its analogues in cancer treatment and wound healing because of the crystallization of its sodium salt within the signal transduction pathway²⁴² as well as its moderate oral bioavailability.²⁴⁴ Conformational

changes to the amide I region of proteins' infrared spectrum were also found to be induced by SOS and sulfated GAGs.²⁴⁸

Knowing the growing application of SOS and related sulfated carbohydrates in the field of pharmaceuticals as well as its use of biological importance, a label-free detection method for measuring its presence would be vital. Current methods used to analyse these sulfated carbohydrates include mass spectrometry,^{249,250} enzymatic digestion or depolymerization followed by capillary electrophoresis (CE),^{251,252} high performance liquid chromatography (HPLC)²⁵³ with UV-Vis/fluorescence detection^{254,255} and nuclear magnetic resonance (NMR) spectrometry.^{256,257} Electro-spray ionization mass spectrometry (ESI-MS) was utilized to survey different counterions and see their effect on the fragmentation of SOS.²⁵⁸ The group of Gunay and co-workers²⁵⁸ reported that quaternary ammonium ions gave good ESI spectra. In a more recent study, Ke and colleagues²⁵⁹ reported a novel liquid chromatography tandem mass spectrometry method to detect SOS in dog plasma and urine samples. Diethylammonium (DEA) was used to form an adduct with SOS that was stable and aided its detection to low ng levels.

Over time, the focus was aligned to electrochemical detection methods since there is the clamour for methods that promise analysis that are fast, low cost and sensitive. One good example is the utilization of potentiometric ion selective electrodes (ISEs) which were used with a polymer membrane containing ion exchangers such as tridodecylmethylammonium (TDMA⁺). These systems were employed to probe molecules that are mostly negatively charged such as pentosan polysulfate,²²⁸ heparin,^{53,227} and carrageenan.²²⁵ In a recent work by Kim and co-workers,²²⁹ an ISE was employed to study species of fucoidan, a sulfated polysaccharide derived from brown seaweeds. Results suggest that ISE response as well as the charge density was dependent on the species of fucoidan, which differ in their polymer backbone.

With the rise of interest on electrochemical techniques, the growing field of electrochemistry at the interface between two immiscible electrolyte solutions (ITIES) was also observed mostly as the basis for novel analytical strategies.^{188,230} With electrochemistry at the ITIES presenting advantages like amenability for miniaturisation⁹⁰ and possibility for label-free detection, it has been explored in the

investigation of molecules with biological importance like proteins,^{189,231} neurotransmitters^{43,127} and carbohydrates.^{52,232} Several polysaccharides have been the subject of studies utilizing this approach, a well-known example of which is the sulfated polysaccharide, heparin.^{50-52,137} Findings reported suggest that binding with an ionophore,⁵² which can also be the organic electrolyte cation used,¹³⁷ affects the adsorption of heparin at the interface. Also, Guo and colleagues⁵⁰ investigated a number of hydrophobic quaternary ammonium cations that served as selective ionophores for heparin. The results revealed that adsorption of heparin was assisted by complexation with the aforementioned cations.

In Chapter 4, the electrochemical behaviour of a sulfated polysaccharide (Fucoidan) was investigated using voltammetry at polarized liquid-organogel microinterfaces. Results show that Fucoidans are electrochemically active at the interface between two immiscible electrolyte solutions and show an adsorption/desorption process. Also, the identity of the organic cation, which served as an ionophore, enhanced the detection of Fucoidan. With these findings, Chapter 5 was designed to study smaller counterparts of Fucoidans, which in this case were sulfated carbohydrates (disaccharides). The idea was to check if these sulfated carbohydrates would also be electrochemically active at the ITIES and can they be detected using the same system. Thus, this chapter reports the electrochemistry of simpler sulfated carbohydrates at the interface between two immiscible electrolyte solutions and explores if this can be a viable alternative method for their detection. The model analytes tested were sucrose octasulfate (SOS), sucrose heptasulfate (SHpS) and sucrose hexasulfate (SHxS) at a liquid-organogel microinterface array via voltammetric techniques. The findings support previous results that counterion interactions enable the detection of these sulfated analytes. Utilizing this discovery, a detection limit of 0.12 μM SOS for 60 s pre-concentration and 0.04 μM for 180 s, in 10 mM LiCl, was achieved while detection of 0.24 μM SOS was achieved in a synthetic urine electrolyte mixture.

5.2 Experimental Method

5.2.1 Reagents

The organic electrolyte salt bis(triphenylphosphoranylidene)ammonium tetrakis(4-chlorophenyl)borate (BTPPATPBCl) was synthesized via a metathesis reaction between equimolar amounts of bis(triphenylphosphoranylidene)ammonium chloride (BTPPACl) and potassium tetrakis(4-chlorophenyl)borate (KTPBCl). Similarly, the other organic electrolyte salt tridodecylmethylammonium tetrakis(4-chlorophenyl)borate (TDMATPBCl) was prepared by the metathesis reaction of equimolar amounts of tridodecylmethylammonium chloride (TDMACl) with potassium tetrakis(4-chlorophenyl)borate (KTPBCl). The organic phase was made by dissolving the organic electrolyte salt (BTPPATPBCl or TDDATPBCl or TDMATPBCl) in 1,6-dichlorohexane (1,6-DCH). The resulting solution (10 mM) was gellified with the addition of low molecular weight poly(vinyl chloride) (PVC) at 10%.¹⁵⁷ Sucrose octasulfate (SOS), was from Toronto Research Chemicals Inc. (TRC) while sucrose heptasulfate (SHpS) and sucrose hexasulfate (SHxS) were obtained from Santa Cruz Biotechnology, Inc. (SCBT). Stock solutions of these sulfated carbohydrates were prepared weekly in aqueous 10 mM LiCl and stored at 4 °C. Similarly, tetrapropylammonium (TPrA⁺) chloride was dissolved in 10 mM LiCl. The matrix effect was tested using a synthetic urine mixture²³⁴ that contains creatinine (1.10 g L⁻¹), urea (25 g L⁻¹), sodium sulfate (2.25 g L⁻¹), sodium chloride (2.295 g L⁻¹) as well as potassium dihydrogen phosphate (1.40 g L⁻¹), potassium chloride (1.60 g L⁻¹), calcium chloride dihydrate (1.103 g L⁻¹) and ammonium chloride (1.00 g L⁻¹). All solutions (aqueous) were prepared using Milli-Q water from a USF Purelab with UV system having a resistivity of 18.2 MΩcm.

5.2.2 Apparatus

Electrochemical measurements were conducted using an AUTOLAB PGSTAT302N electrochemical station (Metrohm, The Netherlands) with the NOVA software. The microITIES array employed was created with the use of a thirty micropore array silicon membrane¹⁷⁴ in a hexagonal arrangement. Each pore had a diameter of 22.4 μm, a pore centre-to-pore centre distance of 200 μm and a thickness of 100 μm. These parameters create a total geometric area of 1.18 x 10⁻⁴ cm². The

silicon microporous membrane was sealed, using a silicon rubber (Selley's glass silicone), onto the mouth of a glass cylinder. The gelled organic phase was placed into the silicon micropore array membrane via the other opening of the glass cylinder using a pre-warmed glass Pasteur pipette. The assembly was then set aside for at least an hour before use. Once ready, the organic reference solution (saturated BTPPACl or TDDATPBCl or TDMATPBCl dissolved in 10 mM LiCl) was introduced into the glass cylinder ensuring that it is on top of the organogel. The whole set-up was then immersed into the aqueous phase (10 mM LiCl, sulfated carbohydrates in 10 mM LiCl and/or TPrA⁺ in 10 mM LiCl) and voltammetric measurements were made. Scheme 5.2. 1 outlines the electrochemical cells utilized.

Cell 1



Cell 2



Cell 3



Cell 4



Scheme 5.2.1 Schematic representation of the electrochemical cells employed, where *x* represents the sulfated carbohydrate (e.g. SOS) concentrations utilized in the study.

5.2.3 Electrochemical Measurements

For all measurements, a pair of Ag/AgCl electrodes with one in each phase were used. Voltammetric investigations (CV and AdSV) were conducted at a sweep rate of 5 mV s⁻¹ unless otherwise stated. Parameters like analyte concentration (sulfated carbohydrates), potential applied and length of pre-concentration were varied accordingly. The reported detection limits were calculated based on three times the standard deviation of the blank (n=3) divided by the best-fit linear calibration line slope. Potentials reported were transposed to the Galvani potential scale based on the

experimental TPrA⁺ mid-point transfer potential along with its formal transfer potential -0.08 V in a water | 1,6-dichlorohexane (DCH) system.²³⁵

5.3 Results and Discussions

5.3.1 Cyclic Voltammetry

Based on the previous findings of the Fucoidan behaviour at the ITIES (Chapter 4), cyclic voltammetry (CV) was used to examine how the simpler sulfated saccharides behave at the ITIES. Different aqueous pH values were tested, and the results suggest the best response was observed at pH 5.5-6 (10 mM LiCl). Figure 5.3.1 (A) illustrates the voltammogram obtained when 10 μ M SOS was present in the aqueous phase using Cell 1 (see Scheme 5.2.1). As observed, there is no distinct peak or response different from the voltammogram obtained in the absence of the SOS. This suggests that SOS at this concentration was not detected for these conditions. What is observed is only the background electrolyte transfer across the liquid-organogel interface as shown in the decline of current going to more negative potentials. This response at the negative side of the potential window denotes the transfer of the cation (BTPPA⁺) from the organic towards the aqueous phase and the anion (Cl⁻) from the aqueous towards the organic phase.

Following on the previous finding (see Chapter 4) that the type of organic electrolyte cation impacts the detection of polysulfated analytes, two other organic electrolyte cations were used to test whether they are capable of enabling the detection of SOS at low micromolar concentrations. Figure 5.3.1 (B) and (C) illustrates the cyclic voltammograms recorded when tetradodecylammonium (TDDA⁺) and tridodecylmethylammonium (TDMA⁺), respectively, were used to replace the commonly used bis(triphenylphosphoranylidene)ammonium (BTPPA⁺) as the organic cation with the presence (black line) of 10 μ M SOS in the aqueous phase. Utilizing these different alkylammonium cations in the organic phase extended the working potential window range on the negative side. This observation can be due to the characteristic of TDDA⁺ to transfer at a more negative potential²³⁸ compared to BTPPA⁺ and since TDMA⁺ is structurally analogous with TDDA⁺, it is assumed to behave similarly. One prime distinction that can be noted in the voltammograms is the difference in the intensity of the SOS response in the presence of TDDA⁺ (Figure 5.3.1

B) and TDMA⁺ (Figure 5.3.1 C) relative to BTPPA⁺ (Figure 5.3.1 A). When 10 μ M SOS was added into the aqueous phase, the distinct peaks observed (Figure 5.3.1 B-C) on the reverse scans represent that SOS is electrochemically active at the liquid-organogel microinterface array. Other polysulfated biomolecules, heparin¹³⁷ and fucoidan²⁶⁰ revealed identical responses. The peak response is representative of an adsorption/desorption process¹ which features a rapid decline in current that is reaching background levels and agrees with a finite amount of material at the interface being depleted. This peak at the reverse scan is presented to be the desorption of SOS from the soft interface which also demonstrates that it undertakes electroadsorption throughout the prior forward scan.

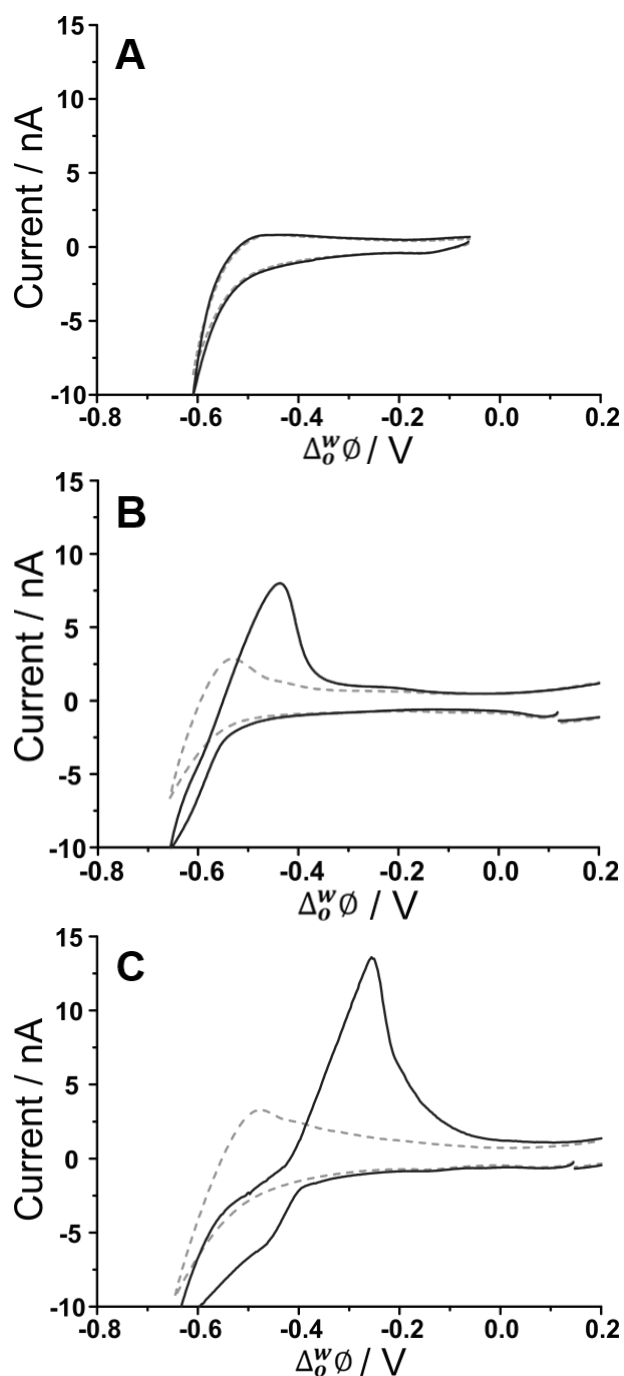


Figure 5.3.1 CV of 10 mM LiCl in the absence (grey dashed line) and presence (black line) of 10 μ M sucrose octasulfate (SOS) using (A) Cell 1, (B) Cell 2 and (C) Cell 3 as shown in Scheme 5.2.1

Cyclic voltammograms of increasing concentration of SOS (0.25 – 6.0 μ M) using Cell 2 (See Scheme 5.2.1) are displayed in Figure 5.3.2 (A).

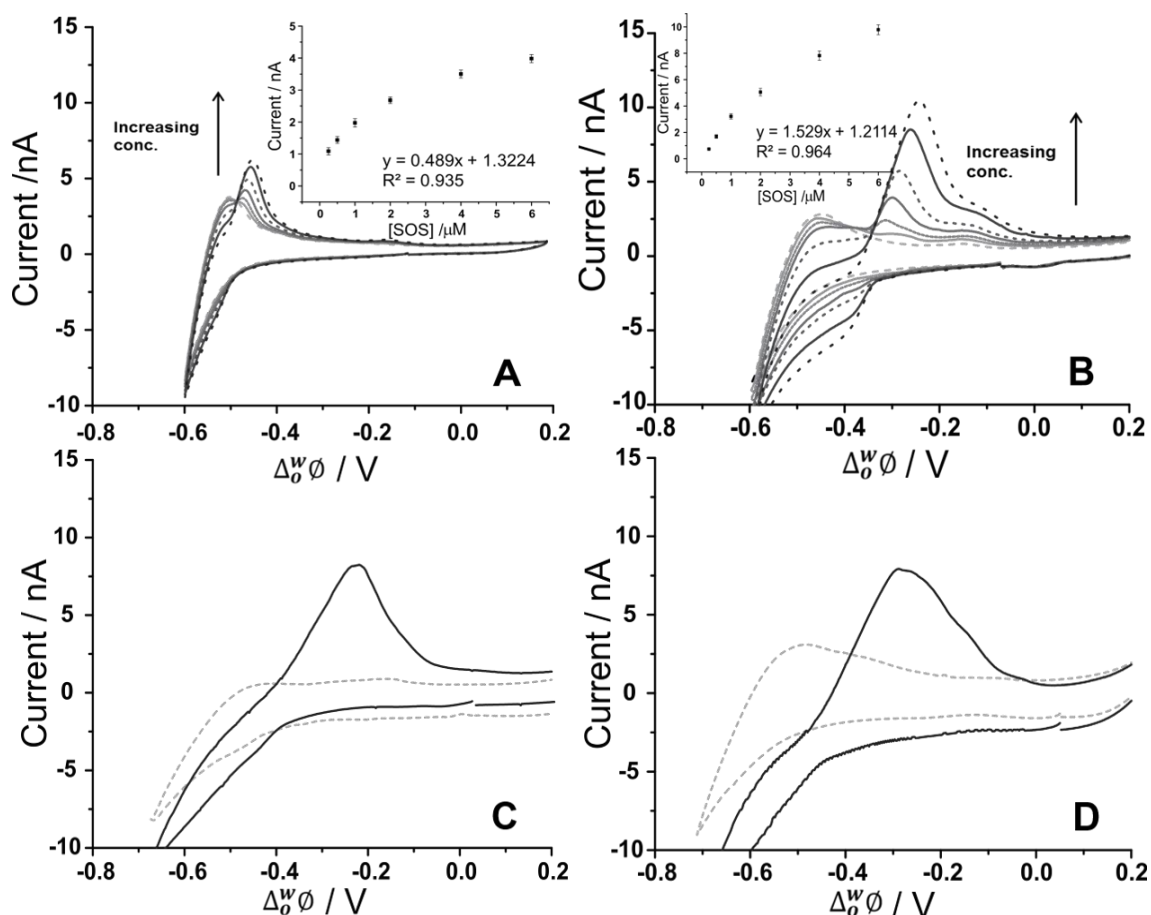


Figure 5.3.2 CV of 10 mM LiCl in the absence (grey dashed line) and presence of increasing concentrations (0.25 – 6.0 μM) of SOS using Cell 2 (A) and Cell 3 (B) while (C) is with 6 μM SHpS and (D) is with 6 μM SHxS, both using Cell 3 (see Scheme 5.2.1).

Going towards the negative potential (forward scan), the negative current increases even with increasing added SOS concentrations. This was previously observed as mentioned earlier (See Figure 5.3.1 B). On the other hand, as the potential is scanned on the reverse direction, a peak response was recorded at *ca.* -0.47 V for 0.5 μM SOS and this peak height intensifies with increasing SOS concentrations. The resulting calibration plot has a sensitivity of 0.489 $\text{nA } \mu\text{M}^{-1}$ and a correlation coefficient of 0.967, which can still be considered fairly linear. In the same way from prior results, the shape of the peak indicates more of an adsorption process than a diffusion-controlled phenomenon. Consequently, the response mechanism for the detection of SOS is proposed to entail the adsorption of SOS at the polarized soft microinterface during the forward (negative-going) scan and integrated with the interaction of the polysulfated analyte with the organic phase cation (TDDA^+), which was also similar to what was discussed for heparin.⁵² The resulting peak on the reverse

(positive-going) scan is then associated with the desorption process including the separation of the formed complex between the anionic (polysulfated) SOS and the organic cation. At the ITIES, these interactions of counterion-polyion have been previously reported.^{144,151,233} This could possibly manifest a common electrochemical detection mechanism for such types of analytes (polyionic).

CVs of increasing SOS concentrations (0.25 – 6.0 μM) now using an organic phase that has 10 mM TDMA⁺ are shown in Figure 5.3.2 B. A peak was observed at *ca.* -0.28 V for 0.25 μM SOS. This is an improvement compared to when TDDA⁺ (peak recorded at a higher concentration) and much more when BTPPA⁺ (no peak observed in these range of concentrations) was used in the organic phase. Figure 5.3.2 B inset reveals an improved sensitivity at 1.529 nA μM^{-1} as well as an improved correlation coefficient of 0.982. This enhancement in the recorded response might be credited to the presence of such alkylammonium organic phase cations and how stronger they interact with SOS as seen for TDDA⁺ or TDMA⁺ compared to BTPPA⁺. Other studies have reported about the formation of complexes of sulfated polysaccharides, such as heparin with cations that acted as ionophores.^{51,137} One finding in these studies discussed that when BTPPA⁺ was used as the organic cation in the organic phase, only weak interactions between heparin and the cation was recorded. However, when hexadecyltrimethylammonium (HDTMA⁺) was utilized, an enhanced interaction was observed. Comparing both cations structurally, it was proposed that HDTMA⁺ offers more flexibility for heparin interaction versus BTPPA⁺ because of the phenyl rings that surround the latter causing steric hindrance and shielding of its positive centre.¹³⁷ This was supported by another study by Guo and colleagues⁵⁰ who found that at the liquid-liquid interface, heparin adsorption was more favoured when there was less steric hindrance observed within the ionophore because this reveals the positive charge of the nitrogen in this quaternary alkylammonium and leaving it more open for electrostatic binding with the negative charges in heparin.

An equivalent situation can be credited for the reported improvement on the electrochemical signal for SOS when the organic cation TDDA⁺ and more so with TDMA⁺ was used in the organic phase because of their structural resemblance with HDTMA⁺. In support of this case, Meyerhoff and group²²⁸ employed polyion-sensitive electrodes that were TDMA⁺-based in detecting pentosan polysulfate (PPS). The group reported that the improved ion-pairing interaction strength with PPS was due to the

more accessible charge density in TDMA⁺. Moreover, quaternary ammonium ions were found to be ideal counterions for SOS-counterion complex formation that resulted to an enhanced ESI-MS analysis as reported by Gunay *et al.*²⁵⁸ Such findings point out that interaction with SOS gets more favoured in the following order: BTPPA⁺ < TDDA⁺ < TDMA⁺ being the organic cation. Therefore, it is suggested that at the liquid-organogel interface, the interaction involves the complexation of SOS with TDDA⁺ or TDMA⁺ then followed by the adsorption of the developed complex during the forward (negative-going) sweep. Then, this adsorbed complex is gradually desorbed during the reverse (positive-going) scan.

Meanwhile, CVs of 10 mM LiCl in the absence (grey-dashed line) and presence (black line) of 6 μM SHpS or SHxS using Cell 3 (See Scheme 5.2.1) are shown in Figure 5.3.2 (C) and (D) respectively. Features in the CV similar to what was observed for SOS were recorded such as the increase of the negative current during the forward scan (negative-going) indicating transfer of background electrolytes (see beginning of Section 5.3.1) and then sharp peaks develop during the reverse (positive-going) scan suggesting that both SHpS and SHxS are also electrochemically active at the ITIES. The interest in considering these analytes was to see the effect of having less sulfation on the disaccharide on its response at the microinterface. Generally, there was no significant decrease on the peak current observed (with the same 6 μM analyte concentration, average of three trials ± one standard deviation) from *ca.* 10.5 ± 1.60 nA for SOS to *ca.* 9.7 ± 2.79 nA for SHpS and *ca.* 9.5 ± 3.22 nA for SHxS. This is suggesting that a difference of a single sulfate group does not make much difference on the electrochemical response at the ITIES so most of the study was then focused on SOS.

5.3.2 Adsorptive Stripping Voltammetry

The utilization of adsorptive stripping voltammetry (AdSV) at the microITIES has been instrumental for the investigation of several polyelectrolytes.^{50,148} The technique involves two stages: first, a constant potential is applied for a chosen time that prompts the adsorption and pre-concentrates the molecule of interest at the interface. Second, a voltammetric scan serves as the detection step when the analyte desorbs away from the interface and yields a peak current that is considered as the analytical signal. For this investigation, the pre-

concentration of SOS was chosen at an appropriate negative potential to stimulate adsorption, then scanning is done towards more positive potentials in order to desorb it from the interface. This yields a peak current that is shown to be dependent on analyte concentration as well as chosen pre-concentration time. The optimization of the parameters for SOS adsorption started with examination of the effect of the applied potential during the adsorption stage. After knowing the potential window where SOS adsorption occurs, potential values were chosen and applied for a definite time. This was then followed by a voltammetric sweep to more positive potentials, thereby desorbing SOS and producing a stripping voltammogram.

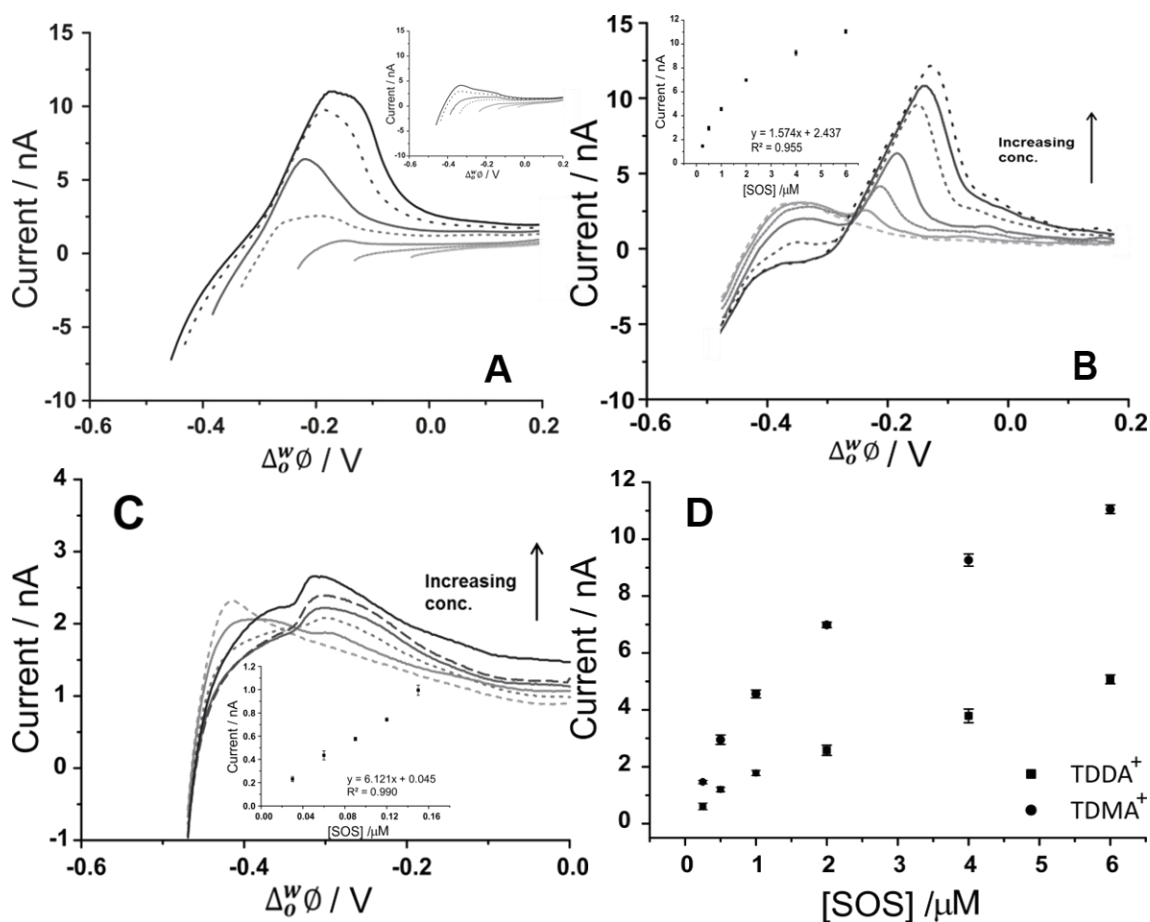


Figure 5.3.3 AdSV of 10 mM LiCl with (A) 5 μM SOS at varying adsorption potentials applied for 60 s using Cell 3 (see Scheme 5.2.1) Inset: Corresponding blank profiles for the said experiment. And (B) 0.25-6.0 μM SOS using the optimized adsorption potential (-0.475 V, 60 s). (C) 0.03-0.15 μM SOS for 180 s. Inset: Current versus concentration plot of the said experiments; (D) Plot of peak current versus SOS concentration using optimized adsorption potentials for each chosen cation at 60 s.

Displayed in Figure 5.3.3 (A) are voltammograms showing the effect of varying the adsorption potential towards SOS detection with TDMA⁺ as the organic

electrolyte cation. Looking at less negative potentials, the resulting stripping voltammograms show no obvious peak. However, at adsorption potentials ≤ -0.375 V, a distinct stripping peak starts to show, demonstrating the influence of applied potential on the adsorption process. Equivalent to what was seen in the CV experiments, the AdSV peaks present a peak shape tantamount to a surface-confined process, which agrees with an adsorption/desorption phenomenon at the interface. In the optimization of the applied adsorption potential, one point to consider is that the region where the background electrolyte signal is seen can also be minimized since it occurs near the SOS adsorption region. Consequently, the chosen adsorption potential is critical in both maximizing the analyte signal as well as minimizing the background electrolyte signal. The data shown in Figure 5.3.3 (A) reveals that the optimized adsorption potential for SOS was *ca.* -0.425 V in the presence of TDMA⁺ at the organic phase.

Moreover, increasing concentrations of SOS were examined using the optimized adsorption parameters. Figure 5.3.3 (B) displays the CVs corresponding for 0.25-6.0 μ M SOS at the aqueous phase using Cell 3 (see Scheme 5.2.1) system. As observed, the peak currents increase proportionately with added concentrations of SOS. The resulting calibration plot (see Inset Figure 5.3.3 B) is generally linear from 0.25 to 2.0 μ M then starts to show a slight curve from 4.0 – 6.0 μ M

Also, the difference in the steepness of the slope (see Figure 5.3.3 D) suggests better interaction of SOS with TDMA⁺ as compared to TDDA⁺ or BTPPA⁺ as the organic phase. This indicates an improvement in sensitivity for TDMA⁺ as the organic electrolyte cation. Similar behaviour is observed if you compare the steepness of the calibration plots in Figure 5.3.2 insets in (A) and (B). Combined AdSV with TDMA⁺ as the organic phase cation resulted to a calculated detection limit of 0.12 μ M SOS. To further lower the detection limit, experiments were done where adsorption time was increased to 180 s and the concentration range studied was lowered to 0.03-0.15 μ M SOS. Resulting voltammograms are displayed in Figure 5.3.3 C. With the longer pre-concentration time and lower concentration range, the sensitivity was improved, and the calculated detection limit was lowered to 0.04 μ M.

5.3.3 Matrix Effect

The interest for most of the investigations involving SOS can be related to its array of biological activities so detection in physiological matrices like urine, blood serum, or plasma is vital and has been the subject of studies.^{259,261} For this investigation, synthetic urine was examined as a working matrix for SOS detection. The preparation of synthetic urine was done following a published method.²³⁴ This was then utilized as the aqueous phase for the electrochemical measurements, replacing 10 mM LiCl as shown in Cell 4 (see Scheme 5.2.1). Figure 5.3.3 (A) displays a CV of the prepared synthetic urine (black line) overlaid on the recorded CV having 10 mM LiCl (grey dashed line) as the aqueous phase.

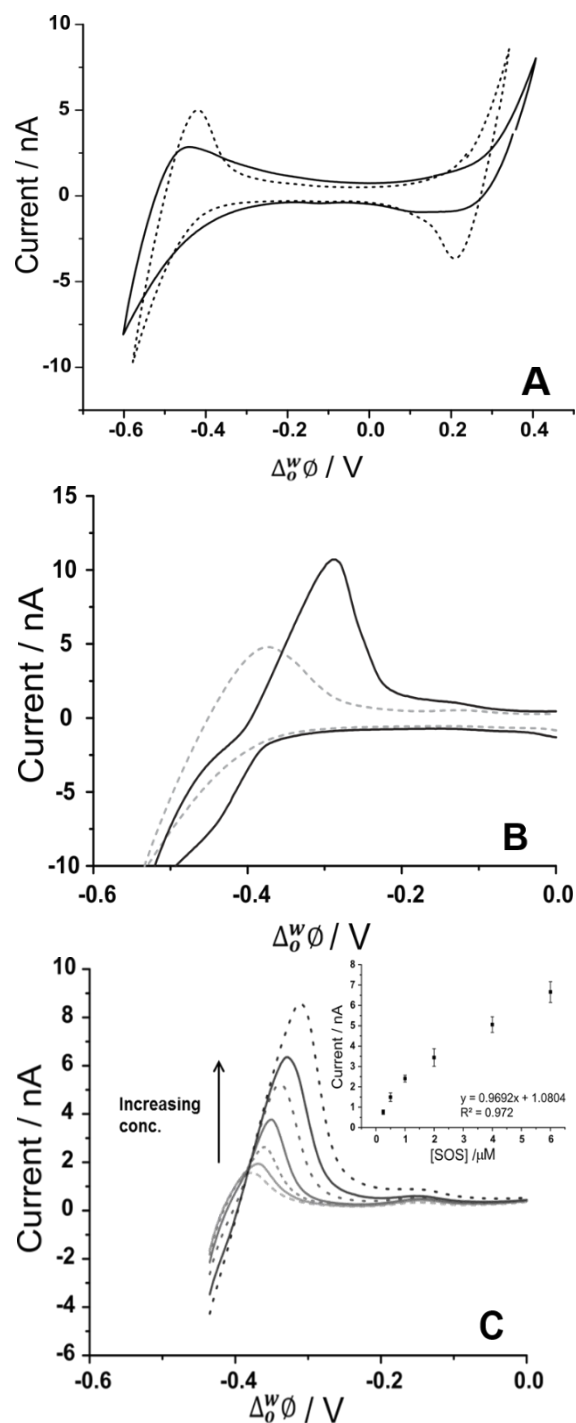


Figure 5.3.4 (A) Cyclic voltammograms of synthetic urine (black line) in contrast to 10 mM LiCl (grey dashed line) as the aqueous phase. (B) CV in the absence (grey dashed line) and presence of 6 μM SOS. (black line) (C) AdSV of increasing SOS concentration (0.25-6.0 μM). Adsorption potential: -0.425 V, pre-concentration time: 60 s, scan rate: 5 mV s^{-1} .

What is observed was the working potential window being shorter when having synthetic urine as the aqueous phase, which could be attributed to the transfer of several component ions in the matrix. This was similar to what was observed in

Chapter 4 (see Section 4.3.3) when the component ions were studied individually and revealed that the cations NH_4^+ , K^+ , Ca^{2+} transfer at lower potentials. These results also support findings of a reported study done in synthetic saliva.²³⁴ However, in spite of the shortened potential window, SOS was still detected, as shown in Figure 5.3.4 (B) when 6 μM SOS was spiked into the synthetic urine. The peak at *ca.* -0.30 V on the reverse (positive-going) scan reveals the detection of SOS in the synthetic urine. This sharp peak shape is suggestive of an adsorption/desorption process, as previously discussed. AdSV using optimized parameters were utilized to improve detection in this biomimetic matrix. Figure 5.3.4 (C) shows AdSV of increasing SOS concentration. The calibration plot (see Inset of Figure 5.3.4 C) for SOS in synthetic urine is generally linear within the concentration range used (0.25-6.0 μM). However, in comparison with the calibration plot for SOS in normal electrolyte (10 mM LiCl) as shown in inset of Figure 5.3.3 (B), the slope of the best fit line is lower. This can be due to the presence of additional species that are considered to be surface-active and these might compete with SOS for adsorption at the interface. In addition, such species present may lower the available potential range and therefore, the potential sufficient to drive the adsorption cannot be attained. Consequently, it can affect the stripping voltammogram if such interferences also adsorb at potentials near to that of SOS and thus could lower the sensitivity. An equivalent phenomenon can be expected in applications with real biological matrices. Nevertheless, prudent optimization of the adsorption potential conditions as well as the chosen electrolyte might aid to diminish this issue, as previously reported for insulin detection with interferences present.¹⁹⁴ Overall, combining AdSV with TDMA⁺ produced a calculated detection limit of 0.24 μM at this biomimetic matrix. Table 5.3.1 summarizes the analytical characteristics of the different organic electrolyte cation employed in this work along with the different voltammetric techniques used.

Table 5.3.1 Summary of analytical characteristics of SOS in the polarized liquid-organogel microarray for different voltammetric methods employed.

Detection Method	Organic Cation	Sensitivity		Limit of		Correlation Coefficient / R
		(calibration graph) $\text{nA } \mu\text{M}^{-1}$	Number of Points / n	Detection (LOD) μM	Concentration Range / μM	
CV	BTPPA ⁺	nd	nd	nd	nd	nd
CV	TDDA ⁺	0.489	6	0.58	0.25-6.0	0.967
CV	TDMA ⁺	1.529	6	0.33	0.25-6.0	0.982
†CV	TDMA ⁺	1.155	6	0.48	0.25-6.0	0.974
AdSV (60 s)	TDDA ⁺	0.745	6	0.35	0.25-6.0	0.995
AdSV (60 s)	TDMA ⁺	1.574	6	0.12	0.25-6.0	0.977
AdSV (180 s)	TDMA ⁺	6.122	5	0.04	0.03-0.15	0.995
†AdSV (60 s)	TDMA ⁺	0.969	6	0.24	0.25-6.0	0.986

† Corresponds to experiments when synthetic urine was used as the aqueous phase. The rest was in 10 mM LiCl. Nd means not detected.

5.4 Conclusions

The electrochemical characteristics of sulfated carbohydrates (SOS) was examined utilizing voltammetry at a liquid-organogel μITIES array. The recorded CV of SOS showed no response on a low μM concentration when BTPPA⁺ was employed in the organic phase. However, a distinct peak at the reverse (negative-going) scan at *ca.* -0.47 V when the organic phase was TDDA⁺ and this moved to *ca.* -0.28 V when

the organic phase cation was substituted with TDMA⁺. This observation is due to the increased binding strength between these specific organic electrolyte cations. The shape of the peak indicates a desorption process, in agreement with an adsorption process during the forward (negative-going) scan. Examination of the optimized adsorption potential for SOS at the micro interface showed that maximum adsorption occurred at a potential near the potential for background electrolyte transfer. With AdSV, having TDMA⁺ in the organic phase and adsorption time of 60 s resulted in a detection limit of 0.12 μM in 10 mM LiCl and 0.24 μM in a synthetic urine solution. When adsorption time was increased to 180 s, the detection limit improved to 0.04 μM (10 mM LiCl). The behaviour reported in this study supports the capacity of employing electrochemistry at the liquid-organogel μTIES array as a bioanalytical label-free tool for the detection of sulfated carbohydrates (SOS). Selectivity (such as distinction between less sulfated species) and enhancing parameters with matrix effects are opportunities for further investigations.

Chapter 6. Behaviour of Aptamers at Soft Polarized Microinterfaces

6.1 Introduction

Since their discovery in 1990s, aptamers have been extensively used in many applications.²⁶² Aptamers, a name derived from the Latin *aptus* meaning “to fit”,²⁶³ are synthetic oligonucleotides (RNA or DNA), obtained through a process known as Systematic Evolution of Ligands by Exponential Enrichment (SELEX)²⁶⁴ and are well known for possessing high affinity and high specificity towards a wide array of target molecules like proteins, drugs, amino acids and more.²⁶⁵ This affinity and specificity is enhanced by their ability to structurally fold upon binding with the target molecule.²⁶⁶ giving it an advantage, among many, from its natural counterparts: antibodies.

Over time, aptamers became increasingly known as vital molecular tools especially in diagnostics and therapeutics.²⁶⁷ They are considered as good reagents for target validation in various disease models.^{268,269} Also, these synthetic oligonucleotides have been evolved to bind with proteins that are affiliated with various disease states paving the way for powerful protein antagonists.²⁷⁰ Generally, aptamers can serve two roles in the therapeutic applications either as a targeting modality or as the therapeutic agent itself. Despite its slow arrival to the clinic due to practical limitations, scientists use chemical modifications along with inventive aptamer selection techniques to further the cause.²⁷¹

Moreover, based on the previously mentioned promising aspects as molecular targeting ligands, aptamers are also studied to enhance molecular imaging (i.e. nuclear imaging with aptamer-based probes).²⁷² Consequently, this has propelled intense interest in research to further understand aptamers and their conformational and ligand-binding properties.^{266,273,274} This increasing interest trend also developed a range of bioassay techniques that utilizes aptamers as receptors or immobilized ligands.^{275,276} and was seen applied to the investigation of numerous target analytes which shaped numerous studies on the analytical application of aptamers.

One well-known target analyte is thrombin, an allosteric serine protease that is Na^+ activated and is the main protease in the coagulation cascade.²⁷⁷ This makes it play a vital role in pathological and physiological coagulation, which is also utilized as an indicator of various diseases like Alzheimer's and some cancers.^{278,279} In order to achieve detection of significantly low concentrations of thrombin, the thrombin binding aptamer (TBA) was the center of several studies.²⁸⁰ The 15-base long oligonucleotide version with the sequence 5'-GGT-TGG-TGT-GGT-TGG-3' was the first example of a potential nucleic acid as therapeutic agent and binds specifically with thrombin at 10 nM concentrations.²⁸¹ Moreover, this 15-mer sequence was found to bind more to alpha-thrombin than to gamma-thrombin²⁸² and was reported to form a folded structure, known as a G-quadruplex structure²⁸³ in a chair-like conformation with an anti-parallel orientation. From then on, more characterization was done on this TBA^{284,285} and how to improve its binding with thrombin.

Several review articles have reported the growing number of studies that involves the detection of thrombin with thrombin-binding aptamer via different analytical approaches.²⁸⁶ In order to deepen the understanding of this analyte-aptamer interaction and given the TBA's array of possible applications, a simple yet direct detection method for measuring the presence of TBA is advantageous. Wu *et al*²⁸⁷ utilized surface enhanced Raman spectroscopy (SERS) to analyse the 15-mer TBA and noted that specific spectral peaks corresponding to the components of TBA were detected. Joseph and colleagues²⁸⁸ reported the use of fluorescent dyes, YO-Pro-1 iodide and YOYO-1 iodide with the 15-mer TBA. They found that the binding constant with these dyes are smaller compared with double-stranded DNA. However, these reports did not mention about limits of detection for the aptamer.

Electrochemical detection techniques were also increasingly being developed for TBA research since it promises fast, affordable and sensitive results. This is more prominent in the development of aptasensors²⁸⁹ which is mostly based on binding-induced detection. Potentiometry with ion-selective electrodes (ISEs) based on polymeric membranes with selective receptors or ionophores have yielded measurements of DNA,²⁹⁰ DNA hybridization,²⁹¹ and protein-binding aptamers.²⁹² Durust and co-workers²²⁶ reported the detection of double-stranded DNA in $\mu\text{g mL}^{-1}$ range via a potentiometric polyion sensor. The DNA interacting with the cationic protamine played a role in its detection. Meanwhile, Shishkanova *et al*.²⁹³ investigated

the use of a single-stranded oligonucleotide as an active component in a polymeric membrane ISE. The group found that membranes modified with cholesterol-oligonucleotides were sensitive toward a 2-80 nM complimentary oligonucleotide.

In recent years, there has been a rise on the utilization of the electrochemistry of the interface between two immiscible electrolyte solutions (ITIES) as the premise of novel analytical strategies.^{188,230} The promise of advantages like amenability for miniaturization and label-free detection⁹⁰ propelled the use of the electrochemistry at the ITIES for the exploration of biologically-vital molecules like proteins^{231,294} and oligonucleotides.⁵⁵ Vagin *et al.*²⁹⁵ described the detection of DNA via a supported liquid-liquid interface. A detection limit of 10 nM was achieved. The use of surfactants with DNA was also explored in ITIES after reports of protein-surfactant complex formation¹⁵⁰ enabled the transfer of proteins at these soft interfaces. Osakai and colleagues²⁹⁶ followed suit by exploring the interaction between a cationic surfactant and DNA. The group found that the transfer of the surfactant was affected by the adsorbed DNA at the interface. In addition, Kivlehan and colleagues⁵⁶ reported the use of acridine-functionalised calix[4]arene at the ITIES which facilitated the transfer of electrolyte anions. However, in the presence of DNA, this transfer response was diminished, and this suggests of DNA binding with the acridine moiety at the ITIES.

To link this chapter from the previous one, it is vital to note that the analytes studied (Chapter 4 – Fucoidans and Chapter 5 - sulfated carbohydrates) are all polyanionic analytes. Starting with Fucoidans presented in Chapter 4, these sulfated polysaccharides were found to be electrochemically active at the ITIES, so to see if that would still be the case, smaller counterparts (sulfated carbohydrates) were studied in Chapter 5. Then, aptamers, being polyanionic analytes as well, are investigated in this chapter to observe if they would also behave similarly to the previously studied analytes. Another connection would be the idea of adding selectivity to the detection of biomolecules at the ITIES. Aptamers are known for this quality so before we are able to maximise their use for that purpose, their electrochemical activity at soft polarized microinterfaces has to be established first. Thus, Chapter 6 was produced to reveal how aptamers behave at the ITIES.

Here, the current work probes the electrochemistry of aptamers at the ITIES and investigates whether it can be a feasible alternative for its quantitative detection.

A 15-mer DNA oligonucleotide thrombin-binding aptamer (TBA) with sequence 5'-GGT-TGG-TGT-GGT-TGG-3' was examined using an array of liquid-organogel microinterfaces for characterization (voltammetric) and detection. The findings reveal that the identity of the organic electrolyte cation aided the detection of the aptamer, which in this case was the surfactant CTA⁺. Also, the presence of the magnesium ion changed the electrochemical response. Meanwhile presence of only thrombin did not produce any peak response in 10 mM LiCl (pH 8.5) but it did for 10 mM HCl (pH 2). Applying this behaviour with only CTATPBCl in the organic phase, a limit of detection value of 0.11 μ M was attained for TBA in 10 mM LiCl (pH 8.5) and 0.29 μ M in synthetic urine

6.2 Experimental Method

6.2.1 Reagents

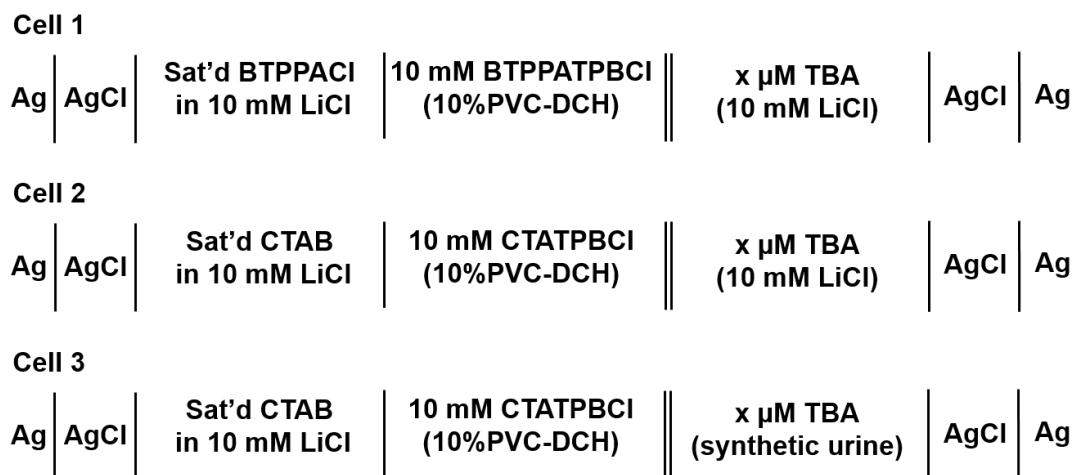
All reagents were purchased from Sigma-Aldrich Australia Ltd and were used as received unless stated otherwise. The organic phase was formulated via dissolving bis(triphenylphosphoranylidene)ammonium tetrakis(4-chlorophenyl) borate (BTPPATPBCl) or cetyltrimethylammonium tetrakis(4-chlorophenyl) borate (CTATPBCl) in 1,6-dichlorohexane (1,6-DCH). The resulting electrolyte solution (10 mM) was gellified via the addition of 10% w/v poly(vinyl) chloride (low molecular weight) as described elsewhere.¹⁵⁷ The organic electrolyte salt, BTPPATPBCl, was produced via a metathesis process of bis(triphenylphosphoranylidene)ammonium chloride (BTPPACl) together with potassium tetrakis(4-chlorophenyl)borate (KTPBCl).¹⁶⁴ In a similar manner, the organic electrolyte salt CTATPBCl was prepared via the metathesis of cetyltrimethylammonium bromide (CTAB) and potassium tetrakis(4-chlorophenyl)borate (KTPBCl) in equimolar amounts.¹⁶⁸ More details of this are presented in Appendix A.3

The unmodified thrombin-binding aptamer (TBA) with sequence: 5'-GGT-TGG-TGT-GGT-TGG-3' was purchased (in lyophilized form) from Integrated DNA Technologies Pte. Ltd. (IDT). The aptamer was resuspended in deionised H₂O to achieve 100 μ M stock solution (the volume needed is provided on aptamer label) then incubated at room temperature for approx. 30 mins. The resulting solution was vortexed for 20 s before centrifuging it (10,000 x g) for 1 min. Aliquots were then

created and stored at $-20\text{ }^{\circ}\text{C}$. Tetrapropylammonium (TPrA⁺) chloride was prepared in 10 mM LiCl while a synthetic urine mixture²³⁴ composed of ammonium chloride (1.00 g L⁻¹), creatinine (1.10 g L⁻¹), calcium chloride dihydrate (1.103 g L⁻¹), potassium dihydrogen phosphate (1.40 g L⁻¹), potassium chloride (1.60 g L⁻¹), sodium sulfate (2.25 g L⁻¹), sodium chloride (2.295 g L⁻¹), and urea (25 g L⁻¹) was prepared. The pH of the aqueous phase was adjusted via dropwise addition of 10 mM NaOH. All aqueous solutions were prepared by using deionised water from a USF Purelab Plus UV system with a resistivity of 18.2 MΩcm.

6.2.2 Apparatus

Electrochemical experiments were conducted using an AUTOLAB PGSTAT302N electrochemical station (Metrohm, The Netherlands) with its corresponding NOVA software. The μ ITIES array utilized in the study was formed via a 30-micropore array silicon membrane,¹⁷⁴ which was in a hexagonal pattern and each pore had a 22.4 μm diameter. The array had a pore centre-to-pore centre distance of 200 μm and a membrane thickness of 100 μm . The total geometric area (total cross-sectional area of the micropores) of the microinterface array was $1.18 \times 10^{-4}\text{ cm}^2$. The silicon membranes were attached onto the lower orifice of glass cylinders using a silicone rubber (acetic acid curing/Selley's glass silicone). The gelled organic phase was introduced into the micropore array through the glass cylinder using the tip of a pre-warmed glass pasteur pipette. The completed set-up was then set aside for at least 1 hour before use. When ready, the organic reference solution, composed of saturated BTTPACl or CTAB in 10 mM LiCl, was introduced into the glass cylinder just enough to sit on top of the organogel. This organogel/silicon membrane assembly was then submerged into the aqueous phase (composition: 10 mM LiCl only, TBA in 10 mM LiCl and/or TPrA⁺ in 10 mM LiCl) to proceed with the the voltammetric experiments. Scheme 6.2.1 summarizes the layout of the electrochemical cells utilized.



Scheme 6.2.1 Schematic illustration of the electrochemical cells utilized in the study. *X* represents the TBA concentrations used.

6.2.3 Electrochemical Measurements

Two Ag/AgCl electrodes, one in each phase were employed in all electrochemical measurements. Cyclic voltammetry (CV) was conducted at a 5 mV s^{-1} scan rate unless otherwise stated. Other experimental parameters such as TBA concentration were varied accordingly. The calculated detection limits were based on three times the standard deviation of the blank ($n=3$) then divided by the slope of the best-fit linear calibration line. All potentials were adjusted to the Galvani potential scale based on the experimental mid-point transfer potential of TPrA^+ and its formal transfer potential (-0.08 V) in the water | 1,6-dichlorohexane system.²³⁵

6.3 Results and Discussions

6.3.1 Cyclic Voltammetry

Cyclic voltammetry (CV) was used to examine the electrochemical behaviour of the thrombin-binding aptamer at the μITIES array. Figure 6.3.1 (A) shows the CVs observed in the absence (grey-dashed line) and presence (black line) of $20 \mu\text{M}$ TBA using Cell 1 in Scheme 6.2.1. Upon scanning from the positive to the more negative potentials (forward scan), a decrease in the current was observed which indicates the transfer of the background electrolytes across the liquid-organogel interface. This process at these more negative potentials equates to the movement of the anions (Cl^-) from the aqueous phase to the organic phase as well as the cations (BTPPA^+) from the organic to the aqueous phase. Despite this, there was no additional peak or response

that would suggest the activity of TBA under these conditions. Previous reports of DNA detection at the ITIES⁵⁵ involved its interaction with organic cations. The group noted that the presence of DNA in the aqueous phase decreased the transfer currents of these cations also in the aqueous phase. Thus, the absence of a response by TBA may be attributed to it having very weak or no interaction with the cation, bis(triphenyl)phosphoranylideneammonium (BTTPA⁺) in the organic phase. Structurally, the positive center of BTTPA⁺ is surrounded by phenyl rings (see inset of Figure 6.3.1 A) which may hinder the generally negative TBA to interact with it. A similar situation was observed for sulfated disaccharides as discussed in Chapter 4.

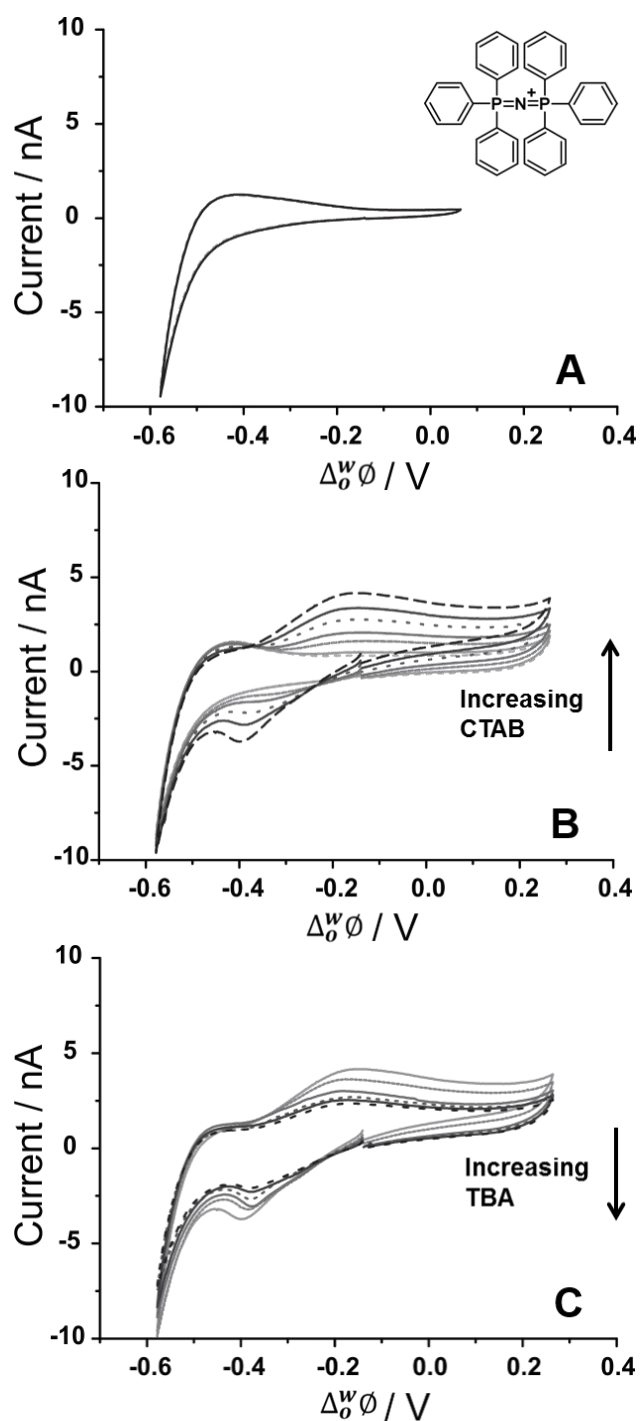


Figure 6.3.1 Cyclic voltammograms of 10 mM LiCl (pH 8.5) (A) without (grey dashed line) and with (black line) 20 μM TBA using Cell 1; (B) with 10-100 μM of CTAB and (C) with 100 μM CTAB plus 5-25 μM TBA. Scan rate was 5 mV s^{-1} .

Based on the previous reports of surfactant transfer facilitated by DNA at the ITIES,²⁹⁶ the use of a surfactant was explored. Cetyltrimethylammonium bromide (CTAB) was chosen for its known interaction with DNA.²⁹⁷ Initially, different concentrations (10-100 μM) of CTAB was added into the aqueous phase and the resulting voltammograms are displayed in Figure 6.3.1 (B). On the forward (negative-going) scan, a peak response starts to

develop at *ca.* -0.40 V and this increases proportionately with increasing CTAB concentrations. Subsequently, a broad peak response was seen at the reverse (positive-going) scan at *ca.* -0.20 V which also increases with added CTAB concentrations. These responses can be attributed to the transfer of CTA^+ as it moves across the interface. The peak currents were proportional to the square root of the scan rate (v) in the range of 5 – 50 mV s^{-1} (data not shown) indicating that the transfer is diffusion-controlled. With the highest CTAB concentration (100 μM) present in the aqueous phase, varying concentrations of TBA (5-25 μM) were spiked and the resulting voltammograms are displayed in Figure 6.3.1 (C). As the TBA concentration added increases, there was a decrease on the peak currents suggesting that the TBA interacted with the CTAB. As more TBA is added and interacts with CTAB, the amount of free CTAB that moves across the interface becomes less resulting to the decreasing peak currents. An equivalent observation was reported by Horrocks *et al.*⁵⁵ when the ion transfer current for methyl viologen (MV^{2+}) decreased in the presence of high-molecular weight DNA.

6.3.2 Effect of Surfactant Concentration

After showing that there was an interaction between CTAB and TBA, the next step was to incorporate the surfactant into the organic phase. This was done by the addition of CTAB to the gelled organic phase during organogel preparation. Since the concentration of the organic electrolyte, BTPPATPBCl, was 10 mM, two different concentrations of CTAB were studied. CVs of 10-50 μM TBA at the aqueous phase while CTAB was mixed with 10 mM BTPPATPBCl at the organic phase is illustrated in Figure 6.3.2. When 5 mM CTAB was added at the organic phase (see Figure 6.3.2 A), no peak response was observed. Only the transfer of background electrolytes, indicated by the decrease in negative currents as the potential is scanned to more negative potentials, is recorded. Meanwhile, when the CTAB concentration added to the organic phase was doubled (10 mM), a distinct peak response was observed around *ca.* -0.54 V. This suggests an aptamer-surfactant interaction because this feature is not seen when surfactant was absent (see Figure 6.3.1 A). The sharp peak response is suggestive of an adsorption/desorption process where upon the scanning of negative potentials, CTA^+ approaches the interface and interacts with TBA. Then as the scan is reversed, TBA desorbs from the interface producing the peak response. Similar observations were seen with other anionic biomolecules interacting with the organic cation as discussed previously (see Chapters 4 and 5) as well as with surfactant-protein

interaction as reported elsewhere.¹⁵³ On the other hand, despite having the surfactant in the organic phase as shown in Figure 6.3.2 (A), its lower concentration (5 mM) as compared to 10 mM BTPPATPBCl means the latter will have the majority effect over it and thus no peak response was recorded.

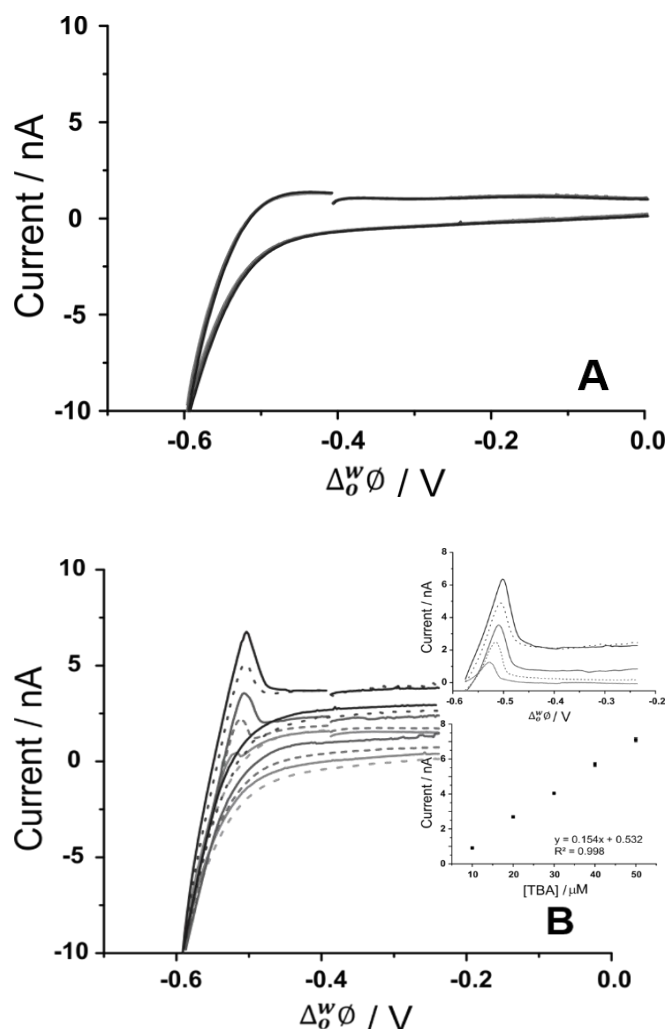


Figure 6.3.2 Cyclic voltammograms of 10 mM LiCl (pH 8.5) with 10-50 μM TBA in aq. phase while (A) 5 mM CTAB + 10 mM BTPPATPBCl and (B) 10 mM CTAB + 10 mM BTPPATPBCl in org. phase; Scan rate was 5 $mV s^{-1}$. Top Inset: Background subtracted CVs (B), Bottom Inset: Calibration plot of top inset.

To further examine the interaction of the surfactant with the aptamer and its role in the detection of the latter, CTATPBCl was employed as the only electrolyte in the organic phase. Having the addition of a hydrophobic salt of the surfactant as the organic phase electrolyte removes any overshadowing of other species and will make the surfactant-aptamer interaction as the focus. Consequently, any electrochemistry observed in the presence of the aptamer can be attributed to the interaction between the anionic aptamer and CTA^+ cation in the organic phase.

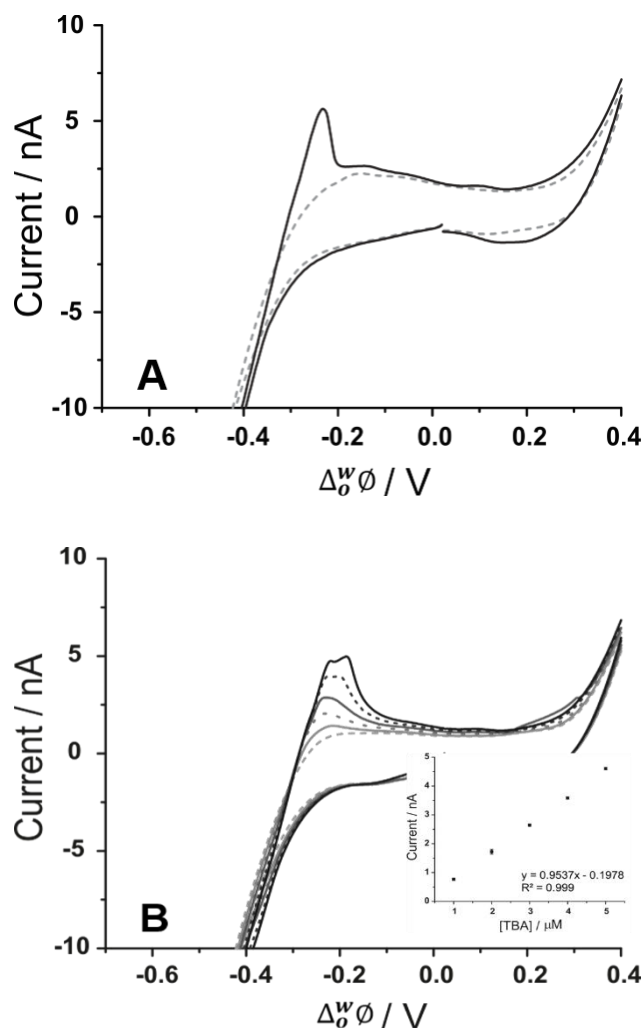


Figure 6.3.3 Cyclic voltammograms of 10 mM LiCl (pH 8.5) using Cell 2 (see Scheme 6.2.1) (A) with (black line) and without (grey dashed line) 10 μM TBA and (B) with varying (1-5 μM) TBA. Scan rate: 5 mV s^{-1} . Inset: Calibration plot of (B).

Figure 6.3.3 shows the cyclic voltammograms obtained when 10 mM CTATPBCl replaced the commonly used BTPPATPBCl in the organic phase. In the presence of 10 μM TBA (black line, Figure 6.3.3 A), a distinct peak response was observed at *ca.* -0.25 V which was clearly not observed in the blank scan (dashed line, Figure 6.3.3 A). Only transfers of background electrolytes were observed when TBA was absent. When compared to the response seen when BTPPATPBCl was present together with CTA^+ at the organic phase (see Figure 6.3.2 B), the peak current corresponding for 10 μM TBA was *ca.* 1 nA. This increased to *ca.* 5 nA (See Figure 6.3.3 A) when only 10 mM CTATPBCl was in the organic phase. As there seems to be a better surfactant-aptamer interaction observed when only 10 mM CTA^+ is in the organic phase, lower TBA concentrations were tested. Illustrated in Figure 6.3.3 (B) are the CVs corresponding to varying lower (1-5 μM) concentrations of TBA were

added into the aqueous phase. As seen, a distinct peak response at *ca.* -0.25 V appears when 2 μM TBA was present. This peak current increased proportionately with increasing concentrations of TBA added. When background subtraction was done (see top inset Figure 6.3.3 B) on the CVs, it reveals that a peak response is already observed even at 1 μM TBA. This arrangement with CTATPBCl in the organic phase afforded a calculated detection limit of 0.11 μM TBA in 10 mM LiCl from a linear calibration of 1-5 μM TBA with a sensitivity of 0.954 nA μM^{-1} .

6.3.3 Effect of Presence of Other Species

The properties of the 15-mer TBA and how it interacts with its designated analyte (thrombin) has been reported to be influenced by various factors.²⁹⁸ One known property of the 15-mer TBA is its folding/unfolding ability in the presence of other species.²⁹⁹ To test this phenomenon and see how it affects the electrochemical response at the μITIES , 1 mM MgCl_2 was used. Previous studies³⁰⁰ include Mg^{2+} as one of the cations that induces folding of the 15-mer thrombin binding aptamer. In fact, this interaction was used to determine total water hardness.³⁰¹

Figure 6.3.4 (A) shows the CVs obtained using Cell 2 (see Scheme 6.2.1) in the absence (grey dashed line) and presence (black dashed line) of 5 μM TBA. As previously observed earlier, a distinct peak response around -0.25 V is seen suggesting the interaction of the surfactant with the aptamer. However, this peak response was no longer observed when 1 mM MgCl_2 was added (grey bold line). This could indicate that Mg^{2+} has induced the folding of the TBA so that it is no longer able to interact with the CTA^+ to produce the distinct desorption peak as previously observed. Also, the effect of the presence of thrombin on the electrochemical response of the aptamer at the ITIES was explored. Displayed in Figure 6.3.4 (B) are the CVs obtained when different concentrations (0.13 and 0.39 mg mL^{-1}) of thrombin was added into the aqueous phase together with 10 μM TBA. The same peak around *ca.* -0.25 V was recorded when 10 μM TBA (grey line) was present. Meanwhile, when 0.13 mg mL^{-1} of thrombin was added into the solution that contained TBA, the peak current of the TBA response decreased. This further decreased when the thrombin concentration was tripled. This is suggestive of the idea that as more thrombin is added, less TBA is being desorbed at the interface as thrombin interacts with the aptamer.

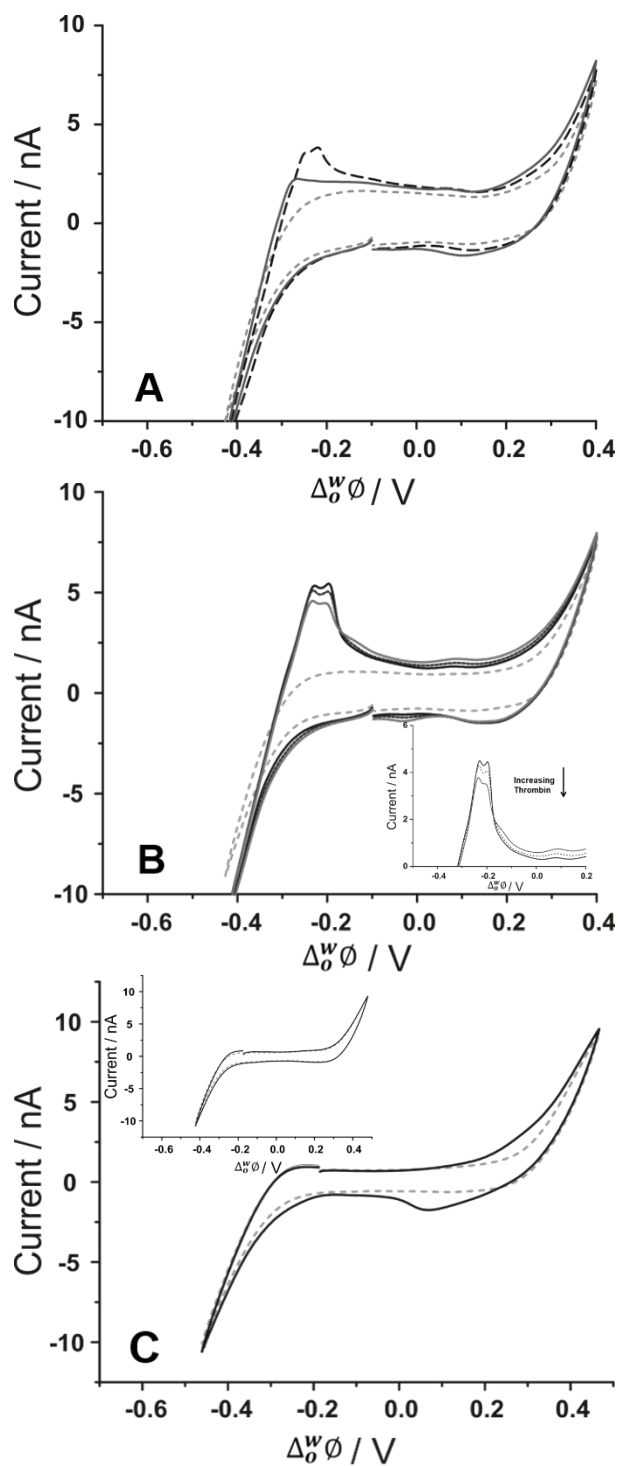


Figure 6.3.4 Cyclic voltammograms of 10 mM LiCl (pH 8.5) using Cell 2 (see Scheme 6.2.1) (A) with (black dashed line) and without (grey dashed line) 5 μM TBA while the dark grey line represent addition of 1 mM MgCl_2 . (B) with (grey line) and without (grey dashed line) 10 μM TBA plus different thrombin concentrations (0.13 – 0.39 mg mL^{-1}). (C) CVs in the absence (grey dashed line) and presence (black line) of 0.26 mg mL^{-1} thrombin in 10 mM HCl. Scan rate: 5 mV s^{-1} . Inset of (B): Background subtracted CVs for (B); Inset of (C): CVs in the absence (grey dashed line) and presence (black line) of 0.26 mg mL^{-1} thrombin in 10 mM LiCl (pH8.5).

Meanwhile, to verify if thrombin is indeed electroactive at this arrangement (Cell 2, see Scheme 6.2.1) where CTATPBCl is the only organic electrolyte, cyclic voltammetry of thrombin in pH 2 (10 mM HCl) was explored. Resulting CVs are shown in Figure 6.3.4 (C) for the absence (grey dashed line) and presence (black line) of 0.26 mg mL⁻¹ thrombin. In the forward scan towards positive potentials, an increase in current is observed which could suggest that thrombin is moving towards the interface and can be adsorbed. Meanwhile, when the scan is reversed towards negative potentials, a peak response is recorded around *ca.* 0.075 V which is indicative of the desorption of thrombin back into the aqueous phase. A similar response was reported for other proteins at this pH.^{49,159,231} On the other hand, when the same concentration of thrombin was added into 10 mM LiCl (pH 8.5) as shown in Figure 6.3.4 (C) inset, no response was observed that would indicate thrombin activity at the interface. Only the response for background electrolyte transfer was recorded.

6.3.4 Matrix Effects

The biological importance of the detection of aptamers at biological systems is expected for most studies. In this light, the electrochemical behaviour of the thrombin-binding aptamer was examined at a synthetic urine matrix. The concoction of the employed synthetic urine was described elsewhere.²³⁴ This was then used as the aqueous phase of the electrochemical measurements following Cell 3 in Scheme 6.2.1. Figure 6.3.5 (A) reveals the CVs obtained using Cell 3 (see Scheme 6.2.1) where the aqueous phase was synthetic urine (black line) overlaid with that of 10 mM LiCl (pH 8.5, grey dashed line). There is a small shift (*ca.* 50 mV) in the potential window. This can be attributed to the presence of other species in the synthetic urine that may transfer at a differential potential than in the usual ITIES set-up. However, in spite of this slight shift in the potential window, TBA was still detected as seen by the distinct peak response at *ca.* -0.32 V and this is displayed in Figure 6.3.5 (B). This peak current is observed to increase linearly with added TBA concentration. As mentioned earlier, this distinct sharp peak is indicative of an adsorption/desorption process. With this explored response, the calculated limit of detection is 0.29 μ M TBA in this biomimetic matrix from a 1-5 μ M TBA calibration and a sensitivity of 0.662 nA μ M⁻¹. This is a lower sensitivity when compared to that achieved with the normal electrolyte. This can

be credited to the presence of other ions in the aqueous phase as discussed earlier. A summary of the analytical characteristics achieved in the study is shown in Table 6.3.1.

Table 6.3-1 Summary of the analytical characteristics attained for TBA using the polarized soft microinterfaces.

Detection Method	Organic Cation	Sensitivity (calibration graph) / nA μM^{-1}	Number of Points / n	Limit of Detection (LOD) / μM	Concentration Range / μM	Correlation Coefficient / R
CV	BTPPA ⁺ /CTA ⁺	0.154	5	1.78	10-50	0.999
CV	CTA ⁺	0.954	5	0.11	1-5	0.999
†CV	CTA ⁺	0.662	5	0.29	1-5	0.977

† Corresponds to experiments when synthetic urine was used as the aqueous phase. The rest was in 10 mM LiCl (pH 8.5).

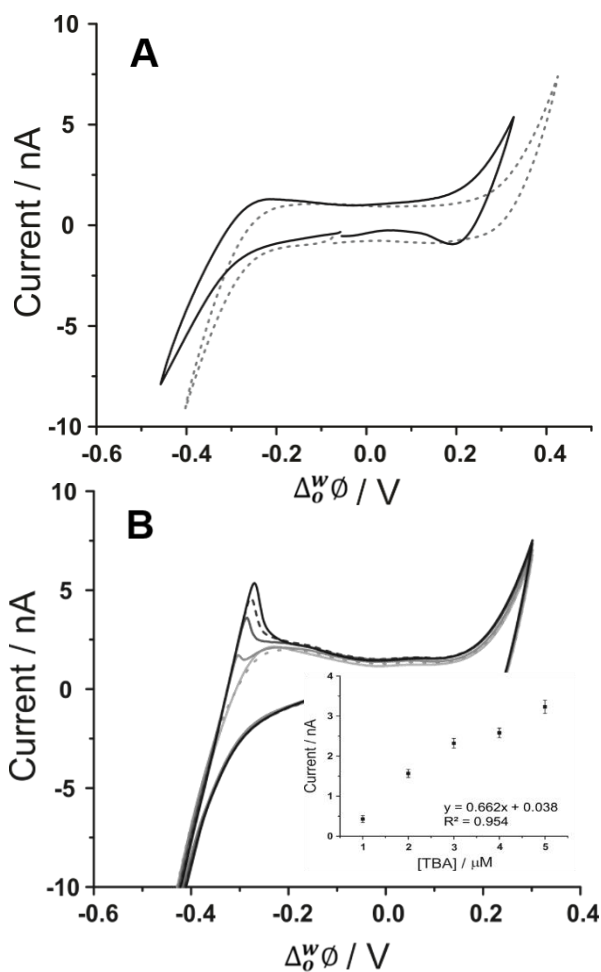


Figure 6.3.5 CVs of synthetic urine (black line) overlaid with that of 10 mM LiCl (pH 8.5) as the aqueous phase. (B) CVs of increasing (1-5 μM) TBA. Scan rate: 5 mV s^{-1} . Inset: Calibration of (B).

6.4 Conclusions

The electrochemistry of ITIES was employed to explore the electrochemical behaviour of a 15-mer thrombin-binding aptamer via voltammetric measurements. No response was observed using the common BTTPATPBCl as the organic phase. However, upon the addition of a surfactant, CTAB, which is known to interact with DNA, a change in the electrochemical response was seen. This was observed as a decrease in the transfer current of CTAB when varying amounts of TBA was added to the aqueous phase. This was further explored by incorporating CTAB in the organic phase along with BTTPATPBCl. The effect of the surfactant concentration was observed to play a role in the detection of TBA since only when 10 mM CTAB was present that a TBA response was seen. A distinct sharp peak around *ca.* -0.54 V was suggestive of an adsorption/desorption process. The surfactant-aptamer interaction

was enhanced when CTATPBCl replaced BTPPATPBCl in the organic phase. This time the peak response for TBA shifted to *ca.* -0.25 V, which can be attributed to the early transfer of CTA⁺ across the interface. This explored surfactant-aptamer interaction afforded a calculated detection limit of 0.11 μM TBA. Moreover, the effect of other species present revealed promising results. In the presence of 1 mM MgCl₂, the peak response previously seen disappears suggesting that Mg²⁺ induces TBA to fold and prevent its interaction with CTAB. Also, thrombin was indirectly detected via the decrease of the peak current produced by the surfactant-aptamer interaction. Then, this explored interaction was further examined in a biomimetic matrix. Despite the presence of other electrochemically active species in the synthetic urine, a calculated detection limit of 0.29 μM for TBA was achieved. The behaviour established here further indicates the viability of using the electrochemistry of μITIES as a label-free analytical tool for the detection of aptamers. Further enhancing this identified behaviour and its application (i.e. thrombin detection) warrants more investigations.

Chapter 7. General Conclusions and Future Outlook

7.1 General Conclusions

The work presented in this thesis chronicles the investigation into utilizing the electrochemistry at the interface between two immiscible electrolyte solutions (ITIES) for the investigation of biologically important molecules. The advent of early disease diagnostics, therapeutics and nutraceuticals have required detection methods that provide rapid, cost-effective and sensitive results. Over the years, the electrochemistry at the ITIES has been employed to explore various biomolecules such as proteins, drugs and other small molecules. This thesis adds to this body of knowledge through exploring an alternative way of preparing the gelled organic phase (Chapter 3), investigation of the electrochemical behaviour of a seaweed-extracted polysaccharide (Chapter 4), simpler versions of it in the form of sulfated disaccharides (Chapter 5) and also the more widely known, synthetic oligonucleotides, aptamers (Chapter 6).

The use of solvent-casting PVC with THF in the preparation of the organic phase of a μ ITIES array was investigated for protein detection with lysozyme as the model. Cyclic voltammetry revealed a distinct peak around *ca.* 0.68 V at the reverse scan for this solvent-casted organogel-liquid interface. Detection was enhanced by optimization of adsorption parameters. Best adsorption potential was at more positive potentials and just below where the transfer of background electrolyte occurred. Also, pre-concentration time obviously affects sensitivity towards lysozyme. AdSV for 300 s afforded a 0.03 μ M detection limit but this was further lowered by using differential pulse voltammetry. Utilization of AdDPSV enabled a quite similar detection limit (0.017 μ M) for only 60 s pre-concentration. Better limits of detection were achieved following 120 s (0.014 μ M) and 300 s (0.010 μ M) pre-concentration, which is lower than previously reported for lysozyme at the μ ITIES.

Then, voltammetric measurements at the μ ITIES array were employed to examine the electrochemical characteristics of fucoidan. Two species, *Undaria pinnatifida* and *Fucus vesiculosus* were initially studied. However, CV showed a more distinct peak for *Undaria p.* at *ca.* -0.50 V with the usual set-up of BTPPA⁺ in the

organic phase. This peak potential, however, shifted to *ca.* -0.30 V and to -0.175 V when the organic phase cation was replaced with TDDA⁺ and TDMA⁺ respectively. This change can be the result of increasing binding strength of the fucoidan with these organic phase cations. Peak shape recorded indicated a desorption process tantamount to an adsorption during the forward (negative-going) scan. When adsorption potential was surveyed, it revealed that optimal adsorption potential occurred at a potential just before the background electrolyte transfer. Employing AdSV and combining a pre-concentration time of 180 s with TDMA⁺ in the organic phase resulted to a detection limit of 1.8 $\mu\text{g mL}^{-1}$ (10 mM NaOH) and 2.3 $\mu\text{g mL}^{-1}$ (pH-adjusted synthetic urine) for *Undaria p. fucoidan*.

To further explore the behaviour of these highly sulfated carbohydrates, simpler versions were examined using voltammetry at the liquid-organogel μ ITIES array. CV showed no response to a low μM SOS concentration when BTPPA⁺ was in the organic phase. Nonetheless, when TDDA⁺ was used instead, a distinct peak was observed at the reverse (negative-going) scan at *ca.* -0.47 V and this shifted to *ca.* -0.28 V when TDMA⁺ was used. As mentioned previously, this can be credited to the increased binding strength between SOS and these organic phase cations. Examination of the peak shape suggests a desorption process following an adsorption during the forward (negative-going) scan. Optimization of the adsorption potential for SOS at the liquid-organogel μ ITIES array revealed that maximum adsorption happens at a potential near that of the background electrolyte transfer. Similar to previous chapters, a combination of TDMA⁺ as the organic electrolyte phase cation and a chosen pre-concentration time, which is 60 s for this instance, resulted to a limit of the detection value of 0.12 μM in 10 mM LiCl and 0.24 μM in a biomimetic matrix (synthetic urine). Moreover, when adsorption time was tripled to 180 s, limit of detection was also lowered down to 0.04 μM (10 mM LiCl).

Furthermore, the electrochemistry of ITIES was employed to explore the electrochemical characteristics of a thrombin-binding aptamer (15-mer) via voltammetric measurements. With the usual organic electrolyte cation, BTPPA⁺, and cyclic voltammetry, no response was recorded for 10 μM TBA. However, when a cationic surfactant, CTAB, was employed, a change in the electrochemical response was shown. CTAB is known to interact with DNA and the results suggest it also interacts with the 15-mer aptamer. This interaction was observed as a decrease in the

transfer current of CTAB upon addition of increasing amounts of TBA in the aqueous phase. Further exploration included the incorporation of CTAB in the organic phase together with BTPPATPBCl. The effect of CTAB concentration in the presence of BTPPA⁺ in the organic phase was observed to play a role in the detection of TBA since only when 10 mM CTAB was present in the organic phase that a response was recorded, which was not seen when 5 mM CTAB was present. This response was again in the form of a sharp peak, this time around *ca.* -0.54 V, indicating an adsorption/desorption process, equivalent to what has been recorded for the other negatively-charged biomolecules discussed previously. This surfactant-aptamer interaction was enhanced when BTPPATPBCl was replaced by CTATPBCl in the organic phase. CV on this system showed a similar peak response for TBA but it was shifted to *ca.* -0.25 V, a phenomenon that can be credited to the early transfer of CTA⁺ across the polarized interface. Using this explored surfactant-aptamer interaction with CTATPBCl in the organic phase, a detection limit of 0.11 μ M TBA was attained. Furthermore, the effect of other species present in the aqueous phase revealed interesting results. When 1mM MgCl₂ was added into the aqueous phase along with the TBA, the peak response previously recorded for TBA disappears indicating Mg²⁺ induces TBA to fold with it and prevent its interaction with CTAB. Then, with CTA⁺ in the organic phase and TBA in the aqueous phase, different amounts of thrombin were spiked with it. This resulted in a decrease on the peak currents produced by the surfactant-aptamer interaction. Meanwhile, the behaviour of TBA in a biomimetic matrix (synthetic urine) was also studied. With CTATPBCl as the organic phase, TBA showed a similar peak response previously seen, even in the synthetic urine as the aqueous phase and this afforded a detection limit of 0.29 μ M.

7.2 Future Outlook

The electrochemistry at the interface between two immiscible electrolyte solutions and its application in understanding biomolecules at the polarized soft interfaces has been one of the key motivations on the research that is presented in this thesis. Since the inception of the technique as an alternative tool for bioanalytical detection, there has been a continuous development in this field. Nevertheless, there is still further investigations needed to establish this technique in a position that can be

commercialized or be used in routinary biomolecular detection. Thus, a few more vital points or research areas in this field can benefit from more research attention.

Despite a growing number of studies detailing protein behaviour at the ITIES, there is still more work that can be done to elucidate the mechanism of interaction at the ITIES. As of now, most protein studies propose a facilitated ion transfer mechanism, which entails the interaction of the protein with the organic anion as the detection method. More detailed investigations into the nature of this interaction and how to enhance the interaction (i.e. exploration of better molecules to complex with proteins) and improve selectivity as well as the sensitivity of the method.

One of the main challenges in biomolecular detection involves detection of biological samples or at complex mixtures. Presented in this thesis is the viability of employing the electrochemistry at the ITIES in the detection of biomolecules in a biomimetic matrix (synthetic urine). In spite of the presence of other species that have been known to interfere with or affect the behaviour of biomolecules at this complex matrix, detection was still possible. The issue is now on being able to achieve physiologically important low concentrations for such biomolecules. Major steps employed in this thesis are optimization of the electrochemical technique of use and the utilization of an ionophore or a molecule that will greatly interact with the analyte. So far, the results in this thesis support the idea that highly negatively charged biomolecules are detected with its interaction with the organic electrolyte cation and the structure of the organic cation influences how effective it is to bind or interact with the anionic biomolecule. Therefore, further exploration on the optimization of such ionophores and enhancement of its interaction with the biomolecule is merited. Also, as revealed by the chapter on thrombin-binding aptamer, the use of surfactants can be studied deeper. Parameters like the type of surfactant, the structure of surfactant as well as the presence of other ions that affect its structure (i.e. folding/unfolding) are avenues for further research.

Optimization of experimental parameters before or during electrochemical measurements is something that also plays a vital role in the detection of biomolecules. From choosing the pH to identifying the optimal adsorption potential or selecting the type of electrolytes at either phase are steps that would greatly affect the electrochemical response attained. In this regard, it is always important to consider the

inherent physical properties of the biomolecule under study. Moreover, inspection or utilizing other electrochemical techniques to enhance detection limits is always beneficial. As most of the results presented in this thesis reveal, adsorptive stripping voltammetry greatly enhances the analyte concentrations being detected. AdDPSV was shown to improve the detection of lysozyme at the solvent-casted organogel-liquid interfaces. Thus, employing such techniques (e.g. differential pulse voltammetry, square wave voltammetry) merits further examination.

Another main advantage of the electrochemistry at the ITIES is the fact that it can be used to deepen the understanding of fundamental biological processes since it is considered to be a simple model of half of a phospholipid bilayer membrane. Interaction of common cations with biomolecules at the lipid bilayer is of research interest for applications such as drug delivery systems. In this thesis, the electrochemistry at the μ ITIES showed that presence of Mg^{2+} in the aqueous phase greatly impacts the electrochemical response recorded for the thrombin-binding aptamer. More investigations on how this supposedly folding of the aptamer can be utilized to study aptamer-protein interactions definitely is warranted. Speaking of aptamer interactions, investigation on the use of aptamers with other biomolecules such as polysaccharides and drug molecules would be of interest. As an example, thrombin is known to interact with SOS so how this interaction can affect their behaviour at the soft polarized interface is a research question that warrants more studies.

References

- (1) Bard, A. J.; Faulkner, L. R. *Electrochemical Methods: Fundamentals and Applications*; John Wiley & Sons, Inc.: New York, **2001**.
- (2) Zoski, C. G. *Handbook of Electrochemistry*; Elsevier: Oxford, **2007**.
- (3) Wieckowski, A. *Interfacial Electrochemistry: Theory: Experiment, and Applications*; CRC Press, **1999**.
- (4) Atkins, P.; De Paula, J. *Elements of Physical Chemistry*; Oxford University Press, **2017**.
- (5) Wang, J. *Analytical Electrochemistry*; John Wiley & Sons: Hoboken, New Jersey, **2006**.
- (6) Wang, Y.; Kakiuchi, T.; Yasui, Y.; Mirkin, M. V. *J. Am. Chem. Soc.* **2010**, *132*, 16945-16952.
- (7) Bond, A. M. *Broadening Electrochemical Horizons: Principles and Illustration of Voltammetric and Related Techniques*; Oxford University Press on Demand, **2002**.
- (8) Gouy, M. *J. Phys. Theor. Appl.* **1910**, *9*, 457-468.
- (9) Chapman, D. L. *The London, Edinburgh, and Dublin philosophical magazine and journal of science* **1913**, *25*, 475-481.
- (10) Collins, C. J. *Liquid-liquid Electrochemistry for the Extraction and Detection of Drug Molecules*. University College Cork, PhD Thesis, **2010**.
- (11) Stern, O. *Z. Elektrochem* **1924**, *30*, 1014-1020.
- (12) Grahame, D. C. *Chemical reviews* **1947**, *41*, 441-501.
- (13) Matsuura, T. *Desalination* **2001**, *134*, 47-54.

- (14) Silvester, D. S. *Electrochemical Studies in Room Temperature Ionic Liquids*. University of Oxford, PhD Thesis, **2008**.
- (15) Scanlon, M. D. *Electrochemical Processes of Bio-Analytical Importance at Micro- and Nano-Liquid/Liquid Interfaces*. University College Cork, PhD Thesis, **2009**.
- (16) Henstridge, M. C.; Compton, R. G. *The Chemical Record* **2012**, *12*, 63-71.
- (17) Samec, Z. *Pure and Applied Chemistry* **2004**, *76*, 2147-2180.
- (18) Arrigan, D. W. M. *Anal. Lett.* **2008**, *41*, 3233-3252.
- (19) Samec, Z.; Mareček, V.; Koryta, J.; Khalil, M. W. *J. Electroanal. Chem. Interfacial Electrochem.* **1977**, *83*, 393-397.
- (20) Taylor, G.; Girault, H. H. *J. Electroanal. Chem. Interfacial Electrochem.* **1986**, *208*, 179-183.
- (21) Shao, Y.; Osborne, M. D.; Girault, H. H. *J. Electroanal. Chem. Interfacial Electrochem.* **1991**, *318*, 101-109.
- (22) Sherburn, A.; Platt, M.; Arrigan, D. W. M.; Boag, N. M.; Dryfe, R. A. W. *Analyst* **2003**, *128*, 1187-1192.
- (23) Lillie, G. C.; Holmes, S. M.; Dryfe, R. A. W. *The Journal of Physical Chemistry B* **2002**, *106*, 12101-12103.
- (24) Sugihara, T.; Hotta, H.; Osakai, T. *PCCP* **2004**, *6*, 3563-3568.
- (25) Herzog, G.; Arrigan, D. W. M. *Analyst* **2007**, *132*, 615-632.
- (26) Koryta, J. *Electrochim. Acta* **1979**, *24*, 293-300.
- (27) Campbell, J. A.; Girault, H. H. *J. Electroanal. Chem. Interfacial Electrochem.* **1989**, *266*, 465-469.
- (28) Campbell, J. A.; Stewart, A. A.; Girault, H. H. *Journal of the Chemical Society, Faraday Transactions 1: Physical Chemistry in Condensed Phases* **1989**, *85*, 843-853.

- (29) Shao, Y.; Mirkin, M. V. *J. Am. Chem. Soc.* **1997**, *119*, 8103-8104.
- (30) Sun, P.; Laforge, F. O.; Mirkin, M. V. *J. Am. Chem. Soc.* **2005**, *127*, 8596-8597.
- (31) Scanlon, M. D.; Arrigan, D. W. M. *Electroanalysis* **2011**, *23*, 1023-1028.
- (32) Rimboud, M.; Hart, R. D.; Becker, T.; Arrigan, D. W. M. *Analyst* **2011**, *136*, 4674-4681.
- (33) Nernst, W.; Riesenfeld, E. H. *Annalen der Physik* **1902**, *313*, 600-608.
- (34) Blank, M.; Feig, S. *Science* **1963**, *141*, 1173-1174.
- (35) Nelson, D. L.; Lehninger, A. L.; Cox, M. M. *Lehninger Principles of Biochemistry*; Macmillan: New York, 2008.
- (36) Gavach, C.; Mlodnick, T.; Guastall, J. *Comptes rendus Hebdomadaires Des Seances De L Academie Des Sciences Serie C* **1968**, *266*, 1196.
- (37) Girault, H. H. *Charge Transfer Across Liquid-Liquid Interfaces*; Plenum Press: New York, **1993**; Vol. 25.
- (38) Zhan, D.; Mao, S.; Zhao, Q.; Chen, Z.; Hu, H.; Jing, P.; Zhang, M.; Zhu, Z.; Shao, Y. *Anal. Chem.* **2004**, *76*, 4128-4136.
- (39) Berduque, A.; Zazpe, R.; Arrigan, D. W. M. *Anal. Chim. Acta* **2008**, *611*, 156-162.
- (40) Ribeiro, J. A.; Miranda, I. M.; Silva, F.; Pereira, C. M. *PCCP* **2010**, *12*, 15190-15194.
- (41) Vanýsek, P.; Hernandez, I. C.; Xu, J. *Microchem. J.* **1990**, *41*, 327-339.
- (42) Marecek, V.; Samec, Z. *Analytical Letters Part B-Clinical and Biochemical Analysis* **1981**, *14*, 1241-1253.
- (43) Colombo, M. L.; Sweedler, J. V.; Shen, M. *Anal. Chem.* **2015**, *87*, 5095-5100.
- (44) Collins, C. J.; Lyons, C.; Strutwolf, J.; Arrigan, D. W. M. *Talanta* **2010**, *80*, 1993-1998.

- (45) Ribeiro, J. A.; Silva, F.; Pereira, C. M. *Anal. Chem.* **2013**, *85*, 1582-1590.
- (46) Huang, X.; Xie, L.; Lin, X.; Su, B. *Anal. Chem.* **2016**, *89*, 945-951.
- (47) Kivlehan, F.; Lanyon, Y. H.; Arrigan, D. W. M. *Langmuir* **2008**, *24*, 9876-9882.
- (48) Scanlon, M. D.; Jennings, E.; Arrigan, D. W. M. *PCCP* **2009**, *11*, 2272-2280.
- (49) Herzog, G.; Kam, V.; Arrigan, D. W. M. *Electrochim. Acta* **2008**, *53*, 7204-7209.
- (50) Guo, J.; Yuan, Y.; Amemiya, S. *Anal. Chem.* **2005**, *77*, 5711-5719.
- (51) Jing, P.; Kim, Y.; Amemiya, S. *Langmuir* **2009**, *25*, 13653-13660.
- (52) Amemiya, S.; Kim, Y.; Ishimatsu, R.; Kabagambe, B. *Anal Bioanal Chem* **2011**, *399*, 571-579.
- (53) Langmaier, J.; Samec, Z.; Samcová, E.; Tůma, P. *Electrochem. Commun.* **2012**, *24*, 25-27.
- (54) Vagin, M. Y.; Trashin, S. A.; Karyakin, A. A.; Mascini, M. *Anal. Chem.* **2008**, *80*, 1336-1340.
- (55) Horrocks, B. R.; Mirkin, M. V. *Anal. Chem.* **1998**, *70*, 4653-4660.
- (56) Kivlehan, F.; Lefoix, M.; Moynihan, H. A.; Thompson, D.; Ogurtsov, V. I.; Herzog, G.; Arrigan, D. W. M. *Electrochim. Acta* **2010**, *55*, 3348-3354.
- (57) Sisk, G. D.; Herzog, G.; Glennon, J. D.; Arrigan, D. W. M. *Electrophoresis* **2009**, *30*, 3366-3371.
- (58) Wilke, S.; Schürz, R.; Wang, H. *Anal. Chem.* **2001**, *73*, 1146-1154.
- (59) Wang, Y.; Kececi, K.; Velmurugan, J.; Mirkin, M. V. *Chemical Science* **2013**, *4*, 3606-3616.
- (60) Lee, H. J.; Girault, H. H. *Anal. Chem.* **1998**, *70*, 4280-4285.

- (61) Scanlon, M. D.; Berduque, A.; Strutwolf, J.; Arrigan, D. W. M. *Electrochim. Acta* **2010**, *55*, 4234-4239.
- (62) Gohara, E.; Osakai, T. *Anal. Sci.* **2010**, *26*, 375-378.
- (63) Rodgers, A. N. J.; Dryfe, R. A. W. *ChemElectroChem* **2016**, *3*, 472-479.
- (64) Huang, X.; Xuan, Y.; Xie, L.; Su, B. *ChemElectroChem* **2016**, *3*, 1781-1786.
- (65) Bian, X.; Scanlon, M. D.; Wang, S.; Liao, L.; Tang, Y.; Liu, B.; Girault, H. H. *Chemical Science* **2013**, *4*, 3432-3441.
- (66) Hirunpinyopas, W.; Rodgers, A. N. J.; Worrall, S. D.; Bissett, M. A.; Dryfe, R. A. W. *ChemNanoMat* **2017**, *3*, 428-435.
- (67) Ozel, F.; Aslan, E.; Sarilmaz, A.; Hatay Patir, I. *ACS Applied Materials & Interfaces* **2016**, *8*, 25881-25887.
- (68) Ge, P.; Olaya, A. J.; Scanlon, M. D.; Hatay Patir, I.; Vrubel, H.; Girault, H. H. *Chem.Phys.Chem* **2013**, *14*, 2308-2316.
- (69) Huang, C.; Cui, M.; Sun, Z.; Liu, F.; Helms, B. A.; Russell, T. P. *Langmuir* **2017**.
- (70) Gschwend, G. C.; Smirnov, E.; Peljo, P.; Girault, H. H. *Faraday Discuss.* **2017**.
- (71) Smirnov, E.; Peljo, P.; Girault, H. H. *Chem. Commun.* **2017**, *53*, 4108-4111.
- (72) Verwey, E. J. W.; Niessen, K. F. *The London, Edinburgh, and Dublin Philosophical Magazine and Journal of Science* **1939**, *28*, 435-446.
- (73) Gavach, C.; Seta, P.; D'Epenoux, B. *J. Electroanal. Chem. Interfacial Electrochem.* **1977**, *83*, 225-235.
- (74) Girault, H. H.; Schiffrin, D. J. *J. Electroanal. Chem. Interfacial Electrochem.* **1983**, *150*, 43-49.
- (75) Senda, M.; Kakiuchi, T.; Osaka, T. *Electrochim. Acta* **1991**, *36*, 253-262.

- (76) Samec, Z.; Mareček, V.; Homolka, D. *Faraday Discuss. Chem. Soc.* **1984**, *77*, 197-208.
- (77) Girault, H. H. J.; Schiffrin, D. J. *J. Electroanal. Chem. Interfacial Electrochem.* **1985**, *195*, 213-227.
- (78) Pereira, C. M.; Schmickler, W.; Silva, F.; Sousa, M. J. *J. Electroanal. Chem.* **1997**, *436*, 9-15.
- (79) Mitrinovic, D. M.; Zhang, Z.; Williams, S. M.; Huang, Z.; Schlossman, M. L. *The Journal of Physical Chemistry B* **1999**, *103*, 1779-1782.
- (80) Luo, G.; Malkova, S.; Yoon, J.; Schultz, D. G.; Lin, B.; Meron, M.; Benjamin, I.; Vanýsek, P.; Schlossman, M. L. *Science* **2006**, *311*, 216-218.
- (81) Laanait, N.; Mihaylov, M.; Hou, B.; Yu, H.; Vanýsek, P.; Meron, M.; Lin, B.; Benjamin, I.; Schlossman, M. L. *Proceedings of the National Academy of Sciences* **2012**, *109*, 20326-20331.
- (82) Mitrinović, D. M.; Tikhonov, A. M.; Li, M.; Huang, Z.; Schlossman, M. L. *Phys. Rev. Lett.* **2000**, *85*, 582.
- (83) Strutwolf, J.; Barker, A. L.; Gonsalves, M.; Caruana, D. J.; Unwin, P. R.; Williams, D. E.; Webster, J. R. P. *J. Electroanal. Chem.* **2000**, *483*, 163-173.
- (84) Benjamin, I. *The Journal of chemical physics* **1992**, *97*, 1432-1445.
- (85) Daikhin, L. I.; Kornyshev, A. A.; Urbakh, M. *J. Electroanal. Chem.* **2000**, *483*, 68-80.
- (86) Girault, H. H. In *Electroanalytical Chemistry: A Series of Advances*, Bard, A. J.; Zoski, C. G., Eds.; CRC Press: Taylor & Francis: Boca Raton, FL, **2010**, p 1.
- (87) Molina, Á.; Serna, C.; Ortuño, J. A.; Torralba, E. *Annual Reports Section "C"(Physical Chemistry)* **2012**, *108*, 126-176.
- (88) Amemiya, S.; Wang, Y.; Mirkin, M. V. *Specialist Periodical Reports In Electrochemistry* **2013**, *12*, 1.

- (89) Liu, B.; Mirkin, M. V. *Electroanalysis* **2000**, *12*, 1433-1446.
- (90) Liu, S.; Li, Q.; Shao, Y. *Chem. Soc. Rev.* **2011**, *40*, 2236-2253.
- (91) Huang, X. J.; O'Mahony, A. M.; Compton, R. G. *Small* **2009**, *5*, 776-788.
- (92) Beattie, P. D.; Delay, A.; Girault, H. H. *J. Electroanal. Chem.* **1995**, *380*, 167-175.
- (93) Shao, Y.; Mirkin, M. V. *Anal. Chem.* **1998**, *70*, 3155-3161.
- (94) Kralj, B.; Dryfe, R. A. W. *PCCP* **2001**, *3*, 5274-5282.
- (95) Lee, H. J.; Beattie, P. D.; Seddon, B. J.; Osborne, M. D.; Girault, H. H. *J. Electroanal. Chem.* **1997**, *440*, 73-82.
- (96) Scanlon, M. D.; Herzog, G.; Arrigan, D. W. M. *Anal. Chem.* **2008**, *80*, 5743-5749.
- (97) Strutwolf, J.; Scanlon, M. D.; Arrigan, D. W. M. *Analyst* **2009**, *134*, 148-158.
- (98) Scanlon, M. I. D.; Strutwolf, J. r.; Blake, A.; Iacopino, D.; Quinn, A. J.; Arrigan, D. W. M. *Anal. Chem.* **2010**, *82*, 6115-6123.
- (99) Alvarez de Eulate, E.; Strutwolf, J. r.; Liu, Y.; O'Donnell, K.; Arrigan, D. W. M. *Anal. Chem.* **2016**, *88*, 2596-2604.
- (100) Cai, C.; Tong, Y.; Mirkin, M. V. *The Journal of Physical Chemistry B* **2004**, *108*, 17872-17878.
- (101) Dryfe, R. A. W.; Kralj, B. *Electrochem. Commun.* **1999**, *1*, 128-130.
- (102) Platt, M.; Dryfe, R. A. W.; Roberts, E. P. L. *Langmuir* **2003**, *19*, 8019-8025.
- (103) Dekker, C. *Nature nanotechnology* **2007**, *2*, 209-215.
- (104) Sairi, M.; Chen- Tan, N.; Neusser, G.; Kranz, C.; Arrigan, D. W. M. *ChemElectroChem* **2015**, *2*, 98-105.
- (105) Arrigan, D. W. M. *Analyst* **2004**, *129*, 1157-1165.

- (106) Arrigan, D. W. M.; Liu, Y. Electroanalytical Ventures at Nanoscale Interfaces Between Immiscible Liquids, *Annual Review of Analytical Chemistry*, 9, **2016** 145-161.
- (107) Osakai, T.; Kakutani, T.; Senda, M. *Bunseki Kagaku* **1984**, 33, E371-E377.
- (108) Kakutani, T.; Ohkouchi, T.; Osakai, T.; Kakiuchi, T.; Senda, M. *Anal. Sci.* **1985**, 1, 219-225.
- (109) Lee, H. J.; Beriet, C.; Girault, H. H. *J. Electroanal. Chem.* **1998**, 453, 211-219.
- (110) Berduque, A.; Sherburn, A.; Ghita, M.; Dryfe, R. A. W.; Arrigan, D. W. M. *Anal. Chem.* **2005**, 77, 7310-7318.
- (111) Fantini, S.; Clohessy, J.; Gorgy, K.; Fusalba, F.; Johans, C.; Kontturi, K.; Cunnane, V. J. *Eur. J. Pharm. Sci.* **2003**, 18, 251-257.
- (112) Rahman, M. A.; Doe, H. *J. Electroanal. Chem.* **1997**, 424, 159-164.
- (113) Bond, A. M.; Luscombe, D.; Oldham, K. B.; Zoski, C. G. *J. Electroanal. Chem. Interfacial Electrochem.* **1988**, 249, 1-14.
- (114) Zoski, C. G.; Mirkin, M. V. *Anal. Chem.* **2002**, 74, 1986-1992.
- (115) Davies, T. J.; Ward-Jones, S.; Banks, C. E.; del Campo, J.; Mas, R.; Munoz, F. X.; Compton, R. G. *J. Electroanal. Chem.* **2005**, 585, 51-62.
- (116) Davies, T. J.; Compton, R. G. *J. Electroanal. Chem.* **2005**, 585, 63-82.
- (117) Saito, Y. *Review of Polarography* **1968**, 15, 177-187.
- (118) Alfred, L. C. R.; Oldham, K. B. *J. Electroanal. Chem.* **1995**, 396, 257-263.
- (119) Fletcher, S.; Horne, M. D. *Electrochem. Commun.* **1999**, 1, 502-512.
- (120) Vanysek, P.; Reid, J. D.; Craven, M. A.; Buck, R. P. *J. Electrochem. Soc.* **1984**, 131, 1788-1791.
- (121) Vanýsek, P.; Sun, Z. *J. Electroanal. Chem. Interfacial Electrochem.* **1990**, 298, 177-194.

- (122) Ohde, H.; Maeda, K.; Yoshida, Y.; Kihara, S. *Electrochim. Acta* **1998**, *44*, 23-28.
- (123) Osakai, T.; Jensen, H.; Nagatani, H.; Fermín, D. J.; Girault, H. H. *J. Electroanal. Chem.* **2001**, *510*, 43-49.
- (124) Beni, V.; Ghita, M.; Arrigan, D. W. M. *Biosensors and Bioelectronics* **2005**, *20*, 2097-2103.
- (125) Ohkouchi, T.; Kakutani, T.; Osakai, T.; Senda, M. *Anal. Sci.* **1991**, *7*, 371-376.
- (126) Lee, H. J.; Beriet, C.; Girault, H. H. *Anal. Sci.* **1998**, *14*, 71-77.
- (127) Ortuño, J. A.; Olmos, J. M.; Torralba, E.; Molina, A. *Sensors and Actuators B: Chemical* **2016**, *222*, 930-936.
- (128) Chen, Y.; Yuan, Y.; Zhang, M.; Li, F.; Sun, P.; Gao, Z.; Shao, Y. *Science in China Series B: Chemistry* **2004**, *47*, 24-33.
- (129) Sawada, S.; Osakai, T. *PCCP* **1999**, *1*, 4819-4825.
- (130) Osakai, T.; Hirai, T.; Wakamiya, T.; Sawada, S. *PCCP* **2006**, *8*, 985-993.
- (131) Bouchard, G.; Pagliara, A.; Carrupt, P.-A.; Testa, B.; Gobry, V.; Girault, H. H. *Pharm. Res.* **2002**, *19*, 1150-1159.
- (132) Ortuno, J. A.; Sanchez-Pedreno, C.; Gil, A. *Anal. Chim. Acta* **2005**, *554*, 172-176.
- (133) Collins, C. J.; Arrigan, D. W. M. *Anal. Chem.* **2009**, *81*, 2344-2349.
- (134) Velický, M.; Tam, K. Y.; Dryfe, R. A. W. *J. Electroanal. Chem.* **2012**, *683*, 94-102.
- (135) Lopes, P.; Katakya, R. *Anal. Chem.* **2012**, *84*, 2299-2304.
- (136) Jeshycka, S.; Han, H. Y.; Lee, H. J. *Electrochim. Acta* **2017**.
- (137) Samec, Z.; Trojánek, A.; Langmaier, J.; Samcová, E. *Electrochem. Commun.* **2003**, *5*, 867-870.

- (138) Ma, S. C.; Yang, V. C.; Meyerhoff, M. E. *Anal. Chem.* **1992**, *64*, 694-697.
- (139) Ma, S. C.; Yang, V. C.; Fu, B.; Meyerhoff, M. E. *Anal. Chem.* **1993**, *65*, 2078-2084.
- (140) Langmaier, J.; Olšák, J.; Samcova, E.; Samec, Z.; Trojánek, A. *Electroanalysis* **2006**, *18*, 115-120.
- (141) Langmaier, J.; Olšák, J.; Samcová, E.; Samec, Z.; Trojánek, A. *Electroanalysis* **2006**, *18*, 1329-1338.
- (142) Rodgers, P. J.; Jing, P.; Kim, Y.; Amemiya, S. *J. Am. Chem. Soc.* **2008**, *130*, 7436-7442.
- (143) Riva, J. S.; Cámara, C. I.; Juarez, A. V.; Yudi, L. M. *J. Appl. Electrochem.* **2014**, *44*, 1381-1392.
- (144) Riva, J. S.; Bierbrauer, K.; Beltramo, D. M.; Yudi, L. M. *Electrochim. Acta* **2012**, *85*, 659-664.
- (145) Méndez, M. A.; Prudent, M.; Su, B.; Girault, H. H. *Anal. Chem.* **2008**, *80*, 9499-9507.
- (146) Méndez, M. A.; Nazemi, Z.; Uyanik, I.; Lu, Y.; Girault, H. H. *Langmuir* **2011**, *27*, 13918-13924.
- (147) Vagin, M. Y.; Malyh, E. V.; Karyakin, A. A. *Electrochem. Commun.* **2003**, *5*, 329-333.
- (148) Amemiya, S.; Yang, X.; Wazenegger, T. L. *J. Am. Chem. Soc.* **2003**, *125*, 11832-11833.
- (149) Yuan, Y.; Amemiya, S. *Anal. Chem.* **2004**, *76*, 6877-6886.
- (150) Shinshi, M.; Sugihara, T.; Osakai, T.; Goto, M. *Langmuir* **2006**, *22*, 5937-5944.
- (151) Trojánek, A.; Langmaier, J.; Samcová, E.; Samec, Z. *J. Electroanal. Chem.* **2007**, *603*, 235-242.

- (152) O'Sullivan, S.; Arrigan, D. W. M. *Electrochim. Acta* **2012**, *77*, 71-76.
- (153) O'Sullivan, S.; Arrigan, D. W. M. *Anal. Chem.* **2013**, *85*, 1389-1394.
- (154) Matsui, R.; Sakaki, T.; Osakai, T. *Electroanalysis* **2012**, *24*, 1164-1169.
- (155) Herzog, G. g.; Roger, A.; Sheehan, D.; Arrigan, D. W. M. *Anal. Chem.* **2009**, *82*, 258-264.
- (156) Zhai, J.; Hoffmann, S. V.; Day, L.; Lee, T.-H.; Augustin, M. A.; Aguilar, M.-I.; Wooster, T. J. *Langmuir* **2012**, *28*, 2357-2367.
- (157) Scanlon, M. D.; Strutwolf, J.; Arrigan, D. W. M. *PCCP* **2010**, *12*, 10040-10047.
- (158) Hartvig, R. A.; van de Weert, M.; Østergaard, J.; Jorgensen, L.; Jensen, H. *Langmuir* **2012**, *28*, 1804-1815.
- (159) Alvarez de Eulate, E.; Arrigan, D. W. M. *Anal. Chem.* **2012**, *84*, 2505-2511.
- (160) Alvarez de Eulate, E.; O'Sullivan, S.; Arrigan, D. W. M. *ChemElectroChem* **2017**, *4*, 898-904.
- (161) Rimboud, M.; Charreteur, K.; Sladkov, V.; Elleouet, C.; Quentel, F.; L'Her, M. *J. Electroanal. Chem.* **2009**, *636*, 53-59.
- (162) Alvarez de Eulate, E.; Qiao, L.; Scanlon, M. D.; Girault, H. H.; Arrigan, D. W. M. *Chem. Commun.* **2014**, *50*, 11829-11832.
- (163) Samec, Z.; Mareček, V.; Weber, J. *J. Electroanal. Chem. Interfacial Electrochem.* **1979**, *96*, 245-247.
- (164) Osakai, T.; Kakutani, T.; Senda, M. *J. Electrochem. Soc.* **1987**, *134*, C520-C520.
- (165) Younan, N.; Hojeij, M.; Ribeaucourt, L.; Girault, H. H. *Electrochem. Commun.* **2010**, *12*, 912-915.
- (166) Rodgers, A. N. J.; Booth, S. G.; Dryfe, R. A. W. *Electrochem. Commun.* **2014**, *47*, 17-20.

- (167) Su, B.; Abid, J.-P.; Fermín, D. J.; Girault, H. H.; Hoffmannová, H.; Krtíl, P.; Samec, Z. *J. Am. Chem. Soc.* **2004**, *126*, 915-919.
- (168) Poltorak, L.; Herzog, G.; Walcarius, A. *Electrochem. Commun.* **2013**, *37*, 76-79.
- (169) Poltorak, L.; Morakchi, K.; Herzog, G.; Walcarius, A. *Electrochim. Acta* **2015**, *179*, 9-15.
- (170) Poltorak, L.; Gamero-Quijano, A.; Herzog, G.; Walcarius, A. *Applied Materials Today* **2017**, *9*, 533-550.
- (171) Bates, R. G.; Macaskill, J. B. *Pure Appl. Chem* **1978**, *50*, 1701-1706.
- (172) Compton, R. G.; Banks, C. E.; Understanding Voltammetry, 2nd Ed., Imperial College Press, **2011**.
- (173) Vanysek, P.; Basaez Ramirez, L. *Journal of the Chilean Chemical Society* **2008**, *53*, 1455-1463.
- (174) Zazpe, R.; Hibert, C.; O'Brien, J.; Lanyon, Y. H.; Arrigan, D. W. M. *Lab on a Chip* **2007**, *7*, 1732-1737.
- (175) Scholz, F. *Electroanalytical Methods*; Springer, **2010**; Vol. 1.
- (176) Osteryoung, J. *Accounts of Chemical Research* **1993**, *26*, 77-83.
- (177) Herzog, G.; Beni, V. *Anal. Chim. Acta* **2013**, *769*, 10-21.
- (178) Strutwolf, J.; Scanlon, M. D.; Arrigan, D. W. M. *J. Electroanal. Chem.* **2010**, *641*, 7-13.
- (179) Paneli, M. G.; Voulgaropoulos, A. *Electroanalysis* **1993**, *5*, 355-373.
- (180) Vocadlo, D. J.; Davies, G. J.; Laine, R.; Withers, S. G. *Nature* **2001**, *412*, 835-838.
- (181) Canfield, R. E.; Liu, A. K. *Journal of Biological Chemistry* **1965**, *240*, 1997-2002.

- (182) Hooper, K. L.; Sheasley, S. L.; Gilbert, H. F.; Thorpe, C. *Journal of Biological Chemistry* **1999**, *274*, 22147-22150.
- (183) Blake, C. C.; Koenig, D. F.; Mair, G. A.; North, A. C.; Phillips, D. C.; Sarma, V. R. *Nature* **1965**, 757-761.
- (184) Serra, C.; Vizoso, F.; Alonso, L.; Rodríguez, J. C.; González, L. O.; Fernández, M.; Lamelas, M. L.; Sánchez, L. M.; García-Muñiz, J. L.; Baltasar, A. *Breast Cancer Res* **2002**, *4*, R16.
- (185) Tahara, E.; Ito, H.; Shimamoto, F.; Iwamoto, T.; Nakagami, K.; Niimoto, H. *Histopathology* **1982**, *6*, 409-421.
- (186) Mishra, O. P.; Batra, P.; Ali, Z.; Anupurba, S.; Das, B. K. *Journal of tropical pediatrics* **2003**, *49*, 13-16.
- (187) Arrigan, D. W. M. *Annu. Rep. Prog. Chem. Sect. C: Phys. Chem.* **2013**, *109*, 167-188.
- (188) Herzog, G. *Analyst* **2015**, *140*, 3888-3896.
- (189) Osakai, T.; Yuguchi, Y.; Gohara, E.; Katano, H. *Langmuir* **2010**, *26*, 11530-11537.
- (190) Hartvig, R. A.; Méndez, M. A.; Weert, M. v. d.; Jorgensen, L.; Østergaard, J.; Girault, H. H.; Jensen, H. *Anal. Chem.* **2010**, *82*, 7699-7705.
- (191) Herzog, G.; Moujahid, W.; Strutwolf, J.; Arrigan, D. W. M. *Analyst* **2009**, *134*, 1608-1613.
- (192) Rosi, N. L.; Mirkin, C. A. *Chemical Reviews* **2005**, *105*, 1547-1562.
- (193) de Eulate, E. A.; Serls, L.; Arrigan, D. W. M. *Anal Bioanal Chem* **2013**, *405*, 3801-3806.
- (194) O'Sullivan, S.; Alvarez de Eulate, E.; Yuen, Y. H.; Helmerhorst, E.; Arrigan, D. W. M. *Analyst* **2013**, *138*, 6192-6196.

- (195) Moody, G. J.; Thomas, J. D. R. In *Ion-Selective Electrodes in Analytical Chemistry*, Freiser, H., Ed.; Springer US: New York, N.Y. 10013, **1978**, pp 287-309.
- (196) Moody, G. J. In *Biosensors and Chemical Sensors in ACS Symposium Series*, Edelman, P. G.; Wang, J., Eds.; American Chemical Society: NW, Washington DC 20036, USA, **1992**, pp 99-110.
- (197) Berduque, A.; Scanlon, M. D.; Collins, C. J.; Arrigan, D. W. M. *Langmuir* **2007**, *23*, 7356-7364.
- (198) Kuramitsu, S.; Hamaguchi, K. *Journal of Biochemistry* **1980**, *87*, 1215-1219.
- (199) Wang, J. *Electroanalytical Techniques in Clinical Chemistry and Laboratory Medicine*; John Wiley & Sons: New Jersey, **1988**.
- (200) Bilan, M. I.; Grachev, A. A.; Ustuzhanina, N. E.; Shashkov, A. S.; Nifantiev, N. E.; Usov, A. I. *Carbohydr. Res.* **2002**, *337*, 719-730.
- (201) Chevolut, L.; Mulloy, B.; Ratiskol, J.; Foucault, A.; Collic-Jouault, S. *Carbohydr. Res.* **2001**, *330*, 529-535.
- (202) Ale, M. T.; Meyer, A. S. *RSC Advances* **2013**, *3*, 8131-8141.
- (203) Berteau, O.; Mulloy, B. *Glycobiology* **2003**, *13*, 29R-40R.
- (204) Morya, V. K.; Kim, J.; Kim, E.-K. *Appl. Microbiol. Biotechnol.* **2011**, *93*, 71-82.
- (205) Mak, W.; Hamid, N.; Liu, T.; Lu, J.; White, W. L. *Carbohydr. Polym.* **2013**, *95*, 606-614.
- (206) Sheng, P. X.; Ting, Y.-P.; Chen, J. P.; Hong, L. *J. Colloid Interface Sci.* **2004**, *275*, 131-141.
- (207) Díaz-Rubio, M. E.; Pérez-Jiménez, J.; Saura-Calixto, F. *Int. J. Food Sci. Nutr.* **2009**, *60*, 23-34.
- (208) Ruocco, N.; Costantini, S.; Guariniello, S.; Costantini, M. *Molecules* **2016**, *21*.

- (209) Kim, E. J.; Park, S. Y.; Lee, J.-Y.; Park, J. H. Y. *BMC Gastroenterol.* **2010**, *10*, 1-11.
- (210) Park, Y. H.; Kim, G.-Y.; Moon, S.-K.; Kim, J. W.; Yoo, H. Y.; Choi, H. Y. *Molecules* **2014**, *19*.
- (211) Aisa, Y.; Miyakawa, Y.; Nakazato, T.; Shibata, H.; Saito, K.; Ikeda, Y.; Kizaki, M. *Am. J. Hematol.* **2005**, *78*, 7-14.
- (212) Fitton, J. H. *Mar. Drugs* **2011**, *9*, 1731-1760.
- (213) Lowenthal, R. M.; Fitton, J. H. *J. Appl. Phycol.* **2014**, *27*, 2075-2077.
- (214) Myers, S. P.; O'Connor, J.; Fitton, J. H.; Brooks, L.; Rolfe, M.; Connellan, P.; Wohlmuth, H.; Cheras, P. A.; Morris, C. *Biol.: Targets Ther.* **2010**, *4*, 33-44.
- (215) Myers, S. P.; O'Connor, J.; Fitton, J. H.; Brooks, L.; Rolfe, M.; Connellan, P.; Wohlmuth, H.; Cheras, P. A.; Morris, C. *Biol.: Targets Ther.* **2011**, *5*, 45-60.
- (216) Hayashi, K.; Nakano, T.; Hashimoto, M.; Kanekiyo, K.; Hayashi, T. *Int Immunopharmacol* **2008**, *8*.
- (217) Cooper, R.; Dragar, C.; Elliot, K.; Fitton, J. H.; Godwin, J.; Thompson, K. *BMC Complement. Altern. Med.* **2002**, *2*, 1-7.
- (218) Schaeffer, D. J.; Krylov, V. S. *Ecotoxicol. Environ. Saf.* **2000**, *45*, 208-227.
- (219) Pielesz, A.; Biniaś, W. *Carbohydr. Res.* **2010**, *345*, 2676-2682.
- (220) Pielesz, A.; Biniaś, W.; Paluch, J. *Carbohydr. Res.* **2011**, *346*, 1937-1944.
- (221) Yamazaki, Y.; Nakamura, Y.; Nakamura, T. *Plant Biotechnol.* **2016**, *33*, 117-121.
- (222) Warttinger, U.; Giese, C.; Harenberg, J.; Krämer, R. *arXiv preprint arXiv:1608.00108* **2016**.
- (223) Irhimeh, M. R.; Fitton, J. H.; Lowenthal, R. M.; Kongtawelert, P. *Methods Find. Exp. Clin. Pharmacol.* **2005**, *27*, 705-710.

- (224) Tokita, Y.; Nakajima, K.; Mochida, H.; Iha, M.; Nagamine, T. *Biosci., Biotechnol., Biochem.* **2010**, *74*, 350-357.
- (225) Hassan, S. S. M.; Meyerhoff, M. E.; Badr, I. H. A.; Abd-Rabboh, H. S. M. *Electroanalysis* **2002**, *14*, 439.
- (226) Dürüst, N.; Meyerhoff, M. E. *J. Electroanal. Chem.* **2007**, *602*, 138-141.
- (227) Fu, B.; Bakker, E.; Yang, V. C.; Meyerhoff, M. E. *Macromolecules* **1995**, *28*, 5834-5840.
- (228) Dürüst, N.; Meyerhoff, M. E. *Anal. Chim. Acta* **2001**, *432*, 253-260.
- (229) Kim, J. M.; Nguyen, L.; Barr, M. F.; Morabito, M.; Stringer, D.; Fitton, J. H.; Mowery, K. A. *Anal. Chim. Acta* **2015**, *877*, 1-8.
- (230) Peljo, P.; Girault, H. H. *Encyclopedia of Analytical Chemistry* **2012**.
- (231) Felisilda, B. M. B.; Alvarez de Eulate, E.; Arrigan, D. W. M. *Anal. Chim. Acta* **2015**, *893*, 34-40.
- (232) Santos, H. A.; García-Morales, V.; Roozeman, R.-J.; Manzanares, J. A.; Kontturi, K. *Langmuir* **2005**, *21*, 5475-5484.
- (233) Riva, J. S.; Iglesias, R.; Yudi, L. M. *Electrochim. Acta* **2013**, *107*, 584-591.
- (234) Collins, C. J.; Berduque, A.; Arrigan, D. W. M. *Anal. Chem.* **2008**, *80*, 8102-8108.
- (235) Katano, H.; Senda, M. *Anal. Sci.* **2001**, *17*, 1027-1029.
- (236) Ho, T. T. M.; Bremmell, K. E.; Krasowska, M.; Stringer, D. N.; Thierry, B.; Beattie, D. A. *Soft Matter* **2015**, *11*, 2110-2124.
- (237) Arooj, M.; Gandhi, N. S.; Kreck, C. A.; Arrigan, D. W. M.; Mancera, R. L. *J. Phys. Chem. B* **2016**, *120*, 3100-3112.
- (238) Wilke, S.; Zerihun, T. *J. Electroanal. Chem.* **2001**, *515*, 52-60.

- (239) Islam, T.; Linhardt, R. J. In *Carbohydrate-Based Drug Discovery*; Wiley-VCH Verlag GmbH & Co. KGaA, 2003, pp 407-439.
- (240) Gandhi, N. S.; Mancera, R. L. *Chem. Biol. Drug Des.* **2008**, *72*, 455-482.
- (241) Capila, I.; Linhardt, R. J. *Angew. Chem. Int. Ed.* **2002**, *41*, 390-412.
- (242) Yeh, B. K.; Eliseenkova, A. V.; Plotnikov, A. N.; Green, D.; Pinnell, J.; Polat, T.; Gritli-Linde, A.; Linhardt, R. J.; Mohammadi, M. *Mol. Cell. Biol.* **2002**, *22*, 7184-7192.
- (243) Bourin, M.-C.; Lindahl, U. *Biochem. J* **1993**, *289*, 313.
- (244) Hiebert, L. M.; Wice, S. M.; Ping, T.; Hileman, R. E.; Polat, T.; Linhardt, R. J. *Pharm. Res.* **2002**, *19*, 838-844.
- (245) Hileman, R. E.; Siegel, M. M.; Tabei, K.; Balagurunathan, K.; Linhardt, R. J. *Electrophoresis* **1998**, *19*, 2677-2681.
- (246) Szabo, S.; Hollander, D. *The American journal of medicine* **1989**, *86*, 23-31.
- (247) Zhu, X.; Hsu, B. T.; Rees, D. C. *Structure* **1993**, *1*, 27-34.
- (248) Prestrelski, S. J.; Fox, G. M.; Arakawa, T. *Arch. Biochem. Biophys.* **1992**, *293*, 314-319.
- (249) Zaia, J. *Mass Spectrom. Rev.* **2004**, *23*, 161-227.
- (250) Wolff, J. J.; Laremore, T. N.; Leach III, F. E.; Linhardt, R. J.; Amster, I. J. *Eur. J. Mass Spectrom.* **2009**, *15*, 275-281.
- (251) Zidkova, J.; Chmelik, J. *Feedback* **1997**, *91*.
- (252) Ruiz-Calero, V.; Puignou, L.; Galceran, M. T. *J. Chromatogr. A* **1998**, *828*, 497-508.
- (253) Skidmore, M. A.; Guimond, S. E.; Dumax-Vorzet, A. F.; Atrih, A.; Yates, E. A.; Turnbull, J. E. *J. Chromatogr. A* **2006**, *1135*, 52-56.
- (254) Deakin, J. A.; Lyon, M. *Glycobiology* **2008**, *18*, 483-491.

- (255) Sinnis, P.; Coppi, A.; Toida, T.; Toyoda, H.; Kinoshita-Toyoda, A.; Xie, J.; Kemp, M. M.; Linhardt, R. J. *Journal of Biological Chemistry* **2007**, *282*, 25376-25384.
- (256) Chuang, W.-L.; McAllister, H.; Rabenstein, D. L. *Carbohydr. Res.* **2002**, *337*, 935-945.
- (257) Guerrini, M.; Naggi, A.; Guglieri, S.; Santarsiero, R.; Torri, G. *Anal. Biochem.* **2005**, *337*, 35-47.
- (258) Gunay, N. S.; Tadano-Aritomi, K.; Toida, T.; Ishizuka, I.; Linhardt, R. J. *Anal. Chem.* **2003**, *75*, 3226-3231.
- (259) Ke, Y.; Li, S. L.; Chang, L. D.; Kapanadze, T. *J. Chromatogr. B* **2015**, *978-979*, 151-156.
- (260) Felisilda, B. M. B.; Alvarez de Eulate, E.; Stringer, D. N.; Fitton, J. H.; Arrigan, D. W. M. *Analyst* **2017**, *142*, 3194-3202.
- (261) Sobolev, V. E.; Jenkins, R. O.; Goncharov, N. V. *Exp. Toxicol. Pathol.* **2017**.
- (262) O'Sullivan, C. K. *Anal Bioanal Chem* **2002**, *372*, 44-48.
- (263) Jayasena, S. D. *Clinical Chemistry* **1999**, *45*, 1628.
- (264) Stoltenburg, R.; Reinemann, C.; Strehlitz, B. *Biomolecular Engineering* **2007**, *24*, 381-403.
- (265) Song, S.; Wang, L.; Li, J.; Fan, C.; Zhao, J. *TrAC Trends in Analytical Chemistry* **2008**, *27*, 108-117.
- (266) Hermann, T.; Patel, D. J. *Science* **2000**, *287*, 820.
- (267) Zhou, J.; Rossi, J. *Nature Reviews Drug Discovery* **2016**, *16*, 181.
- (268) White, R. R.; Sullenger, B. A.; Rusconi, C. P. *The Journal of Clinical Investigation* **2000**, *106*, 929-934.
- (269) Nimjee, S. M.; White, R. R.; Becker, R. C.; Sullenger, B. A. *Annu. Rev. Pharmacool. Toxicol.* **2017**, *57*, 61-79.

- (270) Brody, E. N.; Gold, L. *Rev. Mol. Biotechnol.* **2000**, *74*, 5-13.
- (271) Mattice, C. M. C.; DeRosa, M. C. *Biodrugs* **2015**, *29*, 151-165.
- (272) Wang, A. Z.; Farokhzad, O. C. *J. Nucl. Med.* **2014**, *55*, 353-356.
- (273) Tombelli, S.; Minunni, M.; Mascini, M. *Biosensors and Bioelectronics* **2005**, *20*, 2424-2434.
- (274) Willner, I.; Zayats, M. *Angew. Chem. Int. Ed.* **2007**, *46*, 6408-6418.
- (275) Clark, S. L.; Remcho, V. T. *Electrophoresis* **2002**, *23*, 1335-1340.
- (276) Mairal, T.; Cengiz Özalp, V.; Lozano Sánchez, P.; Mir, M.; Katakis, I.; O'Sullivan, C. K. *Anal Bioanal Chem* **2008**, *390*, 989-1007.
- (277) Di Cera, E. *Mol. Aspects Med.* **2008**, *29*, 203-254.
- (278) Sokolova, E.; Reiser, G. *Thromb Haemost* **2008**, *100*, 576-581.
- (279) Franchini, M.; Mannucci, P. M.; Thieme Medical Publishers, pp 95-101.
- (280) Avino, A.; Fabrega, C.; Tintore, M.; Eritja, R. *Curr. Pharm. Des.* **2012**, *18*, 2036-2047.
- (281) Bock, L. C.; Griffin, L. C.; Latham, J. A.; Vermaas, E. H.; Toole, J. J. *Nature* **1992**, *355*, 564.
- (282) Paborsky, L. R.; McCurdy, S. N.; Griffin, L. C.; Toole, J. J.; Leung, L. L. *Journal of biological chemistry* **1993**, *268*, 20808-20811.
- (283) Macaya, R. F.; Schultze, P.; Smith, F. W.; Roe, J. A.; Feigon, J. *Proceedings of the National Academy of Sciences* **1993**, *90*, 3745-3749.
- (284) Schultze, P.; Macaya, R. F.; Feigon, J. *J. Mol. Biol.* **1994**, *235*, 1532-1547.
- (285) Kelly, J. A.; Feigon, J.; Yeates, T. O.; Elsevier, **1996**.
- (286) Deng, B.; Lin, Y.; Wang, C.; Li, F.; Wang, Z.; Zhang, H.; Li, X.-F.; Le, X. C. *Anal. Chim. Acta* **2014**, *837*, 1-15.

- (287) Wu, T.-C.; Vasudev, M.; Dutta, M.; Stroschio, M. A. *IEEE Trans. NanoBiosci.* **2013**, *12*, 93-97.
- (288) Joseph, M. J.; Taylor, J. C.; McGown, L. B.; Pitner, J. B.; Linn, C. P. *Biospectroscopy* **1996**, *2*, 173-183.
- (289) Liu, J.; Morris, M. D.; Macazo, F. C.; Schoukroun-Barnes, L. R.; White, R. J. *J. Electrochem. Soc.* **2014**, *161*, H301-H313.
- (290) Ammann, D. *Ion-Selective Microelectrodes: Principles, Design and Application*; Springer Science & Business Media, **2013**; Vol. 50.
- (291) Numnuam, A.; Chumbimuni-Torres, K. Y.; Xiang, Y.; Bash, R.; Thavarungkul, P.; Kanatharana, P.; Pretsch, E.; Wang, J.; Bakker, E. *J. Am. Chem. Soc.* **2008**, *130*, 410-411.
- (292) Numnuam, A.; Chumbimuni-Torres, K. Y.; Xiang, Y.; Bash, R.; Thavarungkul, P.; Kanatharana, P.; Pretsch, E.; Wang, J.; Bakker, E. *Anal. Chem.* **2008**, *80*, 707-712.
- (293) Shishkanova, T. V.; Volf, R.; Krondak, M.; Král, V. *Biosensors and Bioelectronics* **2007**, *22*, 2712-2717.
- (294) Imai, Y.; Sugihara, T.; Osakai, T. *The Journal of Physical Chemistry B* **2011**, *116*, 585-592.
- (295) Vagin, M. Y.; Trashin, S. A.; Karyakin, A. A.; Mascini, M. *Anal. Chem.* **2008**, *80*, 1336-1340.
- (296) Osakai, T.; Komatsu, H.; Goto, M. *J. Phys.: Condens. Matter* **2007**, *19*, 375103.
- (297) Mel'nikov, S. M.; Sergeyev, V. G.; Yoshikawa, K. *J. Am. Chem. Soc.* **1995**, *117*, 9951-9956.
- (298) Hianik, T.; Ostatná, V.; Sonlajtnerova, M.; Grman, I. *Bioelectrochemistry* **2007**, *70*, 127-133.
- (299) Vairamani, M.; Gross, M. L. *J. Am. Chem. Soc.* **2003**, *125*, 42-43.

(300) De Rache, A.; Kejnovská, I.; Vorlíčková, M.; Buess- Herman, C. *Chemistry-A European Journal* **2012**, *18*, 4392-4400.

(301) Lerga, T. M.; O'Sullivan, C. K. *Anal. Chim. Acta* **2008**, *610*, 105-111.

Every reasonable effort has been made to acknowledge the owners of copyright material. I would be pleased to hear from any copyright owner who has been omitted or incorrectly acknowledge.

APPENDICES

Appendix A Preparation of Organic Electrolyte Salts

A.1 Metathesis of BTPPATPBCl

The organic electrolyte salt, bis(triphenylphosphoranylidene) ammonium tetrakis (4-chlorophenyl) borate (BTPPATPBCl) was synthesized via a metathesis reaction between bis(triphenylphosphoranylidene) ammonium chloride (BTPPACl) and potassium tetrakis (4-chlorophenyl) borate (KTPBCl). The equimolar reaction is shown in Figure A.1.

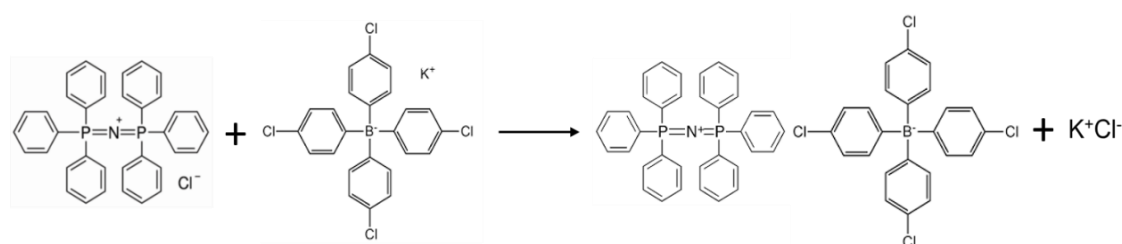


Figure A.1 Metathesis reaction between equimolar BTPPACl and KTPBCl

The procedure for the preparation is described:

- BTPPACl (1.157 g) was dissolved in a H₂O/MeOH mixture (10 mL; 1:2 v/v). Similarly, KTPBCl (1.000 g) was also dissolved in a H₂O/MeOH mixture (20 mL; 1:2 v/v). Then, the BTPPACl solution was added dropwise, with stirring, to the KTPBCl solution. A strong white precipitate was produced.
- The product formed (white precipitate, BTPPATPBCl) was vacuum-filtered using a Buchner funnel. The funnel was then covered with pierced Parafilm and then product was continued to dry under vacuum for approximately 2 hours. The resulting product was then placed in a desiccator for further drying overnight.
- The dried product (BTPPATPBCl) was purified by re-crystallization with acetone. The resulting solution was then filtered (gravity) to separate the impurities. The beaker containing the filtrate was covered with pierced Parafilm and then allowed to dry.
- The re-crystallized product was further washed with a H₂O/Acetone solution (1:1 v/v) and then allowed to dry in a desiccator overnight.

The next day, the product was collected into a vial covered with Aluminium foil and then stored in a cool room. This is necessary since the product is known to be sensitive to light and temperature.

A.2 Metathesis of TDMATPBCl

To explore the effect of a different organic cation towards the detection of the negatively charged analytes presented in this thesis, a new organic electrolyte salt was synthesized. Tridodecylmethylammonium tetrakis (4-chlorophenyl) borate (TDMATPBCl) was prepared via a metathesis reaction of equimolar tridodecylmethylammonium chloride (TDMACl) and potassium tetrakis(4-chlorophenyl) borate (KTPBCl). The reaction is shown in Figure A.2.

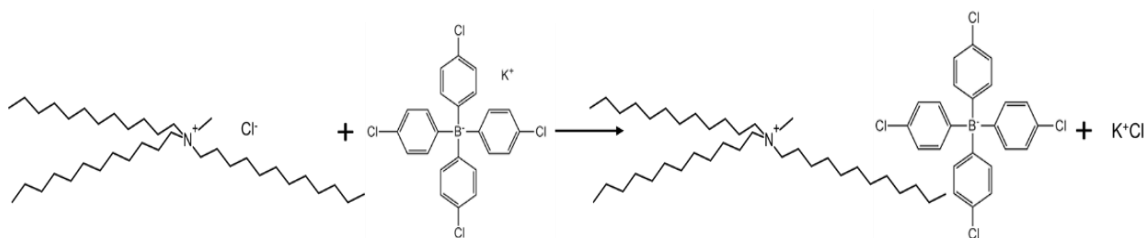


Figure A.2 Metathesis reaction between equimolar TDMACl and KTPBCl

The precipitate TDMATPBCl was produced following the listed steps:

- TDMACl (0.321 g) was dissolved in H₂O/MeOH (2.5 mL, 1:2 v/v) while KTPBCl (0.320 g) was also dissolved in a similar solvent (5.0 mL, 1:2 v/v). The resulting TDMACl solution was then added drop-wise, with stirring, into the KTPBCl solution and this produced a milky-white precipitate.
- The solution was vacuum-filtered to collect the white precipitate. The Buchner funnel was then covered with pierced Parafilm while the vacuum drying was continued for almost 2 hours. Then, the product was allowed to dry further in a desiccator overnight.
- The dried product (TDMATPBCl) was purified by re-crystallization with acetone. The solution was then filtered (gravity). Then, the beaker containing the filtrate was covered with pierced Parafilm and then allowed to dry in the fumehood.
- The TDMATPBCl product was then washed with a H₂O/Acetone solution (1:1 v/v) and then allowed to dry again in a desiccator overnight.

The product TDMATPBCl was then collected into a vial covered with Aluminium foil and stored in a cool room to prevent degradation from light and hot temperature.

A.3 Metathesis of CTATPBCl¹

For the aptamer studies in this thesis, a new organic electrolyte salt was utilized. Cetyltrimethylammonium bromide (CTAB), a surfactant that is known to interact with aptamers, was used. Cetyltrimethylammonium tetrakis(4-chlorophenyl)borate (CTATPBCl) was prepared according to the reaction shown in Figure A.3.

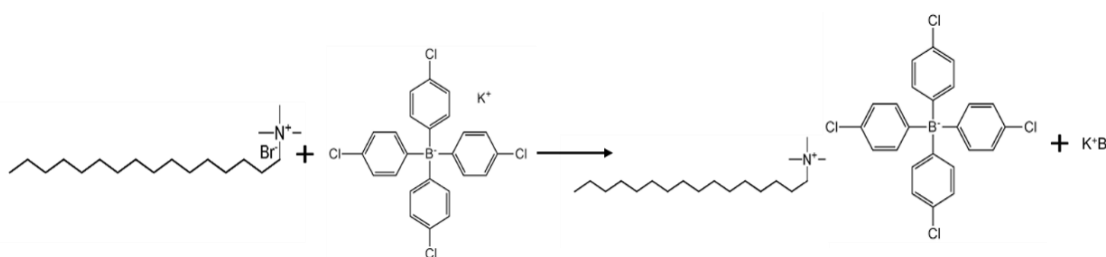


Figure A.3 Metathesis reaction between equimolar CTAB and KTPBCl

The product CTATPBCl was prepared as follows:

- Equimolar amounts of CTAB (0.800 g) and KTPBCl (1.089 g) were dissolved in H₂O:MeOH (1:2 v/v) mixture (5 and 10 mL respectively). The CTAB solution was then added dropwise to the KTPBCl solution with vigorous stirring. The product - white precipitate – was continuously stirred for 48 hours (at 4° C).
- The resulting product was filtered under vacuum and was left in a desiccator overnight for further drying.
- The dried CTATPBCl was dissolved in acetone for purification. The solution was filtered (gravity) and the filtrate was allowed to dry under the fume hood. This was done by covering the funnel with pierced Parafilm to allow acetone evaporation.
- Finally, the product was washed with H₂O:Acetone (1:1 v/v) and then again dried in a desiccator overnight.

The product was then collected in an Aluminium foil-covered vial and stored at 4°C.

¹ G. Herzog, CNRS/University of Lorraine, personal communication (date:24 Nov. 2016).

Appendix B Research Output

B.4 Journal Publications

Published:

- Felisilda, Bren Mark B., Alvarez de Eulate, Eva, Stinger, Damien N., Fitton, J.Helen and Arrigan, Damien. “*Electrochemical behaviour at a liquid-organogel microinterface array of fucoïdan extracted from algae.*” *Analyst*, (2017), 142, 3194-3202.
- Felisilda, Bren Mark B., Alvarez de Eulate, Eva and Arrigan, Damien WM. “*Investigation of a solvent-cast organogel to form a liquid-gel microinterface array for electrochemical detection of lysozyme.*” *Analytica Chimica Acta*, (2015), 893, 34-40.

Submitted:

- Booth, Samuel G., Felisilda, Bren Mark B., Alvarez de Eulate, Eva, Gustafsson, Ove, Dryfe, Robert A.W., Hackett, Mark J., Arrigan, Damien W.M.,” “*Electrochemically Induced Variation in Protein Secondary Structure at Soft Interfaces*” (2018)
- Felisilda, Bren Mark B., Arrigan, Damien W.M., “*Electroactivity of Aptamer at Soft Microinterface Arrays*”. (2018)

In preparation:

- Felisilda, Bren Mark B., Arrigan, Damien W.M., “*Electrochemical Investigation of Sulfated Carbohydrates at a Polarized Microinterface Array*”. (2018)

B.5 Research Presentations

Oral Presentation:

- Felisilda, Bren Mark B., Arrigan, Damien W.M., “*Behaviour of Aptamers at Soft Polarized Microinterfaces*”, 25th Annual RACI R&D Topics Conference, Hobart, Australia, **December 2017**. (*Highly Commended Oral Prize*)
- Felisilda, Bren Mark B., Arrigan, Damien W.M., “*Electrochemical Investigation of Polyelectrolytes at a Liquid-Organogel Microinterface Array*”, RACI Centenary Congress (RACI100), Melbourne, Australia, **July 2017**.
- Felisilda, Bren Mark B., Alvarez de Eulate, Eva, Stinger, Damien N., Fitton, J.Helen and Arrigan, Damien. “*Electrochemical Behaviour of Fucoïdan at a*

Polarized Synthetic Urine-Organogel Micro-Interface Array”, RACI Analytical and Environmental Chemistry Division National Symposium (ANACHEM2016), Adelaide, Australia, **July 2016**. (*RACI Student Travel Award*)

Poster Presentation:

- Felisilda, Bren Mark B., Alvarez de Eulate, Eva, Stinger, Damien N., Fitton, J.Helen and Arrigan, Damien. ”*Electrochemical Behaviour of Fucoidan Extracts from Seaweeds at a Polarized Water-Organogel Interface*”, 19th ISE Topical Meeting and 20th ANZES Symposium, Auckland, New Zealand, **April 2016**.
- Felisilda, Bren Mark B., Alvarez de Eulate, Eva, Stinger, Damien N., Fitton, J.Helen and Arrigan, Damien. “*Electrochemistry of Fucoidans at a Liquid-Liquid Interface*”, RSC Analytical Chemistry Twitter Conference, **March 2016**.
- Felisilda, Bren Mark B., Alvarez de Eulate, Eva and Arrigan, Damien WM. “*Pulse Voltammetric Detection of Lysozyme at the Liquid-Organogel Microinterface Array*”, RSC Analytical Sciences Twitter Conference, **February 2015**.
- Felisilda, Bren Mark B., Alvarez de Eulate, Eva and Arrigan, Damien WM. “*Solvent-cast Organogel in Liquid-Liquid Microinterfaces and its Application for Protein Detection*”, 22nd Annual RACI R&D Topics Conference, Adelaide, Australia, **December 2014**.